

A chronology of late Quaternary southwestern Greenland ice sheet retreat using terrestrial and marine records

By
Kelsey Winsor

A dissertation submitted in partial fulfillment of
the requirements for the degree of

Doctor of Philosophy

(Geoscience)

at the

UNIVERSITY OF WISCONSIN-MADISON

2014

Date of final oral examination: 7/25/2014

This dissertation is approved by the following members of the Final Oral Committee:

D. Clay Kelly, Professor, Geoscience

Stephen R. Meyers, Associate Professor, Geoscience

Bradley Singer, Professor, Geoscience

Basil Tikoff, Professor, Geoscience

Anders E. Carlson, Associate Professor, College of Earth, Ocean, and Atmospheric
Sciences, Oregon State University

ABSTRACT

Examination of past Greenland Ice Sheet (GrIS) responses to changing environmental forcings improves projections of ice loss in a warmer future. Model projections require ice retreat chronologies that can be placed into the context of local, regional, and global forcings of ice mass balance. Here, I discuss results detailing three periods of southwestern GrIS retreat, with each dataset focused on ice margins that are exposed to a unique set of retreat forcings.

During the early last deglaciation (20-15 ka), the southwestern GrIS was located on the continental shelf where the ice margin would have been highly susceptible to changes in oceanic retreat drivers, including warming temperatures and rising sea levels. Using a record of grain size and sedimentation rate changes in a sediment core near the southwestern Greenland shelf, I develop a chronology of ice retreat. During the last glacial maximum (26-19 ka), high sedimentation rates (50-110 cm ka⁻¹) and low sand weight percentages (<11%) suggest a shelf break position before ~20.5 ka and until ~18.1 ka. Highest sedimentation rates occur between ~19.3 and 18.6 ka, contemporaneous with early deglacial sea level rise and increasing boreal summer insolation, suggesting that ice margin fluctuations resulted from these forcings. A subsequent reduction in sedimentation rates (20-40 cm ka⁻¹), an increase in sand weight percentages (20-25%), and a reduction in foraminiferal $\delta^{18}\text{O}$ values to ~3 per mil suggests that the ice margin retracted to and maintained a middle or inner shelf position between ~16.7 and 11.5 ka, despite continued sea-level rise. Terrestrial records, in particular those discussed in Chapter III, indicate that the ice margin pulled back from the modern coastline at ~11 ka, when near-surface Labrador Sea temperatures transitioned from glacial to interglacial values. This last glacial maximum-to-Holocene retreat chronology provides constraints on GrIS behavior during

the early deglaciation, for which records are lacking. Most importantly, it suggests an early response to sea level changes and/or initial rise in boreal summer insolation, followed by slow retreat or stability until influenced by warming waters during the late deglaciation.

A second set of data examines four southwestern GrIS ice margins during the late last deglaciation (15-11 ka) I use ^{10}Be exposure dating of boulders to develop thinning and retreat chronologies of marine- versus land-terminating ice margins. I find that rapid thinning and retreat occurred 12-10.5 ka at the termini of three marine-terminating outlet glaciers, coincident with deglacial warming in the adjacent eastern Labrador Sea. Minimum and maximum thinning rates for these sites were 0.2 m yr^{-1} and infinite, respectively, and retreat rates were between 30 m yr^{-1} and infinite. A fourth record from a land-dominated ice margin indicates earlier high-elevation exposure onset at $17.8 \pm 1.1 \text{ ka}$, thinning at a relatively slow rate of 0.1 to 0.3 m yr^{-1} until low-elevation exposure at $14.8 \pm 0.6 \text{ ka}$. This region experienced prolonged retreat at a rate of 20 m yr^{-1} , much slower than that of the marine-dominated fjord systems. These data suggest that where ice was exposed to a strong marine influence, ocean warming drove rapid ice withdrawal from the coast.

The most recent ice margin retreat examined here occurred during the late Holocene. I present ^{10}Be surface exposure dates on boulders close to the modern margin of the land-terminating Kiagtût sermiat outlet glacier in southernmost Greenland. Results indicate that Kiagtût sermiat reached its late Holocene maximum at $1.51 \pm 0.11 \text{ ka}$, whereas many glaciers in the high northern latitudes reached this maximum later, during the Little Ice Age of the last $\sim 0.5 \text{ ka}$. Boulder ages just outside the Little Ice Age moraine also demonstrate that Kiagtût sermiat did not exceed its Little Ice Age extent after $1.34 \pm 0.15 \text{ ka}$. These data support the hypothesis

that late Holocene southern Greenland experienced temperature trends different from the global average, and demonstrates the importance of observing localized changes in ice mass balance.

ACKNOWLEDGEMENTS

My advisor, Anders Carlson, has watched/forced me to grow up scientifically. Without his focus on the context and implications of our work, I would probably still be standing at my first field site, worrying over whether I was looking at a perfect or semi-perfect rock to sample. Anders has let me be cautious, but not to the point of paralysis, and I don't think I would have developed so much scientifically working under a less enthusiastic or less big-idea person. He's also been marvelous to work with, always kind-hearted and encouraging, with nary an obvious judgment.

Several other people have been integral to my development as a scientific thinker. Basil Tikoff, though he may not realize it, set me up to teach students enough that I would finally learn what it actually means to be a good student. A bit late for me, yes, but never too late. My partner, Scott Johnson, has pushed me to not only learn how to speak about science, but to be aware of the many (many!) psychological impediments to objectively looking at data (e.g., motivated reasoning, confirmation bias, etc.). My parents did the same, using well-developed intuitions for sensing b.s. That sense seems to have been passed on to my sisters, who use it regularly on me.

A slew of scientists and technicians have contributed to the thoughts and data presented in this dissertation. My committee members, Clay Kelly, Brad Singer, Steve Meyers, and Basil Tikoff, have put in valuable time to read and comment on drafts. Clay Kelly put up with the boring bureaucratic duties of an adoptive advisor. My old officemates, Dave Ullman and Richard Becker, were always willing to discuss questions, confusions, or just surprise at the natural world. Richard and Dave, as well as Dan Murray and Julie Harvey, helped with sample preparations and the trading off of lably duties. Beth Welke wrote a fabulous undergraduate

thesis and did grain size analyses for the sediment core discussed in Chapter IV. Amy Leventer and Gene Domack adopted me into their Totten cruise, where I finally started to get the sense of environmental conditions that influence coring and drilling for marine sediments. I know these ideas are still settling into my brain, but I also know I'll now be more aware of potential problems with samples before they even get to the geochemistry stage. The Totten cruise also exposed me to physical oceanography and seismic stratigraphy—and their potential applications to the paleo record—in a more intensive and integrated way than I could have hoped for otherwise.

The Weeks Hall group is a good one, and I'm glad I got to know its people. Lisa Colville aka Siewert, Liz Percak-Dennett, Mel Reusche, Jansi Prabakaran, Alberto Reyes, Sarah Greene, Ian Orland, Mary Schumann, Chlöe Bonamici, Zach Michels, Dan Murray, Kate Smith, Sarah Siewert, Erin Fenlon, Mike Schiltz, Ben Linzmeier, and Miao Du each made being at school friendly and deserve more recognition than there is space for. Sarah Greene, neither of us is sorry that I broke your toe sparring in the basement. Erin, I thought that I wasn't a complainer, but you, my friend, never said a bad word about anyone or anything. Lisa, I hope you get a house with some fruit trees. Mike, thanks for giving me my first disorienting head strike. Chlöe, I think you're awesome, and I wish we could convince each other of how awesome the other is. Liz, maybe a little bit of your confidence rubbed off on me, but maybe not.

I especially thank my nightshift friends, Katy Smith, David Gwyther, and David Morgan, for sharing sunrises, cookies, sea ice, and general confusion. You have inspired me to be a better person and a better scientist. Brendan Reilly, Sarah Strano, Jeremy Hoffman, and John Yang befriended me at Oregon State University, and answered questions about oceanography and

statistics. Brian Haley and Andy Ungerer, also at OSU, have put an immense amount of time into helping me get and analyze data, and I have learned an incredible amount about geochemistry from them.

Finally, the requisite funding acknowledgements: National Science Foundation Graduate Research Fellowship Program, Lewis Weeks Fund, Geological Society of America (twice over), Sigma Xi, National Geographic Society, PRIME Lab, and the Wisconsin Alumni Research Foundation.

Wait, I lied! One more set of really important thanks: everyone at The Blast, and at Rise Martial Arts. You kept me alive and feeling alive. You also kept me from accidentally closing myself out from those not in academia. Some of you think that the government shouldn't fund research, or don't believe in climate change. You are the people who I need to justify my work ethic to, and the people who have taught me to respect and love without politicizing.

Table of Contents

Abstract.....	i
Acknowledgements.....	iv
Chapter I.....	1
INTRODUCTION	
1.1. Motivation.....	1
1.2. Background.....	1
1.2.1. The Last Glacial Maximum to early deglacial southwestern GrIS.....	2
1.2.2. The late deglacial southwestern GrIS.....	3
1.2.3. The late Holocene southwestern GrIS.....	4
1.3. Summary.....	5
References.....	6
Figure Captions.....	9
Figures.....	10
Chapter II.....	12
EARLY DEGLACIAL ONSET OF SOUTHWESTERN GREENLAND ICE-SHEET RETREAT ON THE CONTINENTAL SHELF	
Abstract.....	13
2.1. Introduction.....	13
2.2. Regional Setting.....	15
2.2.1. Core HU87033-008.....	15
2.2.2. Modern and paleo hydrography.....	16
2.3. Methods.....	17
2.3.1. Core sampling and grain size analysis.....	18
2.3.2. Radiocarbon dating.....	18
2.3.3. Oxygen isotope analyses.....	19
2.3.4. Magnetic susceptibility.....	20
2.4. Results.....	20
2.4.1. Core chronology.....	20
2.4.2. Grain size and sedimentation rate.....	21
2.4.3. Oxygen isotopes.....	22
2.4.4. Magnetic susceptibility.....	22
2.5. Discussion.....	23
2.5.1. Interpretation of sediment changes.....	23
2.5.2. LGM and early deglacial sedimentation.....	25
2.5.3. Mid- to late-deglacial sedimentation.....	28
2.6. Conclusions.....	30
Acknowledgements.....	31
References.....	32
Figure captions.....	41
Tables.....	43

Figures.....	47
Chapter III.....	51
RAPID LAST DEGLACIAL THINNING AND RETREAT OF THE MARINE- TERMINATING SOUTHWESTERN GREENLAND ICE SHEET	
Abstract.....	52
3.1. Introduction.....	52
3.2. Geologic Setting and Sampling Locations.....	54
3.2.1. Terrestrial Study Locales.....	55
3.2.1.1. Sisimiut.....	55
3.2.1.2. Nuuk.....	56
3.2.1.3. Paamiut.....	57
3.2.1.4. Qaqortoq.....	58
3.3. Methods and age calculation.....	59
3.3.1. Field and laboratory methods.....	59
3.3.2. Exposure age calculations.....	60
3.4. Results.....	62
3.5. Timing and rates of deglaciation.....	63
3.5.1. Sisimiut.....	63
3.5.2. Nuuk.....	65
3.5.3. Paamiut.....	66
3.5.4. Qaqortoq.....	67
3.5.5. Summary of thinning and retreat rates.....	68
3.6. Environmental influences on southwest Greenland deglaciation.....	69
3.7. Conclusions.....	71
Acknowledgements.....	72
References.....	73
Figure Captions.....	82
Tables.....	84
Figures.....	87
Appendix S3-1.....	94
Chapter IV.....	95
¹⁰BE DATING OF THE NARSARSUAQ MORaine IN SOUTHERNMOST GREENLAND: EVIDENCE FOR A LATE-HOLOCENE ICE ADVANCE EXCEEDING THE LITTLE ICE AGE MAXIMUM	
Abstract.....	96
4.1. Introduction.....	96
4.2. Kiagtût sermiat setting and methodology.....	98
4.3. Results.....	100
4.4. Discussion.....	101
4.4.1. Comparison to other Greenland ice margins.....	102
4.4.2. Late Holocene Greenland climate change.....	106
4.5. Conclusions.....	110

Acknowledgements.....	110
References.....	112
Figure Captions.....	119
Tables.....	121
Figures.....	126
Chapter V.....	130
CONCLUSIONS	
5.1. Summary.....	130
5.2. Retreat Forcings.....	130
5.3. Future research directions.....	131
5.3.1. Early deglaciation shelf retreat.....	131
5.3.2. Marine vs. terrestrial late deglaciation retreat.....	133
5.3.3. Late Holocene glacial maxima.....	134
References.....	136

CHAPTER 1: INTRODUCTION

1.1. Motivation

Interest in past Greenland Ice Sheet (GrIS) behavior is motivated by the general question: how will ice sheets respond to future climate changes, and to the feedbacks associated with them? This response will integrate retreat forcings including atmospheric and oceanic warming, increases in surface radiative forcing, and rising sea level (Rignot and Thomas, 2002). Instrumental records spanning the last several decades enable an understanding of short-term cryosphere responses to short-term changes in forcings. However, not only does the relatively long response time of ice sheets (Alley et al., 2010; Joughin et al., 2014) limit extrapolations of these changes into the far future, but the retreat drivers themselves can take many hundreds to ~10,000 years to adjust to new boundary conditions (Church et al., 2013). Therefore, if we are concerned over ice sheet conditions in a thousand, or several thousand, years, chronicling past ice sheet variations is essential. In this dissertation, I focus on post-Last Glacial Maximum to late Holocene (LGM, 26-19 ka, Figure 1-1, Clark et al., 2009)) retreat of the southwestern GrIS.

1.2. Background

At the modern GrIS margin, outlet glaciers exit the inland ice through valleys that in some cases direct ice into the ocean, creating marine-terminating ice, and in other cases maintain land-terminating ice margins. This difference in termini conditions causes a spatial variation in the retreat (or advance) forcings on the GrIS margin (Funder et al., 2011; Straneo et al., 2013). A land-terminating ice body experiences mass loss primarily via surface melting, with some loss attributed to basal melt. A marine-terminating ice body, however, experiences this melt in

addition to ice loss driven by the ocean (e.g., Sole et al., 2008; Joughin et al., 2012). Calving at the ice margin into the sea generally removes ice much faster than does surface melt (Rignot et al., 2010). Submarine basal melt—though attention has only turned to it in the past decade or so (e.g., Holland et al., 2008; Murray et al., 2010; Straneo et al., 2010; Knutz et al., 2011; Straneo et al., 2013)—can result in as great a rate of ice loss as calving (Rignot et al., 2010). Thus, marine-terminating ice tends to experience more rapid changes in margin position than does land-terminating ice (Rignot et al., 2010; Straneo and Heimbach, 2013).

1.2.1. The Last Glacial Maximum to early deglacial southwestern GrIS

Relatively low boreal summer insolation (Figure 1-1A, Berger and Loutre, 1991), low sea level (Figure 1-1B, Clark et al., 2009; 2012), and cold air (Figure 1-1C; Grootes and Stuiver, 1997; Dahl-Jensen et al., 1998; Rasmussen et al., 2008) and Labrador Sea temperatures (Figure 1-1D, Winsor et al., 2012) controlled the LGM mass balance of the southwestern GrIS (Alley et al., 2010; Funder et al., 2011). At that time, the GrIS extended far past its present-day margin, likely reaching the continental shelf break in many places (Simpson et al., 2009; Alley et al., 2010; Funder et al., 2011). However, constraints on the spatial variability of the LGM margin position are limited.

Discontinuous submarine moraines are mapped on the inner to outer continental shelf (Kelly, 1985), but in very few locales are these moraines dated conclusively to an LGM or last deglaciation time period (Ó Cofaigh et al., 2012). In other regions, no submarine landforms attributed to subglacial or ice margin processes are documented, likely due more to a lack of high-resolution bathymetric mapping rather than to an absence of landforms (Funder et al., 2011). Offshore of southwestern Greenland, limited bathymetric mapping has allowed two

competing views of the LGM ice margin extent—that the GrIS extended to the shelf break (Simpson et al., 2009), or that the ice margin was restricted to the inner to middle shelf (Kelly, 1985)—to persist. I use a sediment core proximal to the shelf (Figure 1-2) to test for southwestern GrIS presence on the shelf break and to develop the first chronology of ice retreat on the shelf in this region. I then place this early deglacial southwestern GrIS margin chronology into the context of changing insolation, air and ocean temperature, and sea level forcings (Chapter II).

1.2.2. The late deglacial southwestern GrIS

Terrestrial records of southwestern GrIS withdrawal onto the modern coastline and then inland to the modern ice margin date the majority of retreat to between 13 and 8 ka, with the onset of rapid withdrawal occurring around the Younger Dryas (Figure 1-1, Simpson et al., 2009; Alley et al., 2010; Funder et al., 2011). In many places, retreat chronology depends on minimum-limiting radiocarbon dates, leading to potential underestimation of the ice margin response to retreat drivers. However, the recent application of ^{10}Be surface exposure dating has allowed direct dating of ice abandonment (Balco, 2011). In southwestern Greenland, Rinterknecht et al. (2009) and Roberts et al. (2009) both report ^{10}Be ages of 18-20 ka near the coastal town of Sisimiut. Levy et al. (2012) and Carlson et al. (in press) date exposure inland of Sisimiut to 6.7 ka. Further to the south, Larsen et al. (2014) document exposure of the modern coastline of Sermilik and Sarqarssuaq fjords at 10.5 ka, and of land adjacent to the modern ice margin at 10.1 ka. Inland of the southwestern Greenland town of Paamiut, Carlson et al. (in press) report exposure at 11.0 ka. In southernmost Greenland, Carlson et al. (in press) date retreat to the

modern ice margin position at 11.3 ka. Yet, without coastal dates from elevation transects and without paired coastal and inland ^{10}Be dates, thinning and retreat rates cannot be calculated.

I use ^{10}Be surface exposure dating to develop thinning chronologies for coastal southwestern to southern Greenland sites. These locales represent fjords ($n=3$) that experienced relatively strong marine influence, and a fourth region exposed to weaker marine influence. I then calculate ice retreat rates using these data and the inland data of Levy et al. (2012), Larsen et al. (2014), and Carlson et al. (in press). With this new, directly dated ice thinning and retreat, I test whether exposure to strong marine influence drove southwestern Greenland ice contraction during the last deglaciation.

1.2.3. The late Holocene southwestern GrIS

Following early to mid-Holocene retreat inland of the present ice margin, the southwestern GrIS once again advanced during the late Holocene (Simpson et al., 2009; Alley et al., 2010; Funder et al., 2011). Across much of the high-latitude northern hemisphere, cool late Holocene temperatures reached a minimum during the Little Ice Age (LIA, Figure 1-1), generally between 600 and 100 years ago (Mann et al., 2009; Funder et al., 2011; Marcott et al., 2013). This cooling was accompanied by glacial advance, in most cases to an ice margin extent that surpassed any previous late-Holocene advances (Grove, 2001). However, the Narsarsuaq moraine in southernmost Greenland is suggested to be late Holocene age (Bennike and Sparrenbom, 2007) but is ice-distal of the local LIA moraine.

In Chapter IV, I use ^{10}Be surface exposure dating to determine if the Narsarsuaq moraine of the Kiagtût sermiat outlet glacier is indeed late Holocene in age. If this southernmost Greenland outlet glacier responded more strongly to a late-Holocene forcing than to general

northern hemisphere LIA cooling, it would support the hypothesis that southern Greenland temperature trends were different from the hemispheric average (Mann et al., 2009).

1.3. Summary

In this dissertation, I discuss data documenting GrIS retreat on three different time scales and under three different forcing conditions. Content in Chapter II examines the evidence for early deglacial behavior of the southwestern GrIS, while its margin rested on the continental shelf. Chapter III surveys the late deglacial chronology of southwest GrIS withdrawal onto the modern coastline, examining ice margins experiencing strong and weak direct marine influence. Chapter IV focuses on the late-Holocene moraine abandonment of a land-terminating outlet glacier in southernmost Greenland and its relation to late-Holocene spatial climate variability. A conclusion summarizing the main findings of these studies and discussing implications for our understanding of GrIS retreat composes Chapter V.

References:

- Alley, R.B., Andrews, J.T., Brigham-Grette, J., Clarke, G.K.C., Cuffey, K.M., Fitzpatrick, J.J., Funder, S., Marshall, S.J., Miller, G.H., Mitrovica, J.X., Muhs, D.R., Otto-Bliesner, B.L., Polyak, L., White, J.W.C., 2010. History of the Greenland Ice Sheet: paleoclimatic insights. *Quaternary Science Reviews*, 29, 1728-1756.
- Balco, G., 2011. Contributions and unrealized potential contributions of cosmogenic-nuclide exposure dating to glacier chronology, 1990-2010. *Quaternary Science Reviews*, 30, 3-27.
- Bennike, O., and Sparrenbom, C.J., 2007. Dating of the Narssarsuaq stade in southern Greenland. *The Holocene*, 17, 279-282.
- Berger, A., and Loutre, M.F., 1991. Insolation values for the climate of the last 10 million years. *Quaternary Science Reviews*, 10, 297-317.
- Carlson, A.E., Winsor, K., Ullman, D.J., Brook, E., Rood, D.H., Axford, Y., LeGrande, A.N., Anslow, F., and Sinclair, G., Earliest Holocene south Greenland ice-sheet retreat within its late-Holocene extent. In press at *Geophysical Research Letters*.
- Church, J.A., Clark, P.U., Cazenave, A., Gregory, J.M., Jevrejeva, S., Levermann, A., Merrifield, M.A., Milne, G.A., Nerem, R.S., Nunn, P.D., Payne, A.J., Pfeffer, W.T., Stammer, D., Unnikrishnan, A.S., and others, 2013. Sea level change: Working Group I Contribution to the Intergovernmental Panel on Climate Change, Fifth Assessment Report, 1137-1216.
- Dahl-Jensen, D., Mosegaard, K., Gundestrup, N., Clow, G.D., Johnsen, S.J., Hansen, A.W., and Balling, N., 1998. Past temperatures directly from the Greenland ice sheet. *Science*, 282, 268-271.
- Funder, S., Kjeldsen, K.K., Kjær, K.H., and Ó Cofaigh, C., 2011. The Greenland Ice Sheet during the past 300,000 years: a review: In Ehlers, J., Gibbard, P.L., and Highes, P.D. (eds), *Developments in Quaternary Science*, 15, Amsterdam, The Netherlands, 699-713.
- Grootes, P.M., and Stuiver, M., 1997. Oxygen 18/16 variability in Greenland snow and ice with 10³ to 10⁵-year time resolution. *Journal of Geophysical Research*, 102, 26455-26470.
- Grove, J.M., 2001. The initiation of the 'Little Ice Age' in regions round the North Atlantic. *Climatic Change*, 48, 53-82.
- Holland, D.M., Thomas, R.H., De Young, B., Ribergaard, M.H., and Lyberth, B., 2008. Acceleration of Jakobshavn Isbræ triggered by warm subsurface ocean waters. *Nature Geoscience*, 1, 659-664

- Joughin, I., Alley, R.B., and Holland, D.M., 2012. Ice-sheet response to oceanic forcing. *Science*, 338, 1172-1176.
- Joughin, I., Smith, B.E., and Medley, B., 2014. Marine ice sheet collapse potentially under way for the Thwaites Glacier Basin, West Antarctica: *Science*, 344, 735-738.
- Kelly, M., 1985. A review of the Quaternary geology of western Greenland. *In* Andrews, J.T. (ed.): *Quaternary Environments Eastern Canadian Arctic, Baffin Bay and Western Greenland*, Allen & Unwin, Boston, USA, 461-501.
- Knutz, P. C., Sicre, M.-A., Ebbesen, H., Christiansen, S., and Kuijpers, A., 2011. Multiple-stage deglacial retreat of the southern Greenland Ice Sheet linked with Irminger Current warm water transport: *Paleoceanography*, 26, PA3204, doi:10.1029/2010PA002053.
- Larsen, N.K., Funder, S., Kjær, K.H., Kjeldsen, K.K., Knudsen, M.F., Linge, H., 2014. Rapid early Holocene ice retreat in West Greenland. *Quaternary Science Reviews*, in press, <http://dx.doi.org/10.1016/j.quascirev.2013.05.027>.
- Levy, L.B., Kelly, M.A., Howley, J.A., Virginia, R.A., 2012. Age of the Ørkendalen moraines, Kangerlussuaq, Greenland: constraints on the extent of the southwestern margin of the Greenland Ice Sheet during the Holocene. *Quaternary Science Reviews*, 52, 1-5.
- Marcott, S.A., Shakun, J.D., Clark, P.U., and Mix, A.C., 2013. A reconstruction of regional and global temperature for the past 11,300 years. *Science*, 339, 1198-1201.
- Murray, T., Scharrer, K., James, T.D., Dye, S.R., Hanna, E., Booth, A.D., Selmes, N., Luckman, A., Hughes, A.L.C., Cook, S., Huybrechts, P., 2010. Ocean regulation hypothesis for glacier dynamics in southeast Greenland and implications for ice sheet mass changes: *Journal of Geophysical Research*, 115, F03026, doi:10.1029/2009JF001522.
- Ó Cofaigh, Andrews, J.T., Jennings, A.E., Dowdeswell, J.A., Hogan, K.A., Kilfeather, A.A., and Sheldon, C., 2013. Glacimarine lithofacies, provenance and depositional processes on a West Greenland trough-mouth fan. *Journal of Quaternary Science*, 28, 13-26.
- Rashid, H., and Piper, D.J.W., 2007. The extent of ice on the continental shelf off Hudson Strait during Heinrich events 1-3. *Canadian Journal of Earth Sciences*, 44, 1537-1549.
- Rasmussen, S.O., Seierstad, I.K., Andersen, K.K., Bigler, M., Dahl-Jensen, D., and Johnsen, S.J., 2008. Synchronization of the NGRIP, GRIP, and GISP2 ice cores across MIS 2 and palaeoclimatic implications. *Quaternary Science Reviews*, 27, 18-28.
- Reyes, A.V., Carlson, A.E., Beard, B.L., Hatfield, R.G., Stoner, J.S., Winsor, K., Welke, W., and Ullman, D.J., 2014. South Greenland ice-sheet collapse during Marine Isotope Stage 11. *Nature*, 510, 525-528.

- Rignot, E., and Thomas, R.H., 2002. Mass balance of polar ice sheets. *Science*, 297, 1502-1506.
- Rignot, E., Koppes, M., Velicogna, I., 2010. Rapid submarine melting of the calving faces of West Greenland glaciers: *Nature Geoscience*, v. 3, p. 187-191.
- Simpson, J.R.M., Milne, G.A., Huybrechts, P., and Long, A.J., 2009. Calibrating a glaciological model of the Greenland ice sheet from the Last Glacial Maximum to present-day using field observations of relative sea level and ice extent. *Quaternary Science Reviews*, 28, 1630-1656.
- Sole, A., Payne, T., Bamber, J., Nienow, P., and Krabill, W., 2008. Testing hypotheses of the cause of peripheral thinning of the Greenland ice sheet: is land-terminating ice thinning at anomalously high rates? *Cryosphere*, 2, 205-218.
- Straneo, F., and Heimbach, P., 2013. North Atlantic warming and the retreat of Greenland's outlet glaciers. *Nature*, 504, 36-43.
- Straneo, F., Hamilton, G.S., Sutherland, D.A., Stearns, L.A., Davidson, F., Hammil, M.O., Stenson, G.B., and Rosing-Asvid, A., 2010. Rapid circulation of warm subtropical waters in a major glacial fjord in East Greenland. *Nature Geoscience*, 3, 182-186.
- Svensson, A., Andersen, K.K., Bigler, M., Clausen, H.B., Dahl-Jensen, D., Davies, S.M., Johnsen, S.J., Muscheler, R., Parrenin, F., Rasmussen, S.O., Röthlisberger, R., Seierstad, I., Steffensen, J.P., and Vinther, B.M., 2008. A 60 000 year Greenland stratigraphic ice core chronology: *Climate of the Past*, 4, 47-57.
- Winsor, K., Carlson, A.E., Klinkhammer, G.P., Stoner, J.S., and Hatfield, R.G., 2012. Evolution of the northeast Labrador Sea during the last interglaciation: *Geochemistry, Geophysics, Geosystems*, 13, doi:10.1029/2012GC004263.

Figure Captions:

Figure 1-1. Paleoclimate context of southwestern Greenland ice retreat during the Holocene and latest Pleistocene. A) Boreal June insolation at 60°N (Berger and Loutre, 1991), B) eustatic sea level (Clark et al., 2009; 2012), C) GISP2 ice core $\delta^{18}\text{O}$ (Grootes and Stuiver, 1997), and D) Labrador Sea Mg/Ca-derived near-surface calcification temperatures using *Neogloboquadrina pachyderma* (sinistral) (Winsor et al., 2012). Vertical bars indicate, from left to right: the Last Glacial Maximum (LGM, Clark et al., 2009), Heinrich event 1 (H1, Rashid and Piper, 2007), the Younger Dryas cold period (YD, Svensson et al., 2008), and the Little Ice Age (LIA, Marcott et al., 2013).

Figure 1-2. Mechanisms of sediment delivery to the lower Greenland rise—the location of sediment core HU87033-008—when the ice margin attains a shelf-break position. Sediment transport mechanisms include ice-rafting, debris flows, and meltwater plumes. Warm surface currents ablate the ice margin. Modified from Reyes et al. (2014).

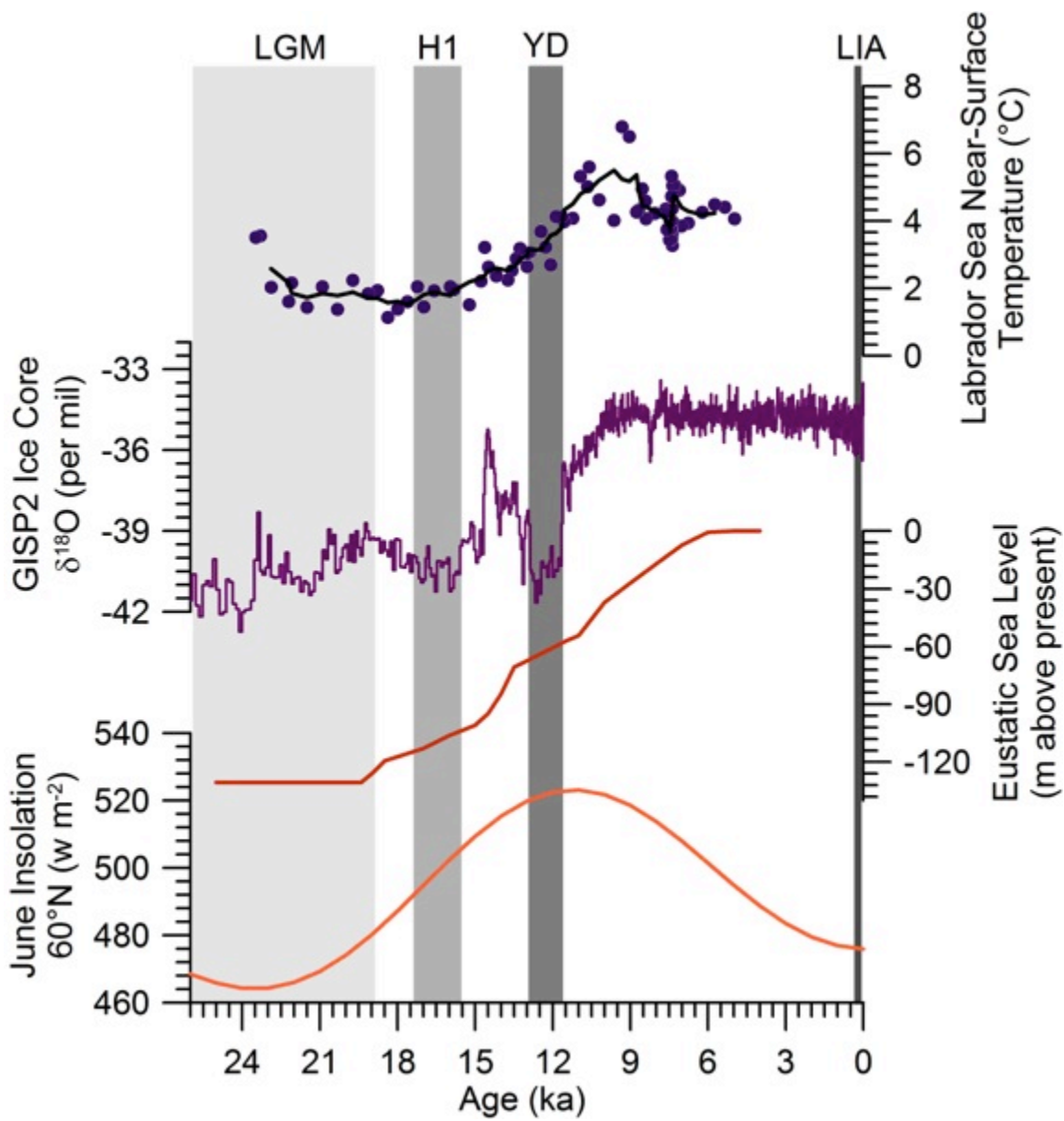


Figure 1-1.

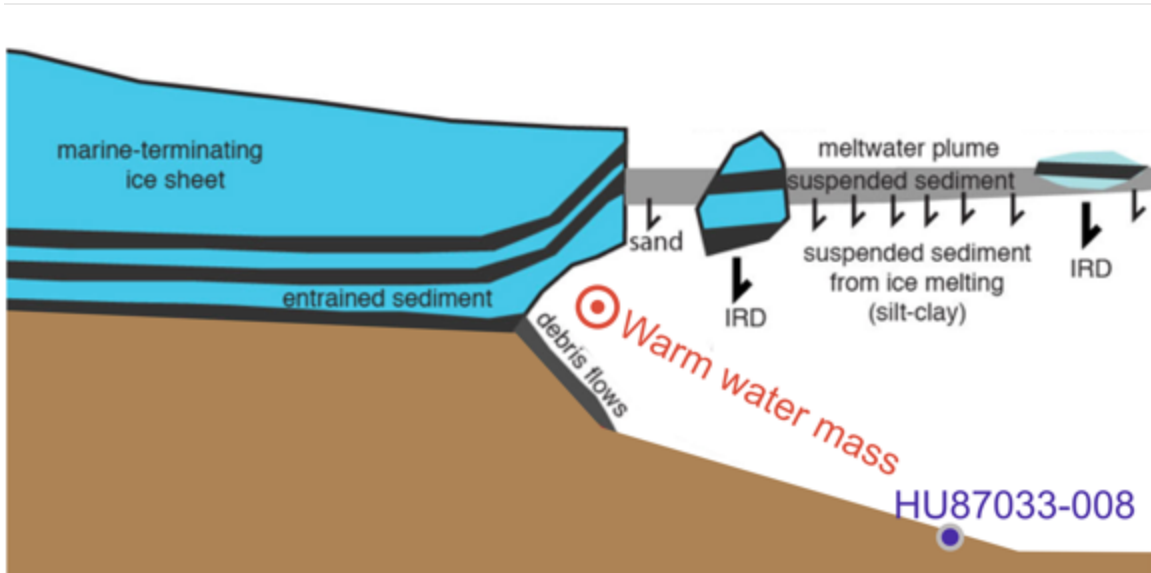


Figure 1-2.

CHAPTER II:
EARLY DEGLACIAL ONSET OF SOUTHWESTERN GREENLAND ICE-SHEET RETREAT ON THE
CONTINENTAL SHELF

Kelsey Winsor¹
Anders E. Carlson^{1,2}
Bethany Welke¹
Brendan Reilly²

¹Department of Geoscience, University of Wisconsin, Madison, WI, 53706, USA

²College of Earth, Ocean, and Atmospheric Sciences, Oregon State University, Corvallis, OR,
97331, USA

³Department of Geosciences, University of Arizona, Tucson, Arizona, 85721, USA

This manuscript will be submitted to *Quaternary Science Reviews*, and is formatted to fit the specifications of that journal.

Abstract

The Greenland ice sheet (GrIS) advanced onto the continental shelf during the last glacial period. While deglacial records for when the GrIS withdrew onto the modern coastline are relatively abundant, the timing of early GrIS retreat on the shelf is poorly constrained. Here we use planktic foraminiferal $\delta^{18}\text{O}$, sediment grain size, sedimentation rates, and ^{14}C ages in southeast Davis Strait core HU87033-008 to develop an early deglaciation chronology of the southwestern GrIS on the continental shelf. Sedimentation rates, and especially silt and clay fluxes, are high between ~ 20.5 and ~ 17.1 ka, suggesting that the GrIS margin was near or at the shelf break, where it released subglacially derived sediment-laden meltwater. A peak in sedimentation rates of ~ 110 cm ka^{-1} between ~ 19.3 ka and ~ 18.6 ka, combined with an initial decrease in planktic $\delta^{18}\text{O}$ of ~ 0.5 per mil, suggests an initial pull back of the GrIS margin from the shelf break with a concurrent increase in surface ocean meltwater discharge. A subsequent planktic $\delta^{18}\text{O}$ decrease of ~ 1.0 per mil combined with a drop in silt and clay sedimentation rates 18-17 ka likely record further GrIS retreat to the middle or inner continental shelf, where terrestrial ^{10}Be surface exposure ages indicate that the GrIS margin remained until ~ 11 ka. Our new records provide the first evidence that the southwestern GrIS margin may have begun to deglaciate at the same time as other Northern Hemisphere ice sheets. Because Labrador Sea water temperatures likely remained near glacial values until after 17 ka, we suggest that initial southwestern GrIS retreat was in response to rising global sea level from retreat of other ice sheets and/or the initial deglacial rise in boreal summer insolation.

2.1. Introduction

Constraints on retreat of the Greenland ice sheet (GrIS) once its margins retracted to the modern ice-free land suggest that much of the terrestrial GrIS deglaciation occurred in the early Holocene (see Funder et al., 2011 for a review). The record of earlier deglaciation when the ice margin rested on the Greenland continental shelf is understandably more limited. Where the shelf is narrow, for example in southern Greenland, the last glacial maximum (LGM, 26-19 ka; Clark et al., 2009) GrIS is generally thought to have extended to the shelf break (e.g., Sommerhoff, 1981; Kelly, 1985; Bennike et al., 2002; Jennings et al., 2006; Simpson et al., 2009; Funder et al., 2011). In regions with a wider shelf, interpretations vary as to the GrIS presence on the shelf break, outer shelf, or inner shelf (e.g., Kelly, 1985; Ó Cofaigh et al., 2004; 2012; 2013; Weidick and Bennike, 2007; Evans et al., 2009; Roberts et al., 2009; Funder et al., 2011; Simon et al., 2013).

Because the GrIS extended onto the shelf during the LGM, the initial timing of ice retreat is difficult to constrain with terrestrial records (Funder et al., 2011) and those that exist suggest a significant lag in GrIS retreat behind rising boreal summer insolation, rising atmospheric greenhouse gas concentrations, and other Northern Hemisphere ice sheets (Clark et al., 2009; 2012). Such a lag could suggest a limited sensitivity of GrIS margins to deglacial climate warming and sea-level rise (Clark et al., 2009). However, ^{10}Be surface exposure ages from west Greenland at $\sim 67^\circ\text{N}$ suggest initial GrIS thinning by 19-18 ka (Rinterknecht et al., 2009; Roberts et al., 2009; Winsor et al., in review). Continental rise sediment records from eastern and southern Greenland show ice retreat commencing by 19-17 ka and ~ 19 ka, respectively (Nam et al., 1995; Andrews et al., 1997; Carlson et al., 2008). In contrast, west Greenland ice streams at $\sim 70^\circ\text{N}$ may have remained near the shelf break until 15-14 ka (Ó Cofaigh et al., 2012; 2013; Simon et al., 2013). Elsewhere on Greenland, our understanding of initial GrIS margin retreat on

the continental shelf is even more restricted. Here, we analyze grain size and sedimentation rates in southeastern Davis Strait sediment core HU87033-008 (Fig. 1A) to constrain the timing of southwestern GrIS presence on the outer shelf. We couple this sediment data with oxygen isotope analyses from the sub-polar to polar planktic foraminifera species *Neogloboquadrina pachyderma* (sinistral) to identify potential near-surface meltwater dilution.

2.2. Regional Setting

2.2.1. Core HU87033-008

Core HU87033-008 was taken by the *CSS Hudson* with a long coring facility in September, 1987 in the southeastern Davis Strait. Located at 62.65°N and 53.88°W, the core was retrieved from 2424 m water depth along the slope from the Labrador Basin to Davis Strait (Fig. 1A), with ~95 percent recovery (Vilks and Powell, 1987). The HU87033-008 site is near core DA04-31P of Knutz et al. (2011) (Fig. 1B). A summary of the shipboard core description is as follows: The upper 11 cm of the core are a dark gray silty mud, with a portion of the core from 0-6 cm being olive gray in color. From 11-128 cm, the core is generally very dark gray, silty mud with mottling and some mm-scale clay clumps. Numerous mm-scale, grayish brown carbonate clasts were observed at 73-86 cm. From 128-253 cm, core material is highly bioturbated, though continues to be a very dark gray, silty clay. For the remainder of our sampling intervals (until 308 cm), the core is of the same color and composition, though scattered sand grains were observed. Mottling was recorded more frequently below 253 cm. Hillaire-Marcel and de Vernal (1989) describe this core and others nearby as being composed chiefly of hemipelagic mud with large amounts of ice-rafted debris (IRD).

2.2.2. Modern and Paleo Hydrography

The Labrador Sea is located south of the Davis Strait, between the northeastern coast of Canada and the southwestern coast of Greenland (Fig 1A). Hydrography of the Labrador Sea is of interest to this study in that it determines the source region for sediments deposited at a given site. Major surface currents enter the area from the westward-flowing arm of the subpolar gyre, and are composed of both Arctic- and Atlantic-sourced waters. Arctic-sourced waters pass through the Fram and Denmark Straits in the East Greenland Current, skirting the Greenland shelf. From the south, the North Atlantic Current delivers relatively warm, saline waters to the Irminger Current, which flows northwest past Iceland and toward southern Greenland (Fig. 1A). Near Cape Farwell, Irminger Water and the East Greenland Current are directed into the West Greenland Current (Coachman and Aagaard, 1974; Cuny et al., 2005).

In the eastern Davis Strait, the West Greenland Current bifurcates into northward and westward components (Cuny et al., 2002). Here, the separation of the Arctic-sourced waters from Baffin Bay and the subtropical-sourced waters carried by the West Greenland Current marks the thermohaline front. Maximum seasonal sea ice extent in the area is approximately at this thermohaline front (Fenty and Heimback, 2013). The westward-flowing segment of the West Greenland Current and the southward-flowing Baffin Island Current mix in the western Davis Strait, forming the surface component of the Labrador Current. The Labrador Current then travels south along the eastern Canadian shelf (Mudie et al., 1984). Thus, ice and runoff entering the Labrador Sea from terrestrial North America are brought southward, as opposed to eastward towards core site HU87033-008.

Below these surface currents, the modern Deep Western Boundary Current passes nearby to, but at lower depth than, our core site, with its main high velocity core at approximately 2800-

3400 m water depth (Fagel et al., 2001; Cuny et al., 2002). At our core site, Labrador Sea Water occupies the water column below the variable-depth surface mixed layer and above Northeast Atlantic Deep Water (Bilodeau et al., 1994). Although Labrador Sea Water possesses relatively low velocity (Dickson and Brown, 1994), it composes part of a recirculation loop of waters from the Labrador Sea, into the Irminger Sea, and back to the Labrador Basin. In the winter, wind-driven cooling and buoyancy loss of Labrador Sea surface waters permit deep overturning circulation in the Labrador Basin (Marshall and Schott, 1999) and formation of Labrador Sea Water. The water column is re-stratified by summertime, with buoyancy gain derived from influx of warm Irminger Water (Cuny et al., 2002). Combined with convection and deep-water formation in the Nordic Seas, Labrador Sea overturning is a primary driver of the strength of Atlantic meridional overturning circulation (e.g., Broecker, 1997; Hillaire-Marcel and Bilodeau, 2000).

At the LGM, deep-water circulation in the Labrador Sea persisted (Ledbetter and Balsam, 1985), though at lower velocities than during present, and with less recirculation outside of the Labrador Basin (Fagel et al., 1999). During the last deglaciation, Deep Western Boundary Undercurrent velocity increased reaching a maximum by ~11 ka (Fagel et al., 1997; 1999). The presence of a circulating Deep Western Boundary Current suggests that the Labrador Current also continued transporting water and ice from North America southward away from our study site (Kirby, 1998). However, sediment from Hudson Strait discharged during Heinrich events of the Laurentide ice sheet were transported to continental rise west of Greenland (Hillaire-Marcel et al., 1994; Fagel et al., 2001).

2.3. Methods

2.3.1. Core Sampling and Grain Size Analysis

We collected sediment from the working half of HU87033-008, kept in ambient storage at the Bedford Institute of Oceanography. Where possible, we sampled at five-cm intervals, avoiding obvious burrows, to a core depth of 308 cm. At the University of Wisconsin-Madison, samples were dried at 30-40°C, then weighed. We wet-sieved each sample to 63 μm using dilute Calgon in deionized water. We then separated the silt (greater than $\sim 5 \mu\text{m}$ for this procedure) from clay using Stoke's Law and timed settling in tubes with deionized water. The silt fraction was dried and weighed, with the residual mass of the total sample being attributed to the clay fraction (Fig. 2B). Accumulation rates of sediment were approximated by linear interpolation between radiocarbon tie points (see below) (Table 1; Fig. 2A). We note that these accumulation rates are uncorrected for sediment density. Density data were not recorded when the core was recovered and the ambient storage of the core precludes the required precise volume measurement of a sample. Weight percentages of sand, silt, and clay (Table S1) were converted to approximate sediment fluxes (e.g., cm of sand accumulated per ka) by multiplying the total uncorrected accumulation rate by each weight percentage.

2.3.2. Radiocarbon Dating

Nine intervals were sampled for radiocarbon dating of planktic foraminifera (Table 1). The core top of the trigger weight core, HU87033-008TWC, was also sampled for dating. Depending on the species assemblage of the sample, a combination of primarily *Neogloboquadrina pachyderma* (sinistral), *N. pachyderma* (dextral), and *Globigerina bulloides* specimens were picked. Radiocarbon analyses were performed at the National Ocean Sciences AMS (NOSAMS) Facility at Woods Hole Oceanographic Institution, using the NBS Oxalic Acid

1 standard and 5568-year half-life (Stuiver and Polach, 1977). Radiocarbon ages were converted to calendar ages using the online Calib7.0 calculator and the Marine04 curve (Stuiver and Reimer, 1993; Stuiver et al., 2005; Table 1). A marine reservoir age of 400 years (ΔR of 0) for all samples was chosen for our initial calculation of calendar years (Fig. 2A). We then recalculated our LGM through deglacial-aged samples ($n=8$) with a marine reservoir age of 600 years (ΔR of 200 years), as performed by Knutz et al. (2011) and others (e.g., Bondevik et al., 2006; Franke et al., 2008). While we use dates calibrated with a 200 year ΔR for our interpretations and discussions, we also calibrated our LGM and deglacial ages with a marine reservoir of 1000 years (ΔR of 600 years) to represent a maximum uncertainty in our ages resulting from high meltwater flux, increased water column stratification, and reduced ventilation (Fig. 2A; Waelbroeck et al., 2001; Knutz et al., 2011). In discussing our ^{14}C data, we refer to the mean probability of the age ranges accompanied by two-sigma standard deviation (Table 1).

2.3.3. Oxygen Isotope Analyses

All intervals possessing sufficient numbers of *N. pachyderma* (s) ($n=44$) were analyzed for $\delta^{18}\text{O}$ (Table S1). Approximately 30 individual *N. pachyderma* (s) tests were picked from the 150-250 μm size fraction for each analysis (Fig. 2C). Foraminifera were not chemically cleaned prior to stable isotope analysis, though samples were chosen for their clean appearance under a light microscope. Stable isotope analyses were performed at the Oregon State University Stable Isotope Laboratory with a Kiel III preparation device and MAT 252 mass spectrometer. Uncertainty on these analyses is 0.05 per mil. We also use $\delta^{18}\text{O}$ from 12 intervals that were published in Hillaire-Marcel et al. (1994) (Table S1).

2.3.4. Magnetic Susceptibility

Uncorrected magnetic susceptibility measurements from the HU87033 cruise report were digitized (Vilks and Powell, 1987) using Digitizeit software (Fig. 3A). Only uncorrected magnetic susceptibilities were available, and we thus discourage the analysis of long-term trends in the magnetic susceptibility data that could be influenced by instrument drift. Measurements were performed shipboard at three-cm resolution using a Barrington Instruments sensor and meter, with a Data General DG-1 computer (Vilks and Powell, 1987). Magnetic susceptibility data were reported in 10^{-6} dimensionless cgs units, which we convert to SI units. We discourage the analysis of long-term trends in the magnetic susceptibility data that could be influenced by instrument drift.

2.4. Results

2.4.1. Core Chronology

With the exception of a single sample at the 116 cm interval of 15.9 ± 0.1 ka that we exclude from our age model, all ^{14}C dates are in stratigraphic order (Table 1; Fig 2A). The sample with the oldest calibrated age dates to 20.1 ± 0.1 ka (287 cm depth), and is followed by five samples from the early deglaciation extending to 16.3 ± 0.1 ka (76 cm depth). A sample at 58 cm depth has an age of 11.4 ± 0.1 ka while another sample from 11 cm depth is from 9.4 ± 0.1 ka. We also dated the core top of the adjacent trigger core, HU87033-008TWC, which is 3.6 ± 0.1 ka. Our age model for core HU87033-008 is based on the eight stratigraphically consistent samples. We linearly interpolate between each of these ^{14}C tie-points, with short extrapolations prior to the oldest age, and after the youngest age (Fig. 2A). Hillaire-Marcel et al. (1994) dated

one *N. pachyderma* (s) sample from 150 cm depth with an age of ~ 14.8 ^{14}C ka (no uncertainty provided), which is close to being in stratigraphic order with our ^{14}C ages.

2.4.2. Grain Size and Sedimentation Rate

The grain size distribution in the upper 308 cm of HU87033-008 shows an abrupt change in weight percent sand and clay between 86 and 76 cm (Fig. 2A). Between 308 and 86 cm, sand remains at or below ~ 11 percent of the total sample weight, though it never reaches zero percent. Silt composes 45-55 weight percent, and clay generally composes 40-55 weight percent. Between 118 and 96 cm, clay increases to a peak of ~ 57 percent. Silt percentage increases again above ~ 45 percent by 76 cm, and then remains at 45-55 percent until the top of the core. Clay percentage decreases following the peak at 96 cm, reaching 25-35 percent by 76 cm and staying at these levels for the remainder of the core. Starting at 86 cm, sand increases above ~ 10 percent to 17-25 percent for most of the remaining sample intervals. At the top of the core (21 to 1 cm), sand percentage varies with an amplitude of greater than ~ 20 percent.

Calculated sedimentation rates (Fig. 3E) vary between ~ 4 cm ka^{-1} and ~ 110 cm ka^{-1} . Rates are high (~ 50 cm ka^{-1}) between 20.5 and 19.3, rise to a peak of ~ 110 cm ka^{-1} until ~ 18.6 ka, then return to average values of ~ 60 cm ka^{-1} until ~ 18.1 ka. Between ~ 18.1 ka and ~ 17.1 ka, sedimentation rates decrease to ~ 40 cm ka^{-1} . Rates decrease again to ~ 25 cm ka^{-1} by ~ 16.3 ka. At this point, sedimentation rates drop to a low of ~ 4 cm ka^{-1} for the next ~ 5 ka, until they increase to ~ 20 cm ka^{-1} by ~ 11.4 ka, where they remain until at least ~ 9.4 ka.

Assuming a constant density due to the lack of shipboard density measurements, changes in the flux of sand, silt, and clay can be broadly estimated by the overall changes in sedimentation rate and the concentration of each grain size (Fig. 3B-D). Fluxes for silt and clay

are $\sim 25 \text{ cm ka}^{-1}$ during the LGM and then increase to $50\text{-}60 \text{ cm ka}^{-1}$ at $\sim 19.3 \text{ ka}$, where they remain until the next ^{14}C age control at $\sim 18.6 \text{ ka}$. During this interval, silt flux is $5\text{-}15 \text{ cm ka}^{-1}$ greater than the clay flux. After $\sim 18.6 \text{ ka}$, silt and clay fluxes decrease to $\sim 10 \text{ cm ka}^{-1}$ by $\sim 16.3 \text{ ka}$. Between the LGM and $\sim 16.3 \text{ ka}$, sand flux generally remains $2\text{-}6 \text{ cm ka}^{-1}$. Between $\sim 16.3 \text{ ka}$ and $\sim 11.4 \text{ ka}$, sand, silt, and clay fluxes all markedly decrease, along with total sedimentation rates. After $\sim 11.4 \text{ ka}$, sand flux increases to $2\text{-}7 \text{ cm ka}^{-1}$, silt flux rises to $\sim 10 \text{ cm ka}^{-1}$, and clay flux increase to $7\text{-}10 \text{ cm ka}^{-1}$.

2.4.3. Oxygen Isotopes

N. pachyderma (s) $\delta^{18}\text{O}$ values are ~ 4.5 per mil during the LGM until $\sim 18.6 \text{ ka}$ when they decrease by ~ 0.5 per mil (Fig. 3F). A second decrease of ~ 0.9 per mil to ~ 3.1 per mil occurs by $\sim 17.6 \text{ ka}$. For the remainder of the core, $\delta^{18}\text{O}$ varies between ~ 2.6 per mil and ~ 3.4 per mil.

2.4.4. Magnetic Susceptibility

Although our magnetic susceptibility measurements may be impacted by instrument drift or sensitivity, we note three large-scale, non-trending features (Fig. 3A). Magnetic susceptibility is variable between $\sim 20.5 \text{ ka}$ and 17.4 ka , but decreases to a low between $\sim 17.4 \text{ ka}$ and $\sim 15.7 \text{ ka}$. Magnetic susceptibility then increases and is relatively constant to the top of the core. The low in magnetic susceptibility $17.4\text{-}15.7 \text{ ka}$ contains brown carbonate clasts that are linked to iceberg and sediment discharge from the Laurentide Ice Sheet through Hudson Strait, which suggests this sediment interval is recording Heinrich event 1 (Vilks and Powell, 1987; Hillaire-Marcel et al., 1994; Stoner et al., 1994; Knutz et al., 2011).

2.5. Discussion

2.5.1. Interpretation of Sediment Changes

Despite indications of bioturbation (Vilks and Powell, 1987), several lines of evidence suggest minimal attenuation of our observed paleoenvironmental signal. The rapid decrease in planktic $\delta^{18}\text{O}$ between ~ 18.6 ka and 17.6 ka (Fig. 3F) covers the majority of the glacial-interglacial change in planktic foraminiferal $\delta^{18}\text{O}$ in Labrador Sea cores (e.g., Hillaire-Marcel et al., 1994). If sediment column mixing had affected our $\delta^{18}\text{O}$ record, we would expect the glacial-interglacial change to be muted, particularly across the primary change in $\delta^{18}\text{O}$. Perhaps more convincing, we calculate very rapid sedimentation rates (>40 cm ka^{-1}) for the core between ~ 20.5 ka and ~ 17.1 ka (Fig. 3E), thus limiting the mixing capacity of burrowing organisms, even with decimeter-scale sea floor penetration. Additionally, we date Heinrich event 1 at the same time as the detrital carbonate event is recorded elsewhere in the Labrador Sea (Hillaire-Marcel et al., 1994; Stoner et al., 1994; Carlson et al., 2008), suggesting our core chronology is not significantly impacted by bioturbation.

Therefore, assuming minimal influence of bioturbation on the stratigraphic integrity of our record, the most marked changes in sedimentation rate and silt, clay, and sand fluxes in core HU87033-008 are: a) overall elevated sedimentation rates between ~ 21 and ~ 17 ka; b) an interval of high (~ 110 cm ka^{-1}) sedimentation and silt/clay flux between ~ 19.3 and 18.6 ka; c) a prolonged interval of apparently very low sedimentation (~ 4 cm ka^{-1}) and silt/clay flux between ~ 16.3 and 11.4 ka; and d) the subsequent partial recovery of sedimentation rates between ~ 11.4 ka and the top of the core (Fig. 2, 3). The primary mechanisms that bring silt and clay to the northern Labrador Sea are ice-rafting (Rashid and Piper, 2007), debris flows (Hesse et al., 2004; Andrews et al., 2012), transport in ice-proximal meltwater plumes (Andrews, 2000), and

suspension in boundary currents (Fagel et al., 1997; 2001; Carlson et al., 2008; Colville et al., 2011). No evidence for turbidite sequences was reported in the core description (Vilks and Powell, 1987), nor were any turbidite sequences observed in nearby core DA04-31P (Fig. 1B) (Knutz et al., 2011). Furthermore, the coherence of our ^{14}C dates (Fig. 2A, Table 1) argues against an influx of much older sediments (greater than 1-2 ka) that formed layers on a greater than centimeter-scale. Therefore, while we acknowledge that the fine-grained tails of turbidity currents are not obvious and may contribute to our data (McCave and Hall, 2006), we suggest that much of the terrigenous sediment was transported to the core site by iceberg rafting, ice-proximal meltwater plumes, and boundary currents.

Iceberg-rafting to core site HU87033-008 would have been controlled by sea ice extent and seasonality (e.g., Hillaire-Marcel and de Vernal, 1989), the position of the GrIS relative to the continental slope (Dowdeswell et al., 1995; Syvitski et al, 1996; Hemming et al, 2002; Jullien et al., 1996), surface water temperatures, (Syvitski et al. 1996; Andrews, 2000; Knutz et al., 2011), and sediment distribution within calved icebergs (Andrews, 2000). Because of the core site's location near the continental slope (Fig. 1B), calving of the GrIS margin likely would have been the main contributor of IRD to HU87033-008 through the LGM and deglaciation (Andrews, 2000), explaining the persistent, though low-magnitude, deposition of sand-sized grains at a relatively constant flux (Fig. 3D).

During the LGM, Deep Western Boundary Undercurrent velocity was slower relative to modern, but generally increased through the deglaciation to peak flow in the early Holocene (Fagel et al., 1997; 1999; 2001). With an increase in velocity came an increase in sediment supply sourced from the Irminger and Iceland Seas, and an increase in the influence of Iceland and East Greenland terrains on Labrador Sea sediments (Fagel et al., 2001). However, the

increase in undercurrent strength was gradual over ~10 ka (Fagel et al., 1997), and would not explain the rapid changes in sedimentation we observe early in the last deglaciation at HU87033-008. Similar abrupt sedimentological changes on the Eirik Ridge off of southern Greenland (Fig. 1A) also seem to be likely related to changes in GrIS sediment supply rather than the Deep Western Boundary Undercurrent (Stoner et al., 1995; Fagel et al., 2004; Carlson et al., 2008; Colville et al., 2011; Reyes et al., 2014). We therefore infer that the observed changes in sedimentation rate and in silt and clay flux were likely driven by changes in ice-margin proximity to the shelf break and to GrIS melting and sediment discharge (Andrews, 2000; Hesse et al., 2004; Andrews et al., 2012; Ó Cofaigh et al., 2013).

2.5.2. LGM and Early Deglacial Sedimentation

We attribute the overall elevated sedimentation rates before ~19.3 ka to the close proximity of the GrIS margin to the shelf break, where high silt and clay discharge to the core site occurred in meltwater plumes at depth. These plumes propagate from high-turbidity layers originating proximal to the grounding line, similar to those observed near modern tidewater glaciers (e.g. Domack and Ishman, 1993; Ashley and Smith, 2000). A meltwater origin is consistent with the sediments being structureless hemipelagic silts and clays (Dowdeswell and Cromack, 1991). The increase in sedimentation rate and silt and clay flux to a maximum between ~19.3 ka and ~18.6 ka could reflect either the maximum extent of the GrIS on the shelf (closest proximity to the core site) or the initiation of GrIS retreat (increased melting and sediment discharge) (Fig. 4E, 4F).

Planktic $\delta^{18}\text{O}$ begins to decrease at ~18.6 ka (Fig. 4D), which would be consistent with increased surface ocean meltwater discharge and would suggest the drop in silt and clay fluxes

by ~18.6 ka reflects the onset of GrIS retreat (Fig. 3B, C). Estimates of Labrador Sea temperatures indicate that near-surface water masses remained close to LGM temperatures during this period (Fig. 4C) (Winsor et al., 2012), suggesting the $\delta^{18}\text{O}$ decrease was driven by an increase in meltwater discharge and not ocean warming. The nearby sediment and $\delta^{18}\text{O}$ records of Knutz et al. (2011) (Fig. 1B) only extend back to ~17 ka, precluding comparison with our early deglaciation records. However, further south on the Eirik Drift (Fig. 1A), an increase in detrital sediment concentration at ~19 ka (Fig. 4G) (Carlson et al., 2008; Colville et al., 2011) is concurrent with the peak in deglacial sediment flux at HU87033-008. Likewise, ^{10}Be surface exposure ages on the western Greenland coast at ~67°N suggest GrIS thinning was underway by 19-18 ka (Rinterknecht et al., 2009; Roberts et al., 2009; Winsor et al., in review). These records therefore support our inference of southwest GrIS initial retreat back from the shelf break beginning by ~18.6 ka.

The further decrease in sedimentation rate and silt and clay flux after ~18.1 ka is concurrent with an abrupt decrease in $\delta^{18}\text{O}$ to near interglacial values (Fig. 4D). As Labrador Sea near-surface temperatures likely remained at glacial levels (Fig. 4C) (Winsor et al., 2012), we attribute the $\delta^{18}\text{O}$ decrease to an increase in meltwater discharge. We suggest that this transition reflects further GrIS margin retreat on the shelf, with attendant discharge of meltwater. Fallout from subglacial melt would have become more spatially restricted with a middle to inner shelf ice margin position (e.g., MacLean et al., 1991; Andrews, 2000; Simon et al., 2013). There, gravity-driven flow would not encounter the Labrador and Greenland down-slopes, but rather gentle and potentially uphill terrain. In glaciated shelf environments, more intense ice scouring of the inner shelf leads to deeper waters proximal to modern coastlines. This topography is compounded during periods of extended ice position due to isostatic depression. These processes

combine to form depocenters for glacially derived sediments, preferentially removing suspended particulate matter while permitting ice-rafted sediments to navigate to deeper waters off the shelf (e.g., Syvitski et al., 1996; Kirby et al., 1997; Andrews, 2000; Ó Cofaigh et al., 2013; Dowdeswell et al., 2013; Simon et al., 2013). This was observed in the Labrador Sea just to the east of the Canadian shelf, where sedimentation rates dropped with the initiation of deglaciation and pull-back of the ice margin from the shelf break (Kirby et al., 1997; Andrews, 2000). The reduction in sedimentation rate and silt and clay fluxes are therefore consistent with a sedimentation model placing the GrIS margin on the middle to inner shelf.

Following the initial deglacial sedimentary and $\delta^{18}\text{O}$ changes, magnetic susceptibility decreases to a low at ~ 17 ka (Fig. 3A), concurrent with deposition of detrital carbonate clasts (Vilks and Powell, 1987). Our timing of this low magnetic susceptibility, detrital carbonate layer in HU87033-008 is in excellent agreement with the detrital carbonate in nearby core DA04-31P, which is attributed to Heinrich event 1 (Knutz et al., 2011). Sedimentological evidence for deposition of Hudson Bay-sourced detrital carbonate during Heinrich events is well documented in the Labrador Sea (e.g., Andrews et al., 1991; 1994; 2012; 2014; Stoner et al., 1994; Hillaire-Marcel et al., 1994; Jennings et al., 1996; Hesse and Khodabakhsh, 1998; Rashid et al., 2003a; b; Hesse et al., 2004; Rashid and Piper, 2007). In the Labrador Sea, Heinrich event layers are also characterized by low magnetic susceptibility (Stoner et al., 1994).

Since Labrador Sea near-surface temperatures were at glacial levels prior to at least 15 ka (Fig. 4C) (Winsor et al., 2012), ocean warming was likely not the cause of initial southwest GrIS retreat from the shelf break. Likewise, Greenland ice core temperatures remained near LGM levels until after ~ 15 ka. We therefore hypothesize that early deglacial changes in sea level (Clark et al., 2004; 2009; 2012) (Fig. 4B) could have destabilized the ice margin on the

continental shelf, driving initial southwest GrIS retreat (Carlson et al., 2008), although the impact of such changes would depend on the ice-sheet source of the sea-level rise (Clark et al., 2002). Alternatively, or in addition, the southwest GrIS margins could have retreated at ~19 ka in response to the gradual rise in boreal summer insolation and attendant increase in incident shortwave radiation that began ~24 ka (Fig. 4A) (Carlson and Winsor, 2012). The increasing radiative forcing may have thinned the ice margin, causing it to eventually grow unstable at the shelf break. Regardless, our sedimentary record suggests southwest GrIS retreat onset concurrent with many other Northern Hemisphere ice sheets (Clark et al., 2009; Carlson and Winsor, 2012) as well as the southern and eastern GrIS margins (Nam et al., 1995; Andrews et al., 1997; Carlson et al., 2008; Rinterknecht et al., 2009; Roberts et al., 2009; Winsor et al., in review). In contrast, similar sedimentary records from the continental slope and rise off of west Greenland at ~70°N suggest the GrIS margin remained near at the shelf break until 15-14 ka (Ó Cofaigh et al., 2012; 2013), significantly lagging the onset of retreat of the southwestern GrIS margin. Ultimately, modeling of ice-sheet dynamics is required to understand the different deglacial behavior of the southwestern and western GrIS margins.

2.5.3. Mid- to Late-Deglacial Sedimentation

Above the Heinrich event 1 layer, sedimentation rates in HU87033-008 drop to an apparent average of ~4 cm ka⁻¹ from ~16.0 to ~11.4 ka (Fig. 4F). Due to the low sedimentation rate and paucity of planktic foraminifera during this period, we cannot resolve rapid or short-term changes in sedimentation rate or flux of the different grain sizes. Even so, our average accumulation rates differ considerably from the DA04-31P record to the west of our core, which

average $\sim 15 \text{ cm ka}^{-1}$ during this period (Knutz et al., 2011). We suggest several mechanisms to explain the low sedimentation rate at HU87033-008.

One possibility is that GrIS-discharged proximal sediments were somehow routed away from HU87033-008 but still reached DA04-31P. However, if the dominant sediment source to the site by $\sim 18 \text{ ka}$ was meltwater transport or iceberg rafting, the gentle seafloor topography (relief of less than several 100 m) between HU87033-008 and DA04-31P would likely not impact sediment transport between the two core sites. A second mechanism is that shifts in the Deep Western Boundary Undercurrent diverted sediments away from HU87033-008, but other records of the undercurrent do not support any abrupt changes (Fagel et al., 1997; 1999). A third possibility is that onset of undercurrent winnowing reduced the deposition of silts and sands. In that case, we would expect to observe higher sand weight percentages than during the bracketing time intervals, but we do not (Fig. 3B, C). Therefore, although no note of their presence was made in DA04-31P or HU87033-008 core descriptions, we submit that erosive processes have affected the core interval between 16.0 to 11.4 ka. We note that sedimentation rates before and after this interval are approximately equal, and that sand percentages very briefly reach values of 15-20 percent between 16.7 and 16.3 ka (Fig. 2), which is approximately where they remain until the top of the core. This offers support to apparent changes in sediment flux being a result of changes in erosion versus changes in sedimentation (Fig. 2).

The 16.7 to 11.4 ka rise in percentage of iceberg-rafted sands and decrease in percentages of clays and silts, which had previously been delivered chiefly by meltwater flows and plumes, suggests a middle- to inner-shelf position for the southwestern GrIS. By $\sim 11.4 \text{ ka}$, net sedimentation increases from a proposed hiatus, discussed above (Fig. 4F). A peak in terrigenous sediment concentration is concurrently observed on the Eirik Drift (Fig. 4G) (Carlson et al.,

2008; Colville et al., 2011). Coastal ^{10}Be surface exposure ages from Paamiut, Nuuk, Sarqarssuaq, and Sermilik—all near our core site (Fig. 1B)—indicate that the southwestern GrIS margin retreated onto the continent ~ 11 ka (Fig. 4H) (Larsen et al., 2014; Winsor et al., in review). This latest interval of southwest GrIS margin retreat is concurrent with warming of the Labrador Sea near-surface and surface temperatures towards their deglacial peak (Fig. 4C) (Solignac et al., 2004; Winsor et al., 2012). Given the likely persistence of the ice margin on the shelf until peak ocean temperatures were reached, we suggest that late deglacial ocean warming may have played an important role in driving the southwest GrIS margin off of the continental shelf.

2.6. Conclusions

We report a new suite of data from southeast Davis Strait core HU87033-008, including a high-resolution radiocarbon chronology for the early deglaciation, grain size analyses, and *N. pachyderma* (s) oxygen isotopes. We suggest a general retreat chronology for the southwestern GrIS from the shelf break to the coastline. The GrIS margin was either at or reached the continental shelf break during the LGM, with retreat commencing from the shelf break before ~ 18.6 ka. The ice margin probably occupied a middle- to inner-shelf position between ~ 16.7 ka and ~ 11 ka. A final stage of ice retreat, with the southwest GrIS margin withdrawing off of the shelf, occurred by ~ 11 ka as indicated by terrestrial data. Our record provides the first evidence for early initiation of southwestern GrIS retreat during the last deglaciation, concurrent with the retreat of other Northern Hemisphere ice sheets (Clark et al., 2009; Carlson and Winsor, 2012). We hypothesize that the initial retreat may have been in response to early deglacial sea-level changes and attendant destabilization of the marine ice margin, and/or due to rising boreal

summer insolation and consequent increase in incident shortwave radiation. The later retreat of the southwestern GrIS margin off of the continental shelf may have been partly driven by warming of the Labrador Sea. We thus suggest that marine-terminating GrIS margins may have responded rapidly to past small changes in oceanic conditions, such as grounding line depth, and also to potentially small increases in surface radiative forcing.

Acknowledgements

We would like to sincerely thank Kate Jarrett (Bedford Institute of Oceanography), who assisted tremendously in core sampling and retrieval of core information. We would also like to thank Elizabeth Siewert (University of Wisconsin-Madison) and Claude Hillaire-Marcel (GEOTOP) for assistance in sediment core sampling, the NOSAMS staff for radiocarbon dating, and June Padman, Andy Ross, and Jennifer McKay (Oregon State University) for stable isotope analyses. The crew and scientists of the *CSS Hudson* 87033 cruise, in particular C. Guilmette who collected magnetic susceptibility data, also deserve acknowledgement. Funds for this project were received from the National Science Foundation Graduate Research Fellowship Program (K.W.), the Geological Society of America (K.W.), the University of Wisconsin-Madison Department of Geoscience (A.E.C., K.W.), and National Science Foundation award ANS-0902571 (A.E.C.). Contribution to the NOSAMS Facility was made by the National Science Foundation (OCE-0753487).

References

- Aksu, A.E., Mudie, P.J., Macko, S.A., and de Vernal, A., 1988. Upper Cenozoic history of the Labrador Sea, Baffin Bay, and the Arctic Ocean: a paleoclimatic and paleoceanographic summary. *Paleoceanography*, 3, 519-538.
- Andrews, J.T., 2000. Explained and unexplained spatial and temporal variability in rates of marine sediment accumulation along the northeast margin of the Laurentide Ice Sheet ≤ 14 ka: *Journal of Sedimentary Research*, 70, 782-787.
- Andrews, J.T., Erlenkeuser, H., Tedesco, K., Aksu, A., and Jull, A.J.T., 1994. Late Quaternary (Stage 2 and 3) meltwater and Heinrich events, NW Labrador Sea: *Quaternary Research*, 41, 26-34.
- Andrews, J.T., Smith, L.M., Preston, R., Cooper, T., and Jennings, A.E., 1997. Spatial and temporal patterns of iceberg rafting (IRD) along the East Greenland margin, ca. 68°N, over the last 14 cal.ka. *Journal of Quaternary Science*, 12, 1-13.
- Andrews, J.T., Barber, D.C., Jennings, A.E., Eberl, D.D., MacLean, B., Kirby, M.E., and Stoner, J.S., 2012. Varying sediment sources (Hudson Strait, Cumberland Sound, Baffin Bay) to the NW Labrador Sea slope between and during Heinrich events 0 to 4. *Journal of Quaternary Science*, 27, 475-484.
- Ashley, G.M., and Smith, N.D., 2000. Marine sedimentation at a calving margin. *Geological Society of America Bulletin*, 112, 657-667.
- Bennike, O., and Björck, S., 2002, Chronology of the last recession of the Greenland Ice Sheet: *Journal of Quaternary Science*, v. 17, p. 211-219.
- Bennike, O., Björck, S., and Lambeck, K., 2002, Estimates of South Greenland late-glacial ice limits from a new relative sea level curve: *Earth and Planetary Science Letters*, v. 197, p. 171-186.
- Bilodeau, G., de Vernal, A., and Hillaire-Marcel, C., 1994. Benthic foraminiferal assemblages in Labrador Sea sediments: relations with deep-water mass changes since deglaciation. *Canadian Journal of Earth Sciences*, 31, 128-138.
- Bond, G.C., and Lotti, R., 1995. Iceberg discharges into the North-Atlantic on millennial time scales during the Last Glaciation. *Science*, 267, 1005-1010, doi:10.1126/science.267.5200.1005.
- Broecker, W.S., 1997. Thermohaline circulation, the Achilles Heel of our climate system: will man-made CO₂ upset the current balance? *Science*, 278, 1582-1588.
- Carlson, A.E., and Winsor, K., 2012. Northern Hemisphere ice-sheet responses to past climate

- warming: *Nature Geoscience*, 5, 607-613.
- Carlson, A. E., J. S. Stoner, J. P. Donnelly, and C. Hillaire-Marcel, 2008. Response of the southern Greenland Ice Sheet during the last two deglaciations. *Geology*, 36, 359-362.
- Clark, P.U., Mitrovica, J.X., Milne, G.A., and Tamisiea, M.E., 2002. Sea-level fingerprinting as a direct test for the source of global meltwater pulse 1A. *Science*, 295, 2438-2441.
- Clark, P.U., McCabe, A.M., Mix, A.C., and Weaver, A.J., 2004. Rapid rise of sea level 19,000 years ago and its global implications. *Science*, 304, 1141-1144.
- Clark, P.U., Dyke, A.S., Shakun, J.D., Carlson, A.E., Clark, J., Wohlfarth, B., Mitrovica, J.X., Hostetler, S.W., and McCabe, A.M., 2009. The Last Glacial Maximum: *Science*, 325, 710-714.
- Clark, P.U., Shakun, J.D., Baker, P.A., Bartlein, P.J., Brewer, S., Brook, E., Carlson, A.E., Cheng, H., Kaufman, D.S., Liu, Z., Marchitto, T.M., Mix, A.C., Morrill, C., Otto-Bliesner, B.L., Pahnke, K., Russell, J.M., Whitlock, C., Adkins, J.F., Blois, J.L., Clark, J., Colman, S.M., Curry, W.B., Flower, B.P., He, F., Johnson, T.C., Lynch-Stieglitz, J., Markgraf, V., McManus, J., Mitrovica, J.X., Moreno, P.I., and Williams, J.W., 2012. Global climate evolution during the last deglaciation. *Proceedings of the National Academy of Sciences*, 109, 1134-1142.
- Coachman, L.K., and Aagaard, K., 1974. Physical oceanography of Arctic and Subarctic seas. In Herman, Y. (ed.), *Marine Geology and Oceanography of the Arctic Seas*, Springer-Verlag, New York, pp. 1-72.
- Colville, E.J., Carlson, A.E., Beard, B.L., Hatfield, R.G., Stoner, J.S., Reyes, A.V., and Ullman, D.J., 2011. Sr-Nd-Pb isotope evidence for ice-sheet presence on southern Greenland during the last interglacial: *Science*, 333, 620-623.
- Cowan, E.A., Seramur, K.C., Cai, J., and Powell, R.D., 1999. Cyclic sedimentation produced by fluctuations in meltwater discharge, tides and marine productivity in an Alaskan fjord. *Sedimentology*, 46, 1109-1126.
- Cuny, J., Rhines, P.B., Pearn, P., and Bacon, S., 2002. Labrador sea boundary currents and the fate of the Irminger Sea Water. *Journal of Physical Oceanography*, 32, 627-647, doi:10.1175/1520-0485(2002)032<0627:LSBCAT>2.0.CO;2.
- Cuny, J., Rhines, P.B., and Kwok, R., 2005. Davis Strait volume, freshwater and heat fluxes. *Deep-Sea Research I*, 52, 519-542.
- de Vernal, A., and C. Hillaire-Marcel, 2008. Natural Variability of Greenland Climate, Vegetation, and Ice Volume During the Past Million Years. *Science*, 320, 1622-1625.

- de Vernal, A., Turon, J.-L., and Guiot, J., 1994. Dinoflagellate cyst distribution in high-latitude marine environments and quantitative reconstruction of sea-surface salinity, temperature, and seasonality. *Canadian Journal of Earth Science*, 31, 48-62.
- de Vernal, A., C. Hillaire-Marcel, W. R. Peltier, and A. J. Weaver, 2002. Structure of the upper water column in the northwest North Atlantic: Modern versus Last Glacial Maximum conditions, *Paleoceanography*, 17, 1050.
- Denton, G.H., Alley, R.B., Comer, G.C., Broecker, W.S., 2005. The role of seasonality in abrupt climate change. *Quaternary Science Reviews*, 24, 1159-1182.
- Deshayes, J., Frankignoul, C., and Drange, H., 2007. Formation and export of deep water in the Labrador and Irminger Seas in a GCM. *Deep-Sea Research I*, 54, 510-532.
- Domack, E.W., and Ishman, S., 1993. Oceanographic and physiographic controls on modern sedimentation within Antarctic fjords. *Geological Society of America Bulletin*, 105, 1175-1189.
- Dodd, P. A., K. J. Heywood, M. P. Meredith, A. C. Naveira-Garabato, A. D. Marca, and K. K. Falkner, 2009. Sources and fate of freshwater exported in the East Greenland Current. *Geophysical Research Letters*, 36, L19608, doi:10.1029/2009GL039663.
- Dowdeswell, J.A., and Cromack, M., 1991. Behavior of a glacier-derived suspended sediment plume in a small Arctic inlet. *Journal of Geology*, 99, 111-123.
- Dowdeswell, J.A., Maslin, M.A., Andrews, J.T., and McCave, I.N., 1995. Iceberg production, debris rafting, and the extent and thickness of Heinrich layers (H-1, H-2) in North Atlantic sediments. *Geology*, 23, 301-304.
- Dowdeswell, J.A., Hogan, K.A., and Ó Cofaigh, C., 2013. Submarine glacial-landform distribution across the West Greenland margin: a fjord-shelf-slope transect through the Uummannaq system (70° to 71°N): In, Dowdeswell, J.A., Canals, M., Jakobsson, M., Todd, B.J., Dowdeswell, E.K., and Hogan, K.A. (eds), *Atlas of Submarine Glacial Landforms: Modern, Quaternary and Ancient*. Geological Society, London, Memoirs, 2015.
- Evans, H. F., J. E. T. Channell, J. S. Stoner, C. Hillaire-Marcel, J. D. Wright, L. C. Neitzke, and G. S. Mountain, 2007. Paleointensity-assisted chronostratigraphy of detrital layers on the Eirik Drift (North Atlantic) since marine isotope stage 11. *Geochemistry, Geophysics, Geosystems*, 8, Q11007, doi:10.1029/2007GC001720.
- Fagel, N., Innocent, C., Stevenson, R.K., and Hillaire-Marcel, C., 1999. Deep circulation changes in the Labrador Sea since the Last Glacial Maximum: new constraints from Sm-Nd data on sediments. *Paleoceanography*, 14, 777-788.

- Fagel, N., Robert, C., Preda, M., and Thorez, J., 2001. Smectite composition as a tracer of deep circulation: the case of the Northern North Atlantic. *Marine Geology*, 172, 309-330.
- Fenty, I., and Heimback, P., 2013. Coupled sea ice–ocean-state estimation in the Labrador Sea and Baffin Bay. *Journal of Physical Oceanography*, 43, 884-904.
- Frajka-Williams, E., Rhines, P.B., and Eriksen, C.C., 2009. Physical controls and mesoscale variability in the Labrador Sea spring phytoplankton bloom observed by Seaglider. *Deep-Sea Research I*, 56, 2144-2161.
- Funder, S., Kjeldsen, K.K., Kjær, K.H., and Ó Cofaigh, C., 2011. The Greenland Ice Sheet during the past 300,000 years: a review: In Ehlers, J., Gibbard, P.L., and Highes, P.D. (eds), *Developments in Quaternary Science*, 15, Amsterdam, The Netherlands, 699-713.
- Grootes, P.M., and M. Stuiver 1997. Oxygen 18/16 variability in Greenland snow and ice with 10^3 and 10^5 -year time resolution. *Journal of Geophysical Research*, 102, 26455-26470.
- Hall, I.R., and Becker, J., 2007. Deep Western Boundary Current variability in the subtropical northwest Atlantic Ocean during marine isotope stages 12-10. *Geochemistry, Geophysics, Geosystems*, 8, Q06013, doi:10.1029/2006GC001518.
- Haskell, B.J., Johnson, T.C., and Showers, W.J., 1991. Fluctuations in deep western North Atlantic circulation on the Blake Outer Ridge during the last deglaciation. *Paleoceanography*, 6, 21-31.
- Hemming, S.R., Vorren, T.O., and Kleman, J., 2002. Provinciality of ice rafting in the North Atlantic: application of $^{40}\text{Ar}/^{39}\text{Ar}$ dating of individual ice rafted hornblende grains. *Quaternary International*, 95-96, 5-85.
- Hesse, R., and Khodabakhsh, S., 1998. Depositional facies of late Pleistocene Heinrich events in the Labrador Sea: *Geology*, 26, 103-106.
- Hesse, R., Rashid, H., and Khodabakhsh, S., 2004. Fine-grained sediment lofting from meltwater-generated turbidity currents during Heinrich events. *Geology*, 32, 449-452.
- Hillaire-Marcel, C., and de Vernal, A., 1989. Isotopic and palynological records of the Late Pleistocene in eastern Canada and adjacent ocean basins. *Géographie physique et Quaternaire*, 43, 263-290.
- Hillaire-Marcel, C., and Bilodeau, G., 2000. Instabilities in the Labrador Sea water structure during the last climatic cycle: *Canadian Journal of Earth Science*, 37, 795-809.
- Hillaire-Marcel, C. and de Vernal, A., 2008. Stable isotope clue to episodic sea ice formation in the glacial North Atlantic: *Earth and Planetary Science Letters*, 268, 143-150.

- Hillaire-Marcel, C., de Vernal, A., Bilodeau, G., and Wu, G., 1994. Isotope stratigraphy, sedimentation rates, deep circulation, and carbonate events in the Labrador Sea during the last ~200 ka. *Canadian Journal of Earth Science*, 31, 63-89.
- Hillaire-Marcel, C., de Vernal, A., and McKay, J., 2011. Foraminiferal isotope study of the Pleistocene Labrador Sea, northwest North Atlantic (IODP Sites 1302/03 and 1305), with emphasis on paleoceanographical differences between its “inner” and “outer” basins, *Marine Geology*, 279, 188-198.
- Hulbe, C.L., 1997. An ice shelf mechanism for Heinrich layer production. *Paleoceanography*, 12, 711-717.
- Jones, E. P., L. G. Anderson, S. Jutterström, and J. H. Swift, 2008. Sources and distribution of fresh water in the East Greenland Current. *Progress In Oceanography*, 78, 37-44.
- Jullien, E., Grousset, F.E., Hemming, S.R., Peck, V.L., Hall, I.R., Jeantet, C., and Billy, I., 2006. Contrasting conditions preceding MIS3 and MIS2 Heinrich events: Global and Planetary Change, 54, 225-238.
- Kelly, M., 1985. A review of the Quaternary geology of western Greenland. *In* Andrews, J.T. (ed.): *Quaternary Environments Eastern Canadian Arctic, Baffin Bay and Western Greenland*, Allen & Unwin, Boston, USA, 461-501.
- Kirby, M.E., 1997. Heinrich event-0 (DC-0) in sediment cores from the northwest Labrador Sea: recording events in Cumberland Sound? *Canadian Journal of Earth Sciences*, 35, 510-519.
- Knutz, P. C., M.-A. Sicre, H. Ebbesen, S. Christiansen, and A. Kuijpers 2011. Multiple-stage deglacial retreat of the southern Greenland Ice Sheet linked with Irminger Current warm water transport: *Paleoceanography*, 26, PA3204, doi:10.1029/2010PA002053.
- Kuijpers, A., Dalhoff, F., Brandt, M.P., Hümbes, P., Schot, T., and Zotova, A., 2007. Giant iceberg plow marks at more than 1 km water depth offshore West Greenland: *Marine Geology*, 246, 60-64.
- Larsen, N.K., Funder, S., Kjær, K.H., Kjeldsen, K.K., Knudsen, M.F., Linge, H., 2013. Rapid early Holocene ice retreat in West Greenland. *Quaternary Science Reviews*, in press, <http://dx.doi.org/10.1016/j.quascirev.2013.05.027>.
- Lucotte, M., Hillaire-Marcel, C., (1994). Identification and distribution of the main water masses in the Labrador and Irminger Seas: *Canadian Journal of Earth Science*, v. 31, p. 5-13, doi:10.1139/e94-002.
- Marcott, S.A., Clark, P.U., Padman, L., Klinkhammer, G.P., Springer, S.R., Liu, Z., Otto-Bleisner, B., Carlson, A.E., Ungerer, A., Padman, J., He, F., Cheng, J., and Schmittner,

- A., 2011. Ice-shelf collapse from subsurface warming as a trigger for Heinrich events. *Proceedings of the National Academy of Sciences*, doi:10.1073/pnas.1104772108.
- McCave, I.N., and Hall, I.R., 2006. Size sorting in marine muds: processes, pitfalls, and prospects for paleoflow-speed proxies. *Geochemistry, Geophysics, Geosystems*, 7, Q10N05, doi:10.1029/2006GC001284.
- McLean, B., ET AL, 1991. Investigations of the Quaternary geology of Hudson Strait and Ungava Bay, Northwest Territories: Geological Survey of Canada, 91-1E, 305-315.
- Mortensen, J., Lennert, K., Bendtsen, J., Rysgaard, S., 2011. Heat sources for glacial melt in a sub-Arctic fjord (Godthåbsfjord) in contact with the Greenland Ice Sheet. *Journal of Geophysical Research* 116, C01013.
- Murray, T., Scharrer, K., James, T.D., Dye, S.R., Hanna, E., Booth, A.D., Selmes, N., Luckman, A., Hughes, A.L.C., Cook, S., Huybrechts, P., 2010. Ocean regulation hypothesis for glacier dynamics in southeast Greenland and implications for ice sheet mass changes: *Journal of Geophysical Research*, 115, F03026, doi:10.1029/2009JF001522.
- Nam, S.I., Stein, R., Grobe, H., and Hubberten, H., 1995. Late Quaternary glacial-interglacial changes in sediment composition at the East Greenland continental margin and their paleoceanographic implications. *Marine Geology*, 122, 243-262.
- Ó Cofaigh, Andrews, J.T., Jennings, A.E., Dowdeswell, J.A., Hogan, K.A., Kilfeather, A.A., and Sheldon, C., 2013. Glacimarine lithofacies, provenance and depositional processes on a West Greenland trough-mouth fan. *Journal of Quaternary Science*, 28, 13-26.
- Ó Cofaigh, C., Dowdeswell, J.A., Jennings, A.E., Hogan, K.A., Kilfeather, A., Hiemstra, J.F., Noormets, R., Evans, J., McCarthy, D.J., Andrews, J.T., Lloyd, J.M., and Moros, M., 2013. An extensive and dynamic ice sheet on the West Greenland shelf during the last glacial cycle: *Geology*, 41, 219-222.
- Pickart, R.S., 1992. Water mass components of the North Atlantic deep western boundary current. *Deep-Sea Research*, 39, 1553-1572.
- Piper, D.J.W., Shaw, J., and Skene, K.I., 2007. Stratigraphic and sedimentological evidence for late Wisconsinan sub-glacial outburst floods to Laurentian Fan. *Palaeogeography, Palaeoclimatology, Palaeoecology*, 246, 101-119.
- Pritchard, H.D., Arthern, R.J., Vaughan, D.G., Edwards, L.A., 2009. Extensive dynamic thinning on the margins of the Greenland and Antarctic ice sheets: *Nature*, v. 461, 971-975.
- Powell, R.D., 1984. Glacimarine processes and inductive lithofacies modelling of ice shelf and tidewater glacier sediments based on Quaternary examples. *Marine Geology*, 57, 1-52.

- Rashid, H., and Piper, D.J.W., 2007. The extent of ice on the continental shelf off Hudson Strait during Heinrich events 1-3. *Canadian Journal of Earth Sciences*, 44, 1537-1549.
- Rashid, H., Hesse, R., and Piper, J.W., 2003a. Evidence for an additional Heinrich event between H5 and H6 in the Labrador Sea. *Paleoceanography*, 18, doi:10.1029/2003PA000913.
- Rashid, H., Hesse, R., and Piper, D.J.W., 2003. Distribution, thickness and origin of Heinrich layer 3 in the Labrador Sea, 205, 281-293.
- Rasmussen, T.L., Oppo, D.W., Thomsen, E., and Lehman, S.J., 2003. Deep sea records from the southeast Labrador Sea: ocean circulation changes and ice-rafting events during the last 160,000 years.
- Reeh, N., Mayer, C., Miller, H., Højmark Thomsen, H., and Weidick, A., 1999. Present and past climate control on fjord glaciations in Greenland: implications for IRD-deposition in the sea: *Geophysical Research Letters*, 26, 1039-1042.
- Reyes, A.V., Carlson, A.E., Beard, B.L., Hatfield, R.G., Stoner, J.S., Winsor, K., Welke, W., and Ullman, D.J., 2014. South Greenland ice-sheet collapse during Marine Isotope Stage 11. *Nature*, 510, 525-528.
- Rignot, E., Koppes, M., Velicogna, I., 2010. Rapid submarine melting of the calving faces of West Greenland glaciers: *Nature Geoscience*, v. 3, p. 187-191.
- Rinterknecht, V., Gorokhovitch, Y., Schaeffer, J., and Caffee, M., 2009, Preliminary ^{10}Be chronology for the last deglaciation of the western margin of the Greenland Ice Sheet: *Journal of Quaternary Science*, v. 24, no. 3, p. 270-278, doi:10.1002/jqs.1226.
- Roberts, D.H., Long, A.J., Schnabel, C., Davies, B., Xu, S., Simpson, M.J.R., and Huybrechts, P., 2009. Ice sheet extent and early deglacial history of the southwestern sector of the Greenland Ice Sheet: *Quaternary Science Reviews*, 28, 2760-2773.
- Simon, Q., Hillaire-Marcel, C., St-Onge, G., and Andrews, J.T., 2013. North-eastern Laurentide, western Greenland and southern Inuitian ice stream dynamics during the last glacial cycle: *Journal of Quaternary Science*, doi:10.1002/jqs.2648.
- Simpson, J.R.M., Milne, G.A., Huybrechts, P., and Long, A.J., 2009. Calibrating a glaciological model of the Greenland ice sheet from the Last Glacial Maximum to present-day using field observations of relative sea level and ice extent. *Quaternary Science Reviews*, 28, 1630-1656.
- Smith, W.H.F., and Sandwell, D.T., 1997. Global seafloor topography from satellite altimetry and ship depth soundings: *Science*, 277, 1957-1962.

- Solignac, S., de Vernal, A., and Hillaire-Marcel, C., 2004. Holocene sea-surface conditions in the North Atlantic—contrasted trends and regimes in the western and eastern sectors (Labrador Sea vs. Iceland Basin). *Quaternary Science Reviews*, 23, 319-334.
- Sommerhoff, G., 1981. Geomorphologische Prozesse in der Labrador und Imingersee. Ein Beitrag zur submarinen Geomorphologie einer subpolaren Meeresregion: *Polarforschung*, 51, 175-191.
- Sparks, R.S.J., Bonnecaze, B., Huppert, H.E., Lister, J.R., Hallworth, M.A., Mader, H., and Phillips, J., 1993. Sediment-laden gravity currents with reversing buoyancy: *Earth and Planetary Science Letters*, 114, 243-257.
- Sparrenbom, C.J., Bennike, O., Björck, S., and Lambeck, K., 2006a. Holocene relative sea-level changes in the Qaqortoq area, southern Greenland: *Boreas*, v. 35, p. 171-187.
- Sparrenbom, C.J., Bennike, O., Björck, S., Lambeck, K., 2006b. Relative sea-level changes since 15 000 cal. yr BP in the Nanortalik area, southern Greenland: *Journal of Quaternary Science*, v. 21, p. 29-48.
- Stoner, J.S., Channell, J.E.T., Hillaire-Marcel, C., and Mareschal, J.-C., 1994. High resolution rock magnetic study of a Late Pleistocene core from the Labrador Sea. *Canadian Journal of Earth Sciences*, 31, 104-114.
- Stoner, J.S., Channell, J.E.T., and Hillaire-Marcel, C., 1995. Magnetic properties of deep-sea sediments off southwest Greenland: evidence for major differences between the last two deglaciations. *Geology*, 23, 241-244.
- Stuiver, M., and Polach, H.A., 1977. Discussion: Reporting of ^{14}C data. *Radiocarbon*, 19, 355-363.
- Stuiver, M., and Reimer, P.J., 1993. Extended ^{14}C database and revised CALIB radiocarbon calibration program: *Radiocarbon*, 35, 215-230.
- Stuiver, M., Reimer, P.J., and Reimer, R.W., 2005. CALIB 5.0 [www.program and documentation].
- Svensson, A., Andersen, K.K., Bigler, M., Clausen, H.B., Dahl-Jensen, D., Davies, S.M., Johnsen, S.J., Muscheler, R., Parrenin, F., Rasmussen, S.O., Röthlisberger, R., Seierstad, I., Steffensen, J.P., and Vinther, B.M., 2008. A 60 000 year Greenland stratigraphic ice core chronology: *Climate of the Past*, 4, 47-57.
- Syvitski, J.P.M., Andrews, J.T., and Dowdeswell, J.A., 1996. Sediment deposition in an iceberg-dominated glaciomarine environment, East Greenland: basin fill implications. *Global and Planetary Change*, 12, 251-270.

- Vilks, G., and Mudie, P.T., 1978. Early deglaciation of the Labrador Shelf: *Science*, 202, 1181-1183.
- Vilks, G., and Powell, C., 1989. Cruise report and preliminary results, CSS Hudson 87-033. 65 pp.
- Waelbroeck, C., Duplessy, J.C., Michel, E., Labeyrie, L., Paillard, D., and Duprat, J., 2001. The timing of the last deglaciation in North Atlantic climate records: *Nature*, 412, 724-727.
- Weidick, A., Kelly, M., and Bennike, O., 2004. Late Quaternary development of the southern sector of the Greenland Ice Sheet, with particular reference to the Qassimiut lobe: *Boreas*, 33, 284-299.
- Winsor, K., Carlson, A.E., Klinkhammer, G.P., Stoner, J.S., and Hatfield, R.G., 2012. Evolution of the northeast Labrador Sea during the last interglaciation: *Geochemistry, Geophysics, Geosystems*, 13, doi:10.1029/2012GC004263.
- Winsor, K., Carlson, A.E., Caffee, M., and Rood, D.H., Rapid last deglacial thinning and retreat of the marine-terminating southwest Greenland Ice Sheet: *in review at Earth and Planetary Science Letters*.
- Woodroffe, S.A., Long, A.J., Lecavalier, B.S., Milne, G.A., Bryant, C.L., 2014. Using relative sea-level data to constrain the deglacial and Holocene history of southern Greenland: *Quaternary Science Reviews*, 92, 345-356.

Figure Captions.

Figure 1. A) North Atlantic surface water bodies and bathymetry (Smith and Sandwell, 1997), and core locations. Currents: LC = Labrador Current, EGC = East Greenland Current, WGC = West Greenland Current, IC = Irminger Current. Sediment cores: 1 = HU87033-008, 2 = DA04-31P, 3 = MD99-2227, 4 = HU90-013-013. Dotted outline shows location of Figure 1B. B) Google Earth image of bathymetry and coastline near southwestern Greenland. An hypothesized general GrIS margin location along the shelf break is outlined in solid orange. An hypothesized mid- to inner-shelf general margin location with ice stream margins extending to the shelf break is outlined in dashed yellow. Also shown are sediment cores HU87033-008 and DA04-31P, and coastal towns of Paamiut and Nuuk discussed in Winsor et al. (in review), and the Sarqarsuaq and Sermilik fjords discussed in Larsen et al. (2014).

Figure 2. Sediment core HU87033-008 age model, with grains size and oxygen isotopes. A) Shown in black diamonds are nine calibrated ^{14}C dates, eight of which are linearly interpolated between to produce the age model (black line), and one of which is an outlier out of stratigraphic order. Also shown are dates calibrated using a ΔR of 0 (red squares and line), and a ΔR of 600 for pre-Younger Dryas samples (orange circles and line). B) Weight percent sand (orange), silt (red), and clay (light green). C) *N. pachyderma* (s) $\delta^{18}\text{O}$ of calcite.

Figure 3. HU87033-008 data against age. A) Uncorrected magnetic susceptibility (Vilks and Powell, 1987), B) calculated clay, C) silt, and D) sand fluxes, E) sedimentation rate (for pre-Younger Dryas samples, sedimentation rates are shown using a marine reservoir correction ΔR of 0 years (pink), 200 years (maroon), and 600 years (light green)), and F) *N. pachyderma* (s)

$\delta^{18}\text{O}$. Black squares are radiocarbon tie-points. Light gray bar is peak flux in silt and clay, and dark gray bar is Heinrich event 1 detrital carbonates. Question marks indicate uncertainty in sedimentation rates and fluxes due to possible erosion at the associated intervals.

Figure 4. Climate context and evidence for southwestern and southern GrIS melt and retreat. A) June insolation at 60°N (Berger & Loutre, 1991), B) eustatic sea level (Clark et al., 2012), C) Mg/Ca-derived calcification temperatures from *N. pachyderma* (s) in MD99-2227 (Winsor et al., 2012), D) *N. pachyderma* (s) $\delta^{18}\text{O}$ for HU87033-008 (dark blue) and MD99-2227 (light blue-green; Evans et al., 2007; Winsor et al., 2012), E) HU87033-008 silt (red) and sand (orange) fluxes, F) MD99-2227 titanium runoff record corrected against calcium (Carlson et al., 2008), and G) ^{10}Be exposure dates from coastal southwestern Greenland (Larsen et al., 2014; Winsor et al., in review). Gray bar is peak sedimentation in HU87033-008, and blue-green bar is GrIS retreat from the modern coastline. Question marks indicate uncertainty in sedimentation rates and fluxes due to possible erosion at the associated intervals.

Table 2-1. Radiocarbon metadata and ages. #Indicates trigger-weight core sample, and *indicates excluded outlier. Uncertainty in ^{14}C and calibrated ages is 2σ . Marine reservoir correction ΔR used here is 200 years (total for samples 287 through 76 cm in depth, and 0 years for samples 58 through core top in depth).

Depth (cm bsf)	^{14}C age (ka)	^{14}C Uncertainty (ka)	$\delta^{13}\text{C}$ (per mil)	ΔR (ka)	ΔR Uncertainty (ka)	Calibrated Upper Range (ka)	Calibrated Lower Range (ka)	Calibrated Mean Probability (ka)	Calibrated Uncertainty (ka)
TWC#	3.72	0.03	0	0.0	0.05	3.81	3.49	3.64	0.06
11	8.70	0.03	0.4	0.0	0.05	9.23	9.49	9.37	0.06
58	10.35	0.04	0.15	0.0	0.05	11.20	11.72	11.40	0.06
76	14.10	0.07	-0.2	0.2	0.1	15.88	16.65	16.25	0.12
96	14.65	0.05	-0.2	0.2	0.1	16.67	17.44	17.07	0.11
			-						
116*	13.80	0.05	0.11	0.2	0.1	15.45	16.19	15.85	0.11
137	15.50	0.06	0.02	0.2	0.1	17.84	18.41	18.12	0.12
			-						
166	15.95	0.06	0.03	0.2	0.1	18.35	18.84	18.61	0.12
			-						
241	16.60	0.08	0.54	0.2	0.1	18.96	19.61	19.30	0.13
287	17.30	0.07	0	0.2	0.1	19.82	20.49	20.15	0.12

Table 2-S1. Stable isotope data from *Neogloboquadrina pachyderma* (s), with starred intervals published in Hillaire-Marcel et al. (1994), and sand, silt, and clay weight percentages.

Depth (cm)	$\delta^{13}\text{C}$ (per mil)	$\delta^{18}\text{O}$ (per mil)	% Sand	% Silt	% Clay
1	0.60	2.56	10	51	40
2	0.51	2.52			
4	0.67	2.74			
6			7	56	37
8	0.59	2.58			
11	0.42	2.71	32	44	24
16			12	48	40
21			28	43	29
26			23	46	31
31			19	46	35
36			16	50	34
41			21	45	35
46			20	50	30
51	-0.03	3.25	19	50	31
53	0.17	3.05	17	51	31
56	-0.06	3.26	19	50	31
57*	0.06	2.83			
58	0.18	2.91	26	49	25
61	-0.24	3.40	18	49	33
63	-0.17	3.16	17	50	33
66	-0.09	3.35	19	52	29
69	0.07	3.29	19	50	31
71	-0.19	3.11	24	46	30
73			18	47	35
75*	-0.03	2.64			
76	-0.18	3.21	21	46	33
81	-0.28	3.03	13	44	43
84	-0.12	3.29	6	41	53
86	-0.20	3.12	17	42	41
91	-0.16	3.01	6	41	53
93	-0.07	3.45	5	42	52
96	0.00	3.44	5	38	57
101	0.08	3.15	5	40	55
106	-0.13	3.17	7	41	52
111			5	46	49

113			4	45	51
116	-0.12	3.09	8	45	47
118			3	44	53
121			5	51	44
123			5	51	44
126			4	49	47
128			4	50	46
131			5	41	53
132*	0.12	4.27			
133	-0.08	4.12	5	52	43
136	-0.06	4.29	5	53	42
138	0.03	4.22	6	53	41
141	0.02	4.33	6	52	43
143*	0.10	3.83			
146	-0.03	4.05	11	49	40
151	-0.10	3.96	5	52	43
155*	0.03	4.53			
156	-0.03	4.14	6	52	42
161			3	48	49
166	0.10	4.46	6	52	42
171	0.00	4.57	7	53	40
176			4	50	45
177*	0.23	4.43			
181			5	47	48
186	0.15	4.70	5	51	44
189*	0.34	4.33			
191			3	51	46
196			4	51	44
200*	0.40	4.63			
206	0.06	4.76	7	51	42
211	0.03	4.23	10	52	39
216			4	52	44
221	-0.17	4.57	6	53	41
223*	0.38	4.33			
226			4	53	44
231			3	53	45
236	0.01	4.67	4	54	42
241	0.01	4.72	2	48	49
246			4	48	48
260			3	45	52
267	-0.13	4.41	5	49	46
268*	0.05	4.33			

276			3	46	51
287	0.03	4.71	7	51	42
291*	0.08	4.53			
297	-0.20	4.61	10	57	32
303*	0.20	4.33			
308	-0.02	4.78	3	46	52

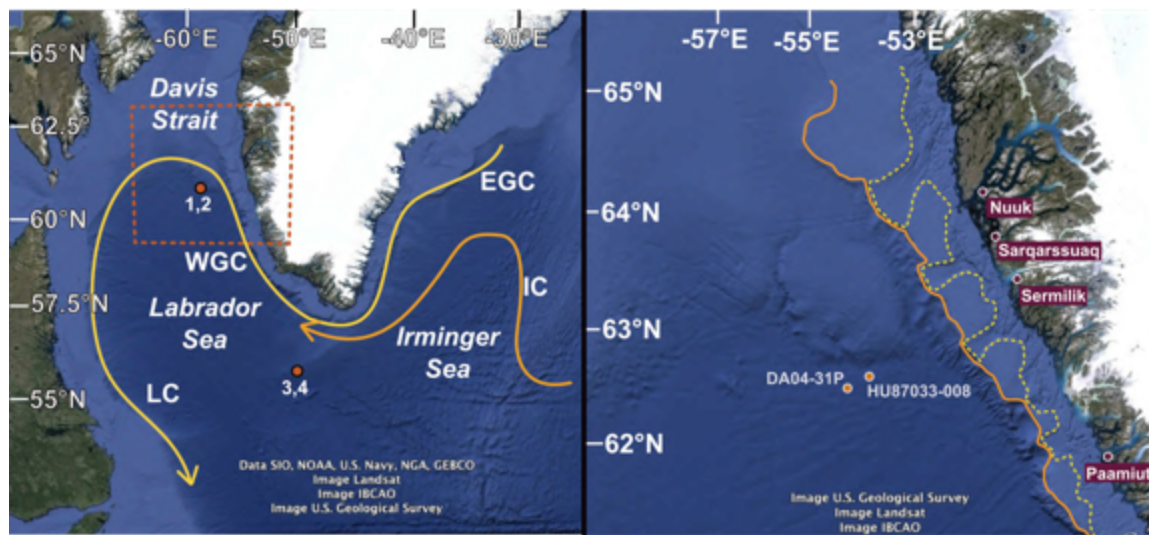


Figure 2-1.

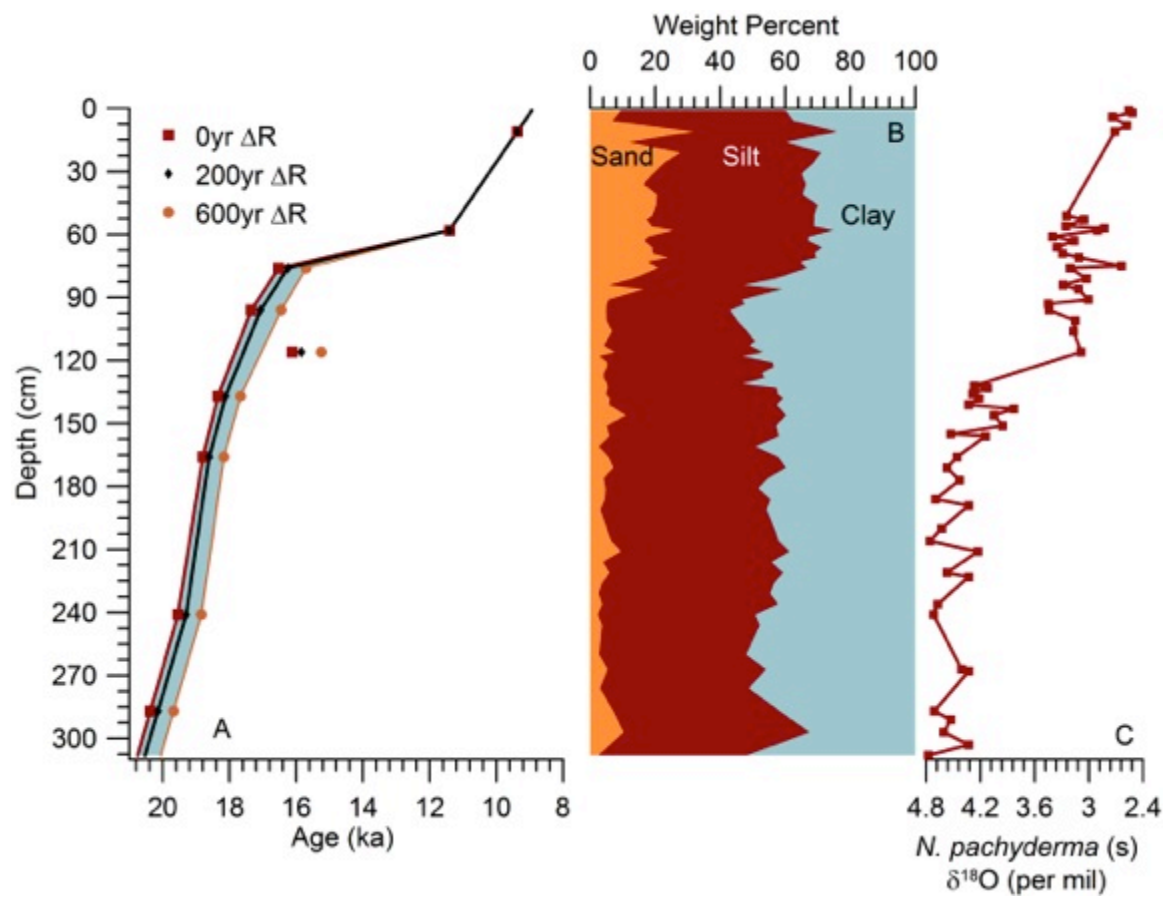


Figure 2-2.

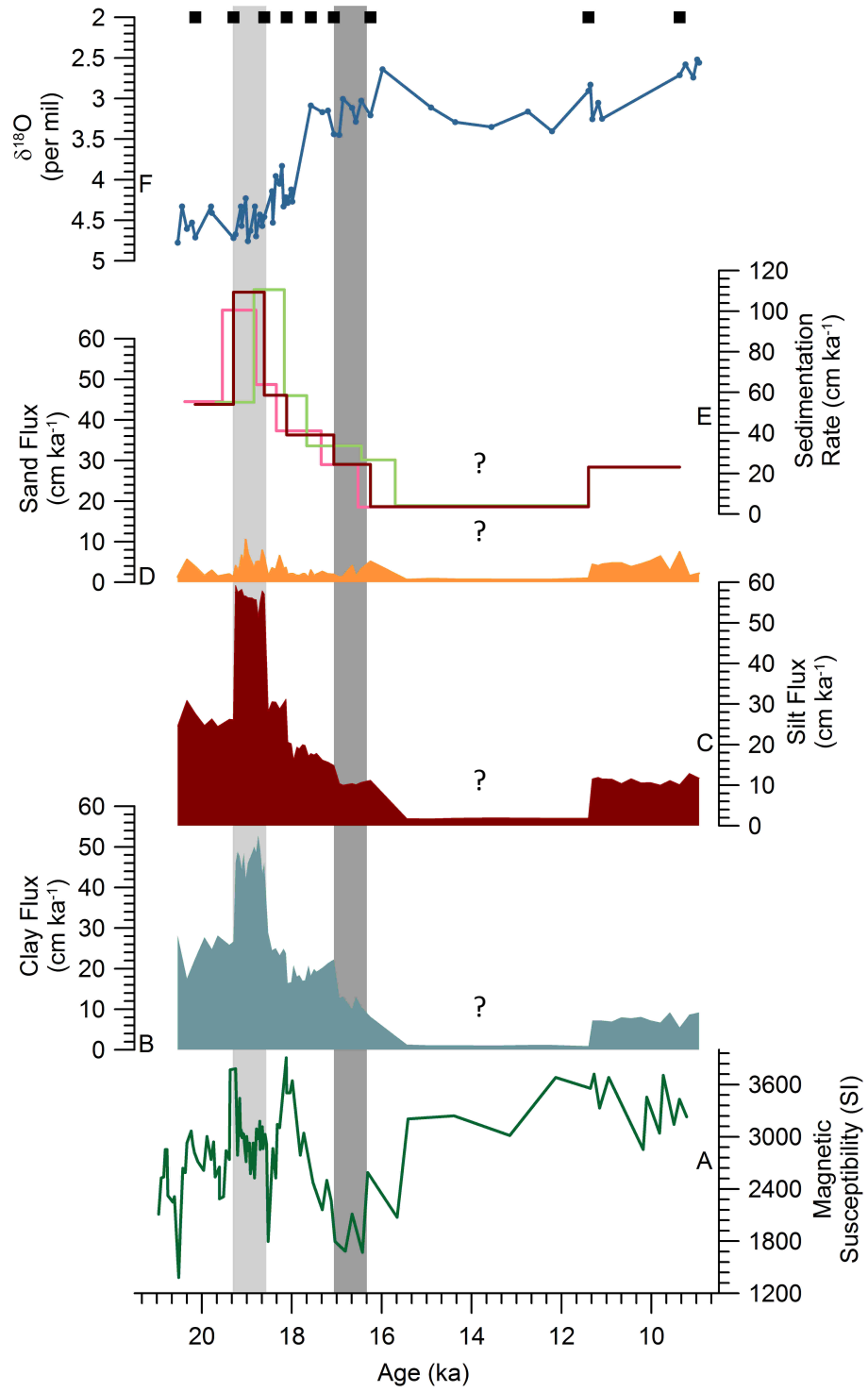


Figure 2-3.

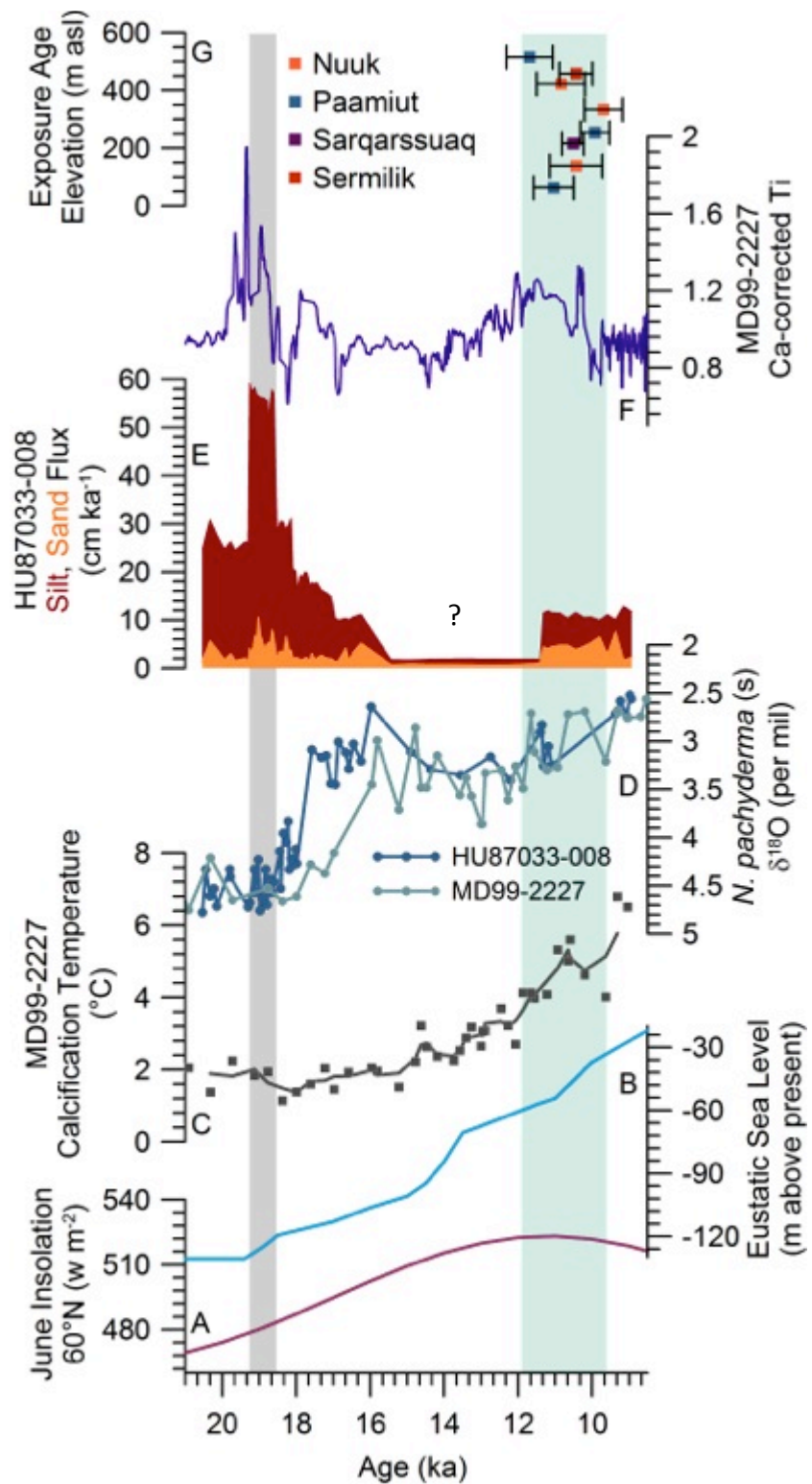


Figure 2-4.

CHAPTER III:**RAPID LAST DEGLACIAL THINNING AND RETREAT OF THE MARINE-TERMINATING SOUTHWEST
GREENLAND ICE SHEET**

Kelsey Winsor¹
Anders E. Carlson^{1,2}
Marc Caffee³
Dylan H. Rood⁴

¹Department of Geoscience, University of Wisconsin, Madison, WI, 53706, USA

²College of Earth, Ocean, and Atmospheric Sciences, Oregon State University, Corvallis, OR,
97331, USA

³Purdue Rare Isotope Measurement Laboratory, Purdue University, West Lafayette, IN, 47907,
USA

⁴Scottish Universities Environmental Research Centre, East Kilbride, G75 0QF, Scotland, UK

This manuscript will be submitted to *Earth and Planetary Science Letters*, and is formatted to fit the specifications of that journal.

Abstract

Marine-terminating outlet glaciers are a major source of modern ice loss from the Greenland Ice Sheet (GrIS). Here, we develop last deglacial outlet glacier retreat chronologies for four sites in southwest and south Greenland in order to improve understanding of spatial variations in centennial- to millennial-scale ice loss during a warming climate. We calculate ^{10}Be surface exposure dates on boulders located in fjords near the towns of Qaqortoq, Paamiut, Nuuk, and Sisimiut. Our northernmost study site, Sisimiut, deglaciated earliest at 17.8 ± 0.8 ka to 14.5 ± 0.6 ka at a thinning rate of $0.1\text{-}0.3$ m yr^{-1} . Inland retreat from Sisimiut to the modern ice margin took ~ 7 ka at a retreat rate of $15\text{-}20$ m yr^{-1} . After retreat from the small coastal Sisimiut fjords, the GrIS margin was mainly land-terminating in this region. In contrast, earliest exposure following ice retreat occurred at ~ 12 ka near Qaqortoq, and $11\text{-}10$ ka near Nuuk and Paamiut. Ice retreat inland from the extensive Nuuk, Paamiut, and Qaqortoq fjord systems to near-present margins occurred in <1 ka, resulting in minimum retreat rates of $25\text{-}60$ m yr^{-1} and a maximum retreat rate of 95 m yr^{-1} to instantaneous within the uncertainty of our measurements. This rapid retreat of marine-terminating southwest GrIS margins is contemporaneous with a foraminiferal Mg/Ca-inferred incursion of relatively warm ocean waters into the Labrador Sea and toward the southwest Greenland coast, suggesting that a warming ocean may have contributed to the more rapid retreat of marine GrIS termini in the Nuuk, Paamiut, and Qaqortoq fjord systems relative to the slower ice retreat inland from Sisimiut.

3.1. Introduction

The southwestern portion of the Greenland Ice Sheet (GrIS) reached its maximum extent at $\sim 24\text{-}19$ ka during the last glacial period (Kelly, 1985; Funder and Hansen, 1996; Weidick et

al., 2004; Fleming and Lambeck, 2004; Alley et al., 2010). Moraine systems on the inner continental shelf suggest that the Last Glacial Maximum (LGM) ice margin may have terminated 10-50 km offshore of the modern coastline (Kelly, 1985; Funder and Hansen, 1996). Modeled southwest GrIS isostatic rebound, on the other hand, suggests that LGM ice extended much further, to the continental shelf break (Bennike et al., 2002; Weidick et al., 2004). Following the local LGM, the southwestern GrIS began to retreat inland from the shelf, eventually exposing glacially scoured coastal terrain. Constraining the timing of onset of retreat is, in most places, hampered by the fact that the LGM margins are now below sea level. However, radiocarbon dates along the southwest Greenland coast generally indicate that ice retreated beyond the modern coastline prior to 11-10 ka (e.g., Bennike and Björck, 2002; Alley et al., 2010; Larsen et al., 2014). Coastal ^{10}Be surface exposure data near 66°N from Rinterknecht et al. (2009) and Roberts et al. (2009) suggest much earlier ice retreat by ~ 18 ka and ~ 20 ka, respectively. Further to the south at $\sim 60^\circ\text{N}$, radiocarbon data suggest first coastal land exposure may have occurred 14.1 ka (Funder, 1989; Bennike and Björck, 2002).

Most datasets for last deglacial outlet glacier retreat on Greenland rely on minimum-limiting radiocarbon dates. These ages can lead to underestimation of the responsiveness of outlet glaciers to climate forcings, and are similarly restricted in their ability to precisely constrain past thinning and retreat rates (Balco et al., 2011). Thus, more accurate pinpointing of deglacial land surface exposure and rates of past ice retreat leads to better assessment of how glacial margins respond to deglacial climate warming.

Here, we present a suite of ^{10}Be surface exposure dates from four outlet glacier fjords in southwestern Greenland, sampled along vertical profiles of coastal slopes. When combined with data from near the current GrIS margin (Larsen et al., 2014; Carlson et al., in press), we are able

to calculate thinning and retreat rates of the ice margins. The purpose of this study is twofold: to construct retreat chronologies that do not rely on minimum-limiting data, and to identify mechanisms that may explain the thinning and retreat rates of different fjords in the region.

3.2. Geologic Setting and Sampling Locations

Cosmogenic nuclide surface exposure samples were collected from boulders in four fjord valleys in southern and southwestern Greenland, near the coastal towns of Sisimiut, Nuuk, Paamiut, and Qaqortoq (Figure 1). In general, the southern and southwestern Greenland coast consists of glacially smoothed hills gaining in elevation as they extend inland. The terrain is punctuated by fjords that vary in length, with some extending to the present GrIS margin (inland ice), and others terminating distal of the ice margin. Predominant orientation of fjords in this region is west-southwest trending.

The northern Labrador Sea abuts southern and southwestern Greenland. Surface and near-surface waters of the Labrador Sea are sourced from the Arctic and North Atlantic, bringing a mix of cooler and fresher water from the north and warmer and more saline water from the south (Coachman and Aagaard, 1974; Holliday et al., 2007). The West Greenland Current flows along the shelf of southwestern Greenland and lies above the intermediate depth Labrador Sea Water (Lucotte and Hillaire-Marcel, 1994; Fagel and Hillaire-Marcel, 2006). Waters of the Labrador Sea enter Greenland fjords, mixing with meltwater and in many cases stratifying the fjord water columns (e.g., Møller et al., 2006; Mortensen et al., 2011).

Modern observations of southeastern and western Greenland fjords demonstrate that the incursion of warm waters—on both seasonal and annual timescales—provides significant heat to fjord systems and has likely contributed to recent glacier acceleration and resultant thinning (e.g.,

Rignot and Kanagaratnam, 2006; Holland et al., 2008; Howat et al., 2008; Murray et al., 2010; Rignot et al., 2010; Straneo et al., 2010; 2011; Straneo and Heimbach, 2013). The influence of open ocean waters on southwestern Greenland fjord systems varies with bathymetry of the fjords, as many fjords possess sills that restrict entry of deeper water (e.g., Møller et al., 2006; Sparrenbom et al., 2006a; b; 2013; Mortensen et al., 2011). This influence also varies with continental shelf depth and width, with some locales having particularly shallow offshore shelves.

Modern air temperatures along coastal southern and southwestern Greenland are heavily modulated by local ocean currents, reaching a monthly average of $\sim 7^{\circ}\text{C}$ in summer, and -11°C in winter (Vinther et al., 2006). While modern precipitation over Greenland has shown some decadal-scale variability, with possibly anti-phased coastal versus inland yearly precipitation values (Mernild et al., 2014), southern coastal precipitation totals are $\sim 1 \text{ m yr}^{-1}$ water equivalent. Further north, e.g. near Sisimiut, climate becomes progressively more arid. Precipitation over the ice sheet is also strongly influenced by synoptic-scale weather events, particularly during the winter (Schuenemann et al., 2013), temperature inversions, and persistent regional high-pressure systems (Steffen and Box, 2001).

3.2.1 Terrestrial Study Locales

3.2.1.1 Sisimiut

Sampling locations near Sisimiut (66.939°N , 53.672°W , also known as Holsteinborg) are located $\sim 150 \text{ km}$ from the modern ice margin to the east, and $\sim 120 \text{ km}$ from the nearest shelf break to the west. LGM ice extent near Sisimiut is uncertain, and may (e.g., Bennike and Björck, 2002; Simpson et al., 2009), or may not (e.g., Funder and Hansen, 1996; Fleming and Lambeck,

2004; Roberts et al., 2010) have reached the shelf edge. The marine limit at this location is ~140 m asl (Bennike et al., 2011). To the south of the town and sampling area, the modern fjord extends only ~35 km inland, well distal of the current inland ice margin. To the north of Sisimiut, a small valley connects the coast to the hills and mountains inland, with 300 m of elevation gain over less than 10 km. Here, a stream dissects proglacial sediment into terraces. Between the two valleys lies a ridge extending to ~400 m above sea level, where previous workers have observed a weathering boundary between smoothed bedrock below, and grussified, felsenmeer-like surfaces above (e.g., Kelly, 1985). This ridge and the proglacial terraces to the north host the sampled boulders (Fig. 2a), with five boulders above the trimline (~590 m above sea level), and four at lower elevations (~160 m above sea level). Low elevation samples were located above the local marine limit. Due to the steepness of the slope leading to the ridge, no samples were collected from middle elevations at this site. Bedrock in this region is predominantly gneiss, with a swath of charnockite in the coastal Sisimiut area (Roberts et al., 2010).

3.2.1.2 Nuuk

The town of Nuuk (64.182°N, 51.715°W) is ~70 km from the shelf break. Like other coastal southwest Greenland sites, the landscape is that of smoothed, glacially scoured bedrock, which in this location is primarily gneiss (Møller et al., 2006). Inland of the town, a network of fjords extends to modern outlet glaciers of the GrIS, located ~100 km to the east (Fig. 2b). The main fjord of this network, termed Nûp Kangerdlua or Godthåbsfjord, possesses an outer sill at ~170 m water depth, although the shelf shallows seaward to ~50 m below sea level (Mortensen et al., 2011). The two smaller fjords of the network possess outer sills at ~350 m below sea level

to the south but shallower sills to the north (Mortensen et al., 2011). Although these sills limit the depth of water masses that can influence GrIS outlet glaciers, modern observations show that relatively warm and saline pulses entrained within the West Greenland Current do enter Nûp Kangerdlua (Mortensen et al., 2011). Subsurface (below ~200 m) West Greenland Current-derived fjord waters are cooler and more saline than the local surface waters in summer, which are influenced by solar heating and meltwater dilution (Møller et al., 2006). However, during the winter, the West Greenland Current is a significant heat source and cause of modern marine-terminating ice melt (Mortensen et al., 2011).

Sampling locations near Nuuk were focused on the hilly, narrow strip of land to the south of Nûp Kangerdlua (Fig. 2b). Four high-elevation samples at ~420 m above sea level were located on a hilltop just outside of town, two middle-elevation samples (~330 m above sea level) were on the adjacent hill slope, and another four were taken from low elevations (~140 m above sea level). Here, the local marine limit is at ~90 m above sea level (Kelly, 1985), and all samples were retrieved from above that altitude.

3.2.1.3 Paamiut

The coastal town of Paamiut (61.597°N, 49.400°W), briefly called Frederikshåb, sits adjacent to Kuannersooq, a branching fjord that extends to the modern inland GrIS (Fig. 2c). Smaller fjords that terminate distal of the outlet glacier terminus lie between Paamiut and the Frederikshåb ice cap. Low-elevation, scoured, and jointed gneissic bedrock stretches from the coast eastward to the sampling sites, which are located where the land rises from ~50 m asl to ~550 m asl. The continental shelf extends ~60 km offshore. The region near Paamiut is relatively unstudied, but LGM ice extent may have reached the shelf edge (e.g., Weidick et al., 2004).

Just to the east of town, we sampled an erratic at the highest accessible elevation (515 m above sea level), and another three from ~70 m below that (Fig. 2c). Two samples were collected from middle elevations (~250 m above sea level), and five from low elevations (~65 m above sea level). The lowest samples from Paamiut were from above, but very close to, the ~50 m marine limit (Kelly, 1985).

3.2.1.4 Qaqortoq

Our southernmost study site is located just northeast of the town of Qaqortoq (60.720°N, 46.037°W) on a ridge rising to ~400 m asl from the shoreline. Bedrock is primarily composed of granite, sandstone, and syenites, and hosts abundant small lakes, some of which have been studied for local sea level reconstruction (Sparrenbom et al., 2006a). Fjords in this area are parallel and NE-SW oriented (Fig. 2d). Beyond the mainland coastline are numerous glacially smoothed bedrock islands. The continental shelf extends ~75 km from the westernmost land near Qaqortoq—the town itself is ~20 km inland of the coast. LGM ice may have extended near to, or reaching, the shelf edge (e.g., Bennike et al., 2002; Weidick et al., 2004), and contributed to overdeepening of fjords in the area, which reach depths of ~600 m below sea level (Sparrenbom et al., 2006a).

Three samples were collected from the highest elevation peak (~400 m above sea level), and an additional four from an adjacent, slightly lower elevation ridge top (~320 m above sea level). Two sets of three samples each were also taken from low-middle (~180 m above sea level) elevations and low (~100 m above sea level) elevations. As for the first three sites, Qaqortoq samples were all sitting above the marine limit, which near Qaqortoq is estimated to be ~50 m (Kelly, 1985).

3.3. Methods and Age Calculation

3.3.1 Field and Laboratory Methods

Our sampling for ^{10}Be surface exposure dating targeted boulders that rested directly on bedrock or on a thin soil covering bedrock. We avoided sampling bedrock directly because of evidence for ^{10}Be inheritance in deglacial samples from southwest Greenland (e.g., Roberts et al., 2009; Larsen et al., 2014). We also avoided sampling moraines to circumvent problems with moraine deflation and reworking (Gosse and Phillips, 2001) that result in erroneously young exposure ages. All boulders were chosen based on the following characteristics: little to no visible weathering on the boulder surface and on the surrounding substrate, a height >1 m, a slightly dipping to horizontal upper surface, a high quartz content, and location that would preclude post-depositional rolling (e.g., on high points rather than on steep slopes). Topographic shielding and GPS coordinates were measured in the field. At most sites, we sampled multiple boulders at each elevation.

At the University of Wisconsin-Madison Cosmogenic Nuclide Laboratory, boulder samples were first cut to <4 cm thick, with average thickness measured. Samples were crushed and sieved to 480-825 μm to obtain grains of single mineral species, then exposed to a Frantz magnetic separator to remove the more magnetic minerals. Non-magnetic sample components were repeatedly acid-etched first using concentrated HCl and then repeatedly using a weak HF/HNO₃ mixture to isolate quartz grains and remove meteoric ^{10}Be contamination (Kohl & Nishiizumi, 1992; Gosse and Philips, 2001). Quartz purity was verified by inductively coupled plasma optical emission spectroscopy at the University of Colorado-Boulder Department of Geological Sciences. Pure samples were fully dissolved in HF acid with a ^9Be carrier, followed

by repeated HClO₄ dissolutions and evaporations to remove fluoride complexes. Through a series of anion and cation exchange columns and pH adjustments, we isolated and then ignited Be(OH)₂. The final BeO product was bound with Nb and packed into targets for accelerator mass spectrometry (AMS) measurement at the Purdue Rare Isotope Measurement (PRIME) Laboratory.

Laboratory blanks using ⁹Be carriers from the commercial Claritas and Merck standards, as well as a custom-made low-level carrier from Oregon State University (OSU Blue; Murray et al., 2012), were processed with each sample set. Average ¹⁰Be/⁹Be blanks for the Claritas carrier were $1.316 \times 10^{-14} \pm 9.937 \times 10^{-16}$ (n=5), for the Merck carrier were $3.42 \times 10^{-15} \pm 3.81 \times 10^{-16}$ (n=3), and for the OSU Blue carrier were $1.63 \times 10^{-15} \pm 3.05 \times 10^{-16}$ (n=14). Complete blank information for each run is present in Supplementary Table 1. PRIME Laboratory measurements were normalized to the 07KNSTD standard, which has a reported ¹⁰Be/⁹Be of 2.85×10^{-12} (Nishiizumi et al., 2007).

3.3.2 Exposure Age Calculation

Surface exposure ages were calculated using the CRONUS online calculator version 2.2, with constants version 2.2 (Balco et al., 2008). We use the Arctic sea-level high-latitude ¹⁰Be production rate of 3.96 ± 0.15 atoms g⁻¹ yr⁻¹ (Young et al., 2013b) with the time-varying spallation production rate-scaling scheme of Lal (1991) and Stone (2000) to account for temporal changes in geomagnetic field strength. This production rate has been successfully used in Greenland and is similar to that found for Scandinavia and the Canadian Arctic (Briner et al., 2012; Young et al., 2013a; b). When other spallation scaling schemes are used (i.e., those of

Dunai (2001), Desilets and Zreda (2003), Desilets et al. (2006), and Lifton et al., (2005)), final calculated ages differ by only ~2 percent.

No correction for snow cover was made due to the size of the boulders (>1 m) (Gosse and Phillips, 2001; Young et al., 2013). Similarly, we do not correct for post-LGM isostatic uplift or late-Holocene subsidence (e.g., Sparrenbom et al., 2006a; b; Long et al., 2011). The marine limit at Qaqortoq, Paamiut, and Nuuk is between 30 and 90 m asl (Kelly, 1985; Bennike et al., 2002; Sparrenbom et al., 2006a; Woodroffe et al., 2014), and taking an average of elevations experienced by samples since exposure yields very small changes from the samples' modern elevations (Kelly et al., 2008; Young et al., 2013). Sisimiut, with a marine limit of ~140 m (Kelly, 1985), has experienced more isostatic rebound, but the effects are still small relative to the uncertainty in the ^{10}Be measurements (Kelly et al., 2008; Rinterknecht et al., 2009; Hughes et al., 2012; Young et al., 2013). We use the Shapiro-Wilk test to determine if the ages within a sample set were normally distributed. We identify potential statistical outliers using Chauvenet's criterion of exclusion (noted in Table 2) and make our decision to exclude based on stratigraphic consistency with both samples from this study and from published studies. For each elevation where we have multiple samples, we calculated an error-weighted mean age and error-weighted mean uncertainty to account for varying analytical uncertainties. The latter is possible because each of our sample sets overlaps within the analytical uncertainty (Bevington and Robinson, 2002).

We use our coastal ^{10}Be ages along elevation transects to calculate ice thinning rates at four study locales along southwest Greenland. We also compare our lower elevation coastal ages to ^{10}Be surface exposure ages from samples inland (Carlson et al., in press; Larsen et al., 2014) of each of our four sites in order to calculate ice retreat rates from the coast to the position of the

modern margin. Data from Roberts et al. (2009), Rinterknecht et al. (2009), Levy et al. (2012), Carlson et al. (in press) and Larsen et al. (2014) were recalculated using the Young et al. (2013) Arctic spallation production rate to facilitate inter-study comparison. We measure retreat distance between coastal and inland locales for the three southern sites using along-fjord lengths measured in Google Earth. For Sisimiut-inland ice, we measure retreat distance linearly between the two sites. Maximum, minimum, and mean thinning and retreat rates are provided in Table 3.

3.4. Results

Surface exposure ages for our four sample locations are presented in Table 2. At our northernmost site, Sisimiut, high elevation samples at ~590 m (n=5) date to between 17.8 ± 1.1 and 37.6 ± 2.1 ka, with all but one samples dating to well before the LGM (Fig. 2, 3, 4). We note that in our presentation of results, we refer to internal uncertainties derived from uncertainty in the AMS ^{10}Be measurement. A full description of uncertainty calculation is provided in Appendix A3.1. External uncertainties incorporating both this uncertainty and that associated with the ^{10}Be production rate are listed in Table 2. At lower elevations (~160 m), Sisimiut samples (n=4) date to between 10.1 ± 0.6 and 15.2 ± 0.9 ka. The 10.1 ka date is likely too young, and does not overlap with the other three dates within uncertainty. Thus, these lower elevation samples yield an error-weighted mean and uncertainty of 14.5 ± 0.6 ka if the 10.1 ka outlier is excluded.

Near Nuuk, high elevation samples at ~420 m (n=4) date between 9.7 ± 1.4 ka and 11.4 ± 2.6 ka (Table 2), produce an error-weighted mean and uncertainty of 10.7 ± 0.6 ka (Figs. 2, 3). Middle elevation samples at ~330 m (n=2) date to between 9.6 ± 0.6 ka and 9.9 ± 0.9 ka, with an

average of 9.7 ± 0.5 ka. Low elevation samples at ~ 140 m ($n=4$) yield ages between 9.7 ± 1.1 and 14.9 ± 2.6 ka, and an error-weighted mean of 11.0 ± 0.7 ka.

The Paamiut sampling location has a high elevation deglacial age ($n=1$) of 11.7 ± 0.6 ka at ~ 515 m (Table 2, Figs. 2, 3). The next sample site downhill at ~ 445 m has ages ($n=3$) between 8.9 ± 1.2 ka and 11.0 ± 2.0 ka. We calculate an error-weighted mean of 10.6 ± 1.0 ka. Middle elevations at ~ 250 m ($n=2$) result in ages of 9.9 ± 0.7 ka and 10.0 ± 0.6 ka, averaging 9.9 ± 0.4 ka. Low elevation ages at ~ 60 m ($n=5$) between 9.7 ± 1.5 ka and 14.3 ± 3.3 ka have an error-weighted mean of 11.2 ± 0.5 ka.

Finally, Qaqortoq high elevation ages at ~ 400 m ($n=3$) date to 9.8 ± 2.2 ka to 11.9 ± 0.8 ka (Table 2, Figs. 2, 3). Here, we calculate an error-weighted mean of 11.7 ± 0.5 ka. Upper-middle elevation ages at ~ 320 m ($n=4$) date to 8.8 ± 2.6 ka to 13.7 ± 4.2 ka with an error-weighted mean of 12.3 ± 1.1 ka. Lower-middle elevation ages at ~ 180 m ($n=3$) date to 10.5 ± 1.1 ka to 12.7 ± 0.6 ka and an error-weighted mean of 12.5 ± 0.4 ka. Low elevation ages at ~ 100 m ($n=3$) date from 7.2 ± 1.0 ka to 9.3 ± 1.2 ka, with an error-weighted mean of 8.6 ± 0.6 ka.

3.5. Timing and Rates of Deglaciation

3.5.1 Sisimiut

Four out of the five high-elevation Sisimiut boulder samples from above the regional trimline (Kelly, 1985) cluster around 36.5 ± 0.8 ka, which pre-dates the global LGM (Clark et al., 2009), with only one sample dating from the last deglaciation. Kelly (1985), Roberts et al. (2009) and Rinterknecht et al. (2009) suggested that the trimline below the high-elevation samples represents an ice-sheet boundary, with ice-free conditions above the weathering limit during the LGM (Fig. 5). Alternatively, the pre-LGM dates at the high elevations near Sisimiut

may be due to the presence of cold-based, less erosive ice during the last glacial period, and contain inherited nuclides.

Roberts et al. (2009) report bedrock exposure ages at high elevations near Sisimiut of 24.2 ± 1.3 ka to 165.7 ± 8.2 ka (Figs. 2A, 4). Rinterknecht et al. (2009) report a boulder age from above the trimline of 21.7 ± 4.1 ka (Figs. 2A, 4), which overlaps with our deglacial-age boulder sample. Given the occurrence of bedrock ^{10}Be ages above the trimline that pre-date the LGM but are much younger than the penultimate deglaciation (Rinterknecht et al., 2009; Roberts et al., 2009) and that at least two boulder samples from above the trimline are deglacial in age (Table 2; Rinterknecht et al., 2009), we suggest that the trimline likely represents an englacial thermal boundary. Above this demarcation cold-based ice cover during the LGM only partly removed bedrock and boulder surfaces that had been previously exposed. This inference of cold-based ice agrees with other studies in Greenland where bedrock surfaces above an erosional trimline contained significant inheritance while boulder surfaces from above the trimline sometimes contained minimal inheritance (Corbett et al., 2013; Roberts et al., 2013; Lane et al., 2014; Larsen et al., 2014). Our single LGM-early deglacial age likely exhibits the least inheritance and is the most accurate date for the deglacial chronology.

Therefore, we use only the younger deglaciation age when calculating thinning from high elevation near Sisimiut. Using this single high-elevation date of 17.8 ± 1.1 ka and the low elevation error-weighted mean of 14.5 ± 0.6 ka, ~ 440 m of thinning occurred at this location over the course of ~ 3 ka. Thinning rates are between 0.1 - 0.3 m yr^{-1} .

Our ^{10}Be ages, and those of Rinterknecht et al. (2009) and Roberts et al. (2009), suggest an early onset of deglaciation from the coast near Sisimiut, around the onset of Northern Hemisphere deglaciation (e.g., Clark et al., 2009; Carlson and Winsor, 2012). While limited,

there is evidence for retreat of southeast and east GrIS margins before ~17 ka (Nam et al., 1995; Andrews et al., 1997; Carlson et al., 2008). Our timing of the pull back of the GrIS from the Sisimiut coast at ~14.8 ka is earlier than, but not inconsistent with, reconstructions based on minimum-limiting ^{14}C dates (Long et al., 2009; Bennike et al., 2011). Our timing of coastal retreat is concurrent with the initial retreat of the west GrIS margin from the continental shelf break west of Disko Bugt (O’Cofaigh et al., 2013). ^{10}Be ages on valley glacier moraines in Scoresby Sund also show that the much larger LGM outlet glacier had retreated from the shelf before ~14 ka (Kelly et al., 2008). Therefore, the GrIS retreat recorded around Sisimiut may not be an isolated phenomenon as there is limited evidence elsewhere on Greenland for such early deglacial thinning and retreat.

While exposure at the coast occurred in the early part of the last deglaciation, the GrIS margin retreated to its present extent by the middle Holocene. The Carlson et al. (in press) and Levy et al. (2012) ^{10}Be exposure ages from near the inland ice margin average 6.7 ± 0.2 ka ($n=16$). Using our low elevation error-weighted mean ^{10}Be age of 14.5 ± 0.6 ka, calculated retreat rates from Sisimiut to the inland ice are $15\text{-}20$ m yr^{-1} . A prolonged retreat from Sisimiut to the modern GrIS margin is consistent with persistent glacially derived sediments deposited in the Kangerlussuaq fjord until ~7 ka (Storms et al., 2012). This slow retreat of the southwest GrIS margin from Sisimiut is also reconstructed by Rinterknecht et al. (2009), which has the ice margin ~20 km west of its present extent at ~9 ka.

3.5.2 Nuuk

Exposure ages from coastal Nuuk indicate that ice thinned ~280 m between 10.7 ± 0.6 ka and 11.0 ± 0.7 ka. Our middle elevation average age at Nuuk of 9.7 ± 0.5 ka overlaps within

uncertainty with the overall thinning history. The minimum estimated thinning rate is $\sim 0.3 \text{ m yr}^{-1}$ and the maximum thinning rate is essentially instantaneous within the uncertainties of our measurements. The timing of coastal retreat is consistent with minimum-limiting ^{14}C ages in the fjord west of our Nuuk samples of ~ 10.7 to ~ 11.4 ka (Larsen et al., 2014). Likewise, three coastal ^{10}Be boulder ages several fjords south of Nuuk range from 10.4 ± 0.4 ka to 10.8 ± 0.7 ka (Larsen et al., 2014), in excellent agreement with our ^{10}Be ages. The similarity between our dataset and that of Larsen et al. (2014) provides support for the high degree of reproducibility of ^{10}Be exposure ages in this region.

We calculate a minimum retreat rate from Nuuk of $\sim 65 \text{ m yr}^{-1}$ (Table 3), using an error-weighted mean age of 10.1 ± 0.3 ka from published ^{10}Be ages ($n=3$) just to the south of the head of Nûp Kangerdlua (Larsen et al., 2014), and our low elevation date of 11.0 ± 0.7 ka. The maximum retreat is essentially instantaneous within the uncertainty of these dates. This range somewhat lower than that estimated by Larsen et al. (2014) of $90\text{-}210 \text{ m yr}^{-1}$. We note that the lack of ^{10}Be ages at the head of Nûp Kangerdlua preclude a more precise retreat rate, but our retreat rates are consistent with minimum-limiting radiocarbon ages from the Nûp Kangerdlua fjord (Weidick, 1976; Larsen et al., 2014).

3.5.3 Paamiut

At Paamiut, ~ 450 m of surface exposure occurred between 11.7 ± 0.6 ka and 11.2 ± 0.5 ka. Our highest elevation site is only dated by one boulder sample, but another three boulder samples from ~ 70 m lower are 10.6 ± 1.0 ka in age. The middle elevation site mean age of 9.9 ± 0.4 ka is almost within stratigraphic order. We estimate thinning rates between infinite and ~ 0.3

m yr⁻¹. Our timing of retreat from the coast at ~11.2 ka agrees with the oldest minimum-limiting ¹⁴C date in the region of ~11 ka (Woodroffe et al., 2014).

Carlson et al. (in press) dated the GrIS margin nearing its current extent up-fjord from Paamiut at 10.4 ± 0.4 ka (n=4), which overlaps with our low elevation date of 11.2 ± 0.5 ka. Another five boulder dates from high elevations (~740 m asl) near the inland GrIS margin averaged 10.7 ± 0.1 ka. (Carlson et al., in press). Therefore, simultaneous deglacial exposure at the coastal Paamiut site and the modern outlet glacier terminus, ~40 km away, is possible within uncertainty (Table 3). We calculate a minimum retreat rate of ~25 m yr⁻¹. The timing of retreat from the coast up-fjord is in general agreement with the last pulse in ice-rafted debris north of Paamiut ~11 ka to ~9 ka (Fig. 1) (Knutz et al., 2011), where icebergs would be transported in the West Greenland Current.

3.5.4 Qaqortoq

At the low elevation Qaqortoq site (~100 m above sea level), the error-weighted mean is 8.5 ± 1.0 ka (Table 3). Minimum-limiting ¹⁴C ages show ice-free conditions in fjords near Qaqortoq by ~11 ka (Sparrenbom et al., 2006a). Therefore, we suggest that the three lowest elevation Qaqortoq boulders are erroneously young and may have experienced post-depositional rolling or delayed exposure due to sediment uncovering. As a result, we calculate thinning rates over ~220 m between our highest elevation site (11.7 ± 0.5 ka) and our second lowest elevation site (~180 m; 12.5 ± 0.4 ka). Rates imply nearly instantaneous (within a few centuries) exposure of high and low elevation samples, being between ~2 m yr⁻¹ to infinite within the uncertainty of our measurements (Table 3). Our estimated occurrence of ice-free conditions at the coast of 12.5 ± 0.4 ka is ~1 ka earlier than the earliest exposure inferred from surrounding ¹⁴C dates (Bennike

& Björck, 2002; Weidick et al., 2004; Sparrenbom et al., 2006a; 2006b), but is still consistent given the limiting nature of the ^{14}C dates. Our ^{10}Be ages also agree with the oldest minimum-limiting age from the outermost island southwest of Qaqortoq suggesting ice-free conditions by ~ 14.1 ka (Bennike & Björck, 2002; Sparrenbom et al., 2006b).

Inland of Qaqortoq near the present ice margin near the town of Narsarsuaq, surface exposure boulder ages ($n=4$) date to 11.1 ± 0.2 ka (Carlson et al., in press). This data and our lowest in situ elevation Qaqortoq boulder date (12.5 ± 0.4 ka) suggest retreat rates from Qaqortoq inland of $35\text{-}95$ m yr^{-1} (Table 3). Using mainly minimum-limiting ^{14}C dates, Larsen et al. (2011) estimated a minimum retreat rate of ~ 30 m yr^{-1} , which is slightly slower than our ^{10}Be -based estimates. A GrIS runoff record from south of Qaqortoq on the Eirik Drift (Fig. 1) shows the major peak in GrIS deglaciation occurring ~ 13.0 ka to ~ 10.5 ka (Carlson et al., 2008; Fig. 6h), concurrent with our ^{10}Be dated ice retreat in southernmost Greenland.

3.5.5. Summary of thinning and retreat rates

We have calculated thinning rates at the coast, and retreat rates inland of these sites, using a combination of new ^{10}Be ages and previously analyzed ^{10}Be samples (Table 3, Figs. 3, 7; Larsen et al., 2014; Carlson et al., in press). Coastal thinning occurred slowly at Sisimiut (0.1 to 0.3 m yr^{-1}), more rapidly at Nuuk and Paamiut (0.3 m yr^{-1} to instantaneous exposure), and extremely rapidly at Qaqortoq (2 m yr^{-1} to instantaneous exposure) (Fig. 7). Retreat inland from Sisimiut was also relatively slow, at a rate of $15\text{-}20$ m yr^{-1} . Retreat from Qaqortoq was faster, at $35\text{-}95$ m yr^{-1} . From coastal Paamiut, minimum retreat was 25 m yr^{-1} , and the maximum retreat rate implies instantaneous exposure within our uncertainties. Retreat from Nuuk is estimated to

have had a minimum value of 65 m yr^{-1} and a maximum that, like at Paamiut, implies instantaneous exposure within uncertainty (Fig. 7).

These retreat rates are similar to, though potentially faster than, those estimated for other GrIS margins. Roberts et al. (2013) estimated deglacial retreat of the Uummannaq ice stream (71.0°N , 53.7°W ; Fig. 1), west Greenland, at $\sim 30 \text{ m yr}^{-1}$. This is slower than all but one of our retreat rates for Qaqortoq, Paamiut, and Nuuk, and faster than maximum rates at Sisimiut (Table 2, Fig. 3). Just south of Nuuk, Larsen et al. (2014; Fig. 1) calculated a retreat rate of $90\text{--}210 \text{ m yr}^{-1}$. Our minimum retreat rate from Nuuk is identical to their minimum value, with our maximum rate of infinite-within-uncertainty being greater than the Larsen et al. (2014) maximum estimate. In southeastern Greenland, Hughes et al. (2012) document late deglacial retreat rates of $\sim 80 \text{ m yr}^{-1}$ for Helheim Glacier in Sermilik Fjord (65.9°N , 37.8°W ; Fig 1), with exposure onset at $\sim 13 \text{ ka}$ to $\sim 10 \text{ ka}$ and no difference in exposure times at the head versus mouth of the fjord. This is comparable to our minimum retreat rate estimates at Nuuk, our maximum estimate at Qaqortoq, and between our minimum and maximum values at Paamiut (Table 2, Fig. 3). The Helheim retreat rates are, however, certainly much swifter than at Sisimiut (Fig. 3; Hughes et al., 2012).

3.6. Environmental Influences on southwest Greenland Deglaciation

Why did retreat inland from Sisimiut occur at a slower average pace than at the three more southern sites? We suggest that this difference is primarily due to the relatively weak marine influence on the transect inland from Sisiumt. The Sisimiut fjord system is less extensive than the fjords around Qaqortoq, Paamiut, and Nuuk (Fig. 2). This means that the ice margin near Sisimiut would have become isolated from deep marine influences before reaching Kangerlussuaq, even with a marine limit of $\sim 140 \text{ m}$ above modern sea level (Kelly, 1985). Just

to the west of Kangerlussuaq (Fig 2), Kelly (1985) observed a marine limit of 65 m asl, and at Mt. Keglen (~ 15 km distal of the modern margin) a marine limit of ~50 m asl. These are consistent with minimum marine limit estimates of Ten Brink (1974) (Storms et al., 2012). Modern minimum elevation in these shallow valleys are on the order of 100-150 m asl, permitting ~250-300 m of maximum water depth at the retreating ice margin close to the modern coastline, and ~100-150 m maximum depth close to the modern inland ice. However, low elevation valleys are very narrow and winding in this region, with much intervening topography that would have limited the areal contact of the ice margin with the penetrating marine system. Considering this topography inland of our Sisimiut study location, and as suggested by Bennike and Björck (2002), the glaciers of this region would therefore lose mass primarily via surface melting as opposed to by calving and submarine basal melting.

Compared to Sisimiut, the sites of Nuuk, Paamiut and Qaqortoq experienced relatively strong marine influence on retreat. The outer sill at Nuuk is ~170 m below modern sea level (Mortensen et al., 2011), and with a coastal marine limit of ~90 m (Kelly, 1985), this restricted deglacial seawaters deeper than ~260 m from entering the fjord. Unlike the fjords near Sisimiut, the fjord inland of Nuuk deepens. The two southernmost outlet glaciers entering Nûp Kangerdlua (Fig. 2b) are estimated to be grounded below sea level near their modern margin (Morlighem et al., 2014). Although fjord bathymetry is not constrained at Paamiut, Morlighem et al. (2014) indicate that subglacial bed topography upstream from the modern outlet-glacier terminus is below sea level. The bed of outlet glacier Kragtût Sermiat, at the head of our Qaqortoq transect, (Fig. 2d), is above modern sea level, although other nearby glacier termini are grounded below sea level and fjords do extend inland close to the Kragtût Sermiat terminus (Morlighem et al., 2014). This relatively shallow topography may help explain the slower maximum retreat rate

estimated at Qaqortoq, compared to those at Nuuk and Paamiut (Fig. 3). However, considered as a whole, the fjords of Nuuk, Paamiut, and Qaqortoq are wider and deeper than the fjords near Sisimiut and extend inland close to or at the modern GrIS margin. It is therefore likely that calving and submarine melting played a larger role for GrIS mass loss near Nuuk, Paamiut and Qaqortoq relative to mass loss near Sisimiut. These additional ablation mechanisms may thus explain the more rapid thinning and retreat inland near Nuuk, Paamiut, and Qaqortoq relative to Sisimiut.

Ocean forcings on ablation is supported by regional paleoclimate records. Deglacial warming of the eastern Labrador Sea began ~13 ka and reached maximum warmth by ~10 ka, likely due to the influx of warm Irminger Current waters (Solignac et al., 2004; Knutz et al., 2011; Winsor et al., 2012; Fig 6f). This warming is concurrent with up-fjord ice retreat at our three southern locations. The strong contrast between the timing and rate of thinning and retreat at Sisimiut, which is less exposed to marine influences (Møller et al., 2006; Mortensen et al., 2011), and the other sites that have extensive fjord systems, could therefore be explained by the relative strength of marine influence on local ice margins.

3.7. Conclusions

We present a new deglacial thinning and retreat chronology of four outlet glaciers in southwestern Greenland using ^{10}Be surface exposure dating. Our data show that ice retreat in three of the fjords occurred at 13.0-11.0 ka at rates $>25\text{-}65\text{ m yr}^{-1}$ (Table 3). Ice retreat in a fourth fjord with relatively little marine influence (being shallow and short) occurred comparatively earlier (~17.8 ka to ~14.6 ka), but at a rate of only $\sim 20\text{ m yr}^{-1}$. Together, our fjord retreat chronology suggests that ocean warming—and transfer of ocean heat to the outlet glacier

systems—played an important role in the timing and rate of southwestern GrIS retreat. Such a marine influence on ice retreat is consistent with modern observations of accelerated outlet glacier thinning and retreat coeval with the incursion of warmer waters into Greenland fjord systems (e.g., Holland et al., 2008; Murray et al., 2010; Straneo et al., 2010). Interestingly, modern ice thinning rates for marine margins are in some places $>0.2 \text{ m yr}^{-1}$ (Pritchard et al., 2009). Our deglacial ^{10}Be chronology suggests that such rates could be sustained for centuries in marine-terminating settings, with attendant significant mass loss from the GrIS.

Acknowledgements

The authors would like to thank Elizabeth Siewert, Elizabeth Obbink, Sarah Strano, Robert Hatfield, and David Ullman for assistance in field sample collection. Fred Luiszer, Daniel S. Murray, David J. Ullman, Brent Goehring, Shaun Marcott, and Richard A. Becker aided in laboratory preparation of cosmogenic nuclide samples. Alberto V. Reyes provided helpful comments on an earlier draft. Funding for this study was provided by National Geographic Society (award 8687-09; AEC), the National Science Foundation Graduate Fellowship Research Program (KW), the Geological Society of America (KW), and the University of Wisconsin-Madison Department of Geoscience (KW, AEC).

References

- Alley, R.B., Clark, P.U., Huybrechts, P., and Joughin, I., 2005, Ice-sheet and sea-level changes: *Science*, 310, 456-460.
- Anderson, N.J., Bennike, O., Christofferson, K., Jeppesen, E., Markager, S., Miller, G., and Renberg, I., 1999, Limnological and palaeolimnological studies of lakes in south-western Greenland: *Geology og Greenland Survey Bulletin*, 183, 68-74.
- Andresen, C.S., Björck, S., Bennike, O., Bond, G., 2004. Holocene climate changes in southern Greenland. *Journal of Quaternary Science*, 18, 783-795.
- Andrews, J.T., Smith, L.M., Preston, R., Cooper, T., and Jennings, A.E., 1997. Spatial and temporal patterns of iceberg rafting (IRD) along the East Greenland margin, ca. 68°N, over the last 14 cal.ka. *Journal of Quaternary Science*, 12, 1-13.
- Axford, Y., Lose, S., Briner, J.P., Francis, D.R., Langdon, P.G., Walker, I.R., 2013. Holocene temperature history at the western Greenland Ice Sheet margin. *Quaternary Science Reviews*, 59, 87-100.
- Balco, G., 2011. Contributions and unrealized potential contributions of cosmogenic-nuclide exposure dating to glacier chronology, 1990-2010. *Quaternary Science Reviews*, 30, 3-27.
- Balco, G., Stone, J.O., Lifton, N.A., Dunai, T.J., 2008. A complete and easily accessible means of calculating surface exposure ages or erosion rates from ^{10}Be and ^{26}Al measurements. *Quaternary Geochronology*, 3, 174-195.
- Balco, G., Briner, J., Finkel, R.C., Rayburn, J.A., Ridge, J.C., Schaefer, J.M., 2009. Regional beryllium-10 production rate calibration for late-glacial northeastern North America. *Quaternary Geochronology*, 4, 93-107.
- Bennike, O., and Weidick, A., 2001, Late Quaternary history around Nioghalvfjærdsfjorden and Jokelbugten, North-East Greenland: *Boreas*, v. 30, p 205-227.
- Bennike, O., and Bjorck, S., 2002, Chronology of the last recession of the Greenland Ice Sheet: *Journal of Quaternary Science*, v. 17, p. 211-219.
- Bennike, O., Bjorck, S., and Lambeck, K., 2002, Estimates of South Greenland late-glacial ice limits from a new relative sea level curve: *Earth and Planetary Science Letters*, v. 197, p. 171-186.
- Bennike, O., Wagner, B., Richter, A., 2011. Relative sea level changes during the Holocene in the Sisimiut area, south-western Greenland: *Journal of Quaternary Science*, v. 26, p. 353-361.

- Bevington, P. and Robinson, D.K., 2002. *Data Reduction and Error Analysis for the Physical Sciences*. McGraw-Hill, Boston, USA, 336 pgs.
- Briner, J.P., Young, N.E., Goehring, B.M., Schaefer, J.M., 2012. Constraining Holocene ^{10}Be production rates in Greenland. *Journal of Quaternary Science*, 27, 2-6.
- Carlson, A.E., and Winsor, K., 2012. Northern Hemisphere ice-sheet responses to past climate warming: *Nature Geoscience*, 5, 607-613.
- Carlson, A.E., Stoner, J.S., Donnelly, J.P., and Hillaire-Marcel, C., 2008, Response of the southern Greenland Ice Sheet during the last two deglaciations: *Geology*, v. 36, p. 359-362
- Carlson, A.E., Winsor, K., Ullman, D.J., Brook, E., Rood, D.H., Axford, Y., LeGrande, A.N., Anslow, F., and Sinclair, G., Earliest Holocene south Greenland ice-sheet retreat within its late-Holocene extent. in review at *Geophysical Research Letters*.
- Clark, P.U., Dyke, A.S., Shakun, J.D., Carlson, A.E., Clark, J., Wohlfarth, B., Mitrovica, J.X., Hostetler, S.W., and McCabe, A.M., 2009. The Last Glacial Maximum: *Science*, 325, 710-714
- Corbett, L.B., Young, N.E., Bierman, P.R., Briner, J.P., Neumann, T.A., Rood, D.H., Graly, J.A., 2011. Paired bedrock and boulder ^{10}Be concentrations resulting from early Holocene ice retreat near Jakobshavn Isfjord, western Greenland. *Quaternary Science Reviews*, 30, 1739-1749.
- Cuffey, K.M., Clow, G.D., 1997. Temperature, accumulation, and ice sheet elevation in central Greenland through the last deglacial transition. *Journal of Geophysical Research*, 102, 26,383-26,396.
- Dahl-Jensen, D., Mosegaard, K., Gundestrup, N., Clew, G.D., Johnsen, S.J., Hansen, A.W., Balling, N., 1998. Past temperatures directly from the Greenland ice sheet. *Science*, 282, 268-271.
- de Vernal, A., Hillaire-Marcel, C., Turon, J-L., and Matthiessen, J., 2000, Reconstruction of sea-surface temperature, salinity, and sea-ice cover in the northern North Atlantic during the last glacial maximum based on dinocyst assemblages: *Canadian Journal of Earth Sciences*, v. 37, no. 5, p. 725-750.
- de Vernal, A., Rosell-Melè, A., Kucera, M., Hillaire-Marcel, C., Eynaud, F., Weinelt, M., Dokken, T., and Kageyama, M., 2006, Comparing proxies for the reconstruction of LGM sea-surface conditions in the northern North Atlantic: *Quaternary Science Reviews*, v. 25, p. 2820-2834.

- Desilets, D., and Zreda, M., 2003. Spatial and temporal distribution of secondary cosmic-ray nucleon intensities and applications to in-situ cosmogenic dating: *Earth and Planetary Science Letters*, 2006. 21-42.
- Desilets, D., Zreda, M., and Prabu, T., 2006. Extended scaling factors for in situ cosmogenic nuclides: new measurements at low latitude. *Earth and Planetary Science Letters*, 246, 265-276.
- Dowdeswell, J.A., 2006, The Greenland Ice Sheet and global sea-level rise: *Science*, v. 311, no. 5763, p. 963-964.
- Dunai, T.J., 2001, Influence of secular variation of the geomagnetic field on production rates of in situ produced cosmogenic nuclides: *Earth and Planetary Science Letters*, v. 193, p. 197-212.
- Fagel, N., Hillaire-Marcel, C., 2006. Glacial/interglacial instabilities of the Western Boundary Under Current during the last 365 kyr from Sm/Nd ratios of the sedimentary clay-size fractions at ODP site 646 (Labrador Sea): *Marine Geology*, v. 232, p. 87-99, doi:10.1016/j.margeo.2006.08.006.
- Fleming, K., Lambeck, K., 2004. Constraints on the Greenland Ice Sheet since the Last Glacial Maximum from sea-level observations and glacial-rebound models. *Quaternary Science Reviews* 23, 1053-1077.
- Funder, S., Hansen, L., 1996. The Greenland ice sheet; a model for its culmination and decay during and after the last glacial maximum. *Bulletin of the Geological Society of Denmark* 42, 137-152.
- Funder, S., Kjeldsen, K.K., Kjær, Ó Cofaigh, C., 2011. The Greenland Ice Sheet during the past 300,000 years: a review. In: Ehlers, J., Gibbard, P.L., and Hughes, P.D., (Eds.) *Developments in Quaternary Science*, v. 15, Amsterdam, The Netherlands, pp. 699-713.
- Gosse, J.C., and Phillips, F.M., 2001, Terrestrial in situ cosmogenic nuclides: theory and application: *Quaternary Science Reviews*, v. 20, p. 1475-1560.
- Grootes, P.M., Stuiver, M., 1997. Oxygen 18/16 variability in Greenland snow and ice with 10^3 to 10^5 -year time resolution: *Journal of Geophysical Research*, v. 102, p. 26455-26470.
- Håkansson, L., Briner, J., Alexanderson, H., Aldahan, A., and Possnert, G., 2007, ^{10}Be ages from central east Greenland constrain the extent of the Greenland ice sheet during the Last Glacial Maximum: *Quaternary Science Reviews*, v. 26, 2316-2321.
- Håkansson, L., Graf, A., Strasky, S., Ivy-Ochs, S., Kubik, P.W., Hjort, C., and Schluchter, C., Cosmogenic ^{10}Be -ages from the Store Koldewey Island, NE Greenland: *Swedish Society for Anthropology and Geography*, 89A (3), p. 195-202.

- Håkansson, L., Briner, J.P., Aldahan, A., and Possnert, G. (submitted). ^{10}Be and ^{26}Al exposure ages of tors and meltwater channels on Jameson Land, east Greenland: Implications for the Late Quaternary glaciation history. *Quaternary Research*.
- Håkansson, L., Alexanderson, H., Hjort, H., Möller, C., Briner, J.P., Aldahan, A. and Possnert, G. (in press). The late Pleistocene glacial history of Jameson Land, central East Greenland derived from cosmogenic ^{10}Be and ^{26}Al exposure dating. *Boreas*.
- Holland, D.M., Thomas, R.H., de Young, B., Ribergaard, M.H., and Lyberth, B., 2008, Acceleration of Jakobshavn Isbrae triggered by warm subsurface ocean waters: *Nature Geoscience*, v. 1, p. 659-664.
- Howat, I.M., Joughin, I., Fahnestock, M., Smith, B.E., and Scambos, T.A., 2008. Synchronous retreat and acceleration of southeast Greenland outlet glaciers 2000-06: ice dynamics and coupling to climate: *Journal of Glaciology*, 54, 646-660.
- Hughes, A.L.C., Rainsley, E., Murray, T., Fogwill, C.J., Schnabel, C., Xu, S., 2012. Rapid response of Helheim Glacier, southeast Greenland, to early Holocene climate warming: *Geology*, 40, 427-430.
- Jansen, E., Overpeck, J., Briffa, K.R., Duplessy, J.-C., Joos, F., Masson-Delmotte, V., Olago, D., Otto-Bliesner, B., Peltier, W.R., Rahmstorf, S., Ramesh, R., Raynaud, D., Rind, D., Solomina, O., Villalba, R., Zhange, D., 2007. Paleoclimate. In: Solomon, S., Qin, D., Manning, M., Chen, Z., Marquis, M., Averyt, K.B., Tignor, M., Miller, H.L. (Eds.), *Climate Change 2007: the Physical Science Basis. Contribution of Working Group I to the Fourth Assessment Report of the Intergovernmental Panel on Climate Change*. Cambridge University Press, Cambridge, United Kingdom and New York, NY, USA.
- Johnsen, S.J., Dahl-Jensen, D., Gundestrup, N., Steffensen, J.P., Clausen, H.B., Miller, H., Masson-Delmotte, V., Sveinbjönsdóttir, A.E., White, J., 2001. Oxygen isotope and paleotemperature records from six Greenland ice-core stations: Camp Century, Dye-3, GRIP, GRIP2, Renland and NorthGRIP: *Journal of Quaternary Science*, v. 16, p. 299-307.
- Kelly, M., 1980. The status of the Quaternary geology of western Greenland. *Rapport Grønlands GeoloGISke Undersøgelse*, 96, 24 pp.
- Kelly, M., 1985. A review of the Quaternary geology of western Greenland. In Andrews, J.T. (ed.): *Quaternary Environments Eastern Canadian Arctic, Baffin Bay and Western Greenland*, Allen & Unwin, Boston, USA, 461-501.
- Kelly, M.A., Lowell, T.V., 2009. Fluctuations of local glaciers in Greenland during latest Pleistocene and Holocene time. *Quaternary Science Reviews*, 28, 2088-2106.

- Kelly, M.A., Lowell, T.V., Hall, Shaefer, J.M., Finkel, R.C., Goehring, B.M., Alley, R.B., Denton, G.H., 2008, A ^{10}Be chronology of lateglacial and Holocene mountain glaciation in the Scoresby Sund region, east Greenland: implications for seasonality during lateglacial time: *Quaternary Science Reviews*, doi:10.1016/j.quascirev.2008.08.004.
- Kohl, C.P., and Nishiizumi, K., 1992, Chemical insolation of quartz for measurement of in-situ-produced cosmogenic nuclides: *Geochimica et Cosmochimica Acta*, v. 56, p. 3583-3587.
- Knutz, P.C., Sicre, M.-A., Ebbesen, H., Christiansen, S., Kuijpers, A., 2011. Multiple-stage deglacial retreat of the southern Greenland Ice Sheet linked with Irminger Current warm water transport: *Paleoceanography*, v. 26, PA3204, doi:10.1029/2010PA002053.
- Lal, D., 1991, Cosmic ray labeling of erosion surfaces: in situ nuclide production rates and erosion models: *Earth and Planetary Science Letters*, v. 104, p. 424-439.
- Lane, T.P., Roberts, D.H., Rea, B.R., Ó Cofaigh, C., Vieli, A., and Rodés, A., 2014. Controls upon the Last Glacial Maximum deglaciation of the northern Uummannaq Ice Stream System, West Greenland: *Quaternary Science Reviews*, 92, 324-344.
- Larsen, N.K., Kjær, K.H., Olsen, J., Funder, S., Kjeldsen, K.K., Nørgaard-Pedersen, N., 2011. Restricted impact of Holocene climate variations on the southern Greenland Ice Sheet. *Quaternary Science Reviews*, 30, 3171-3180.
- Larsen, N.K., Funder, S., Kjær, K.H., Kjeldsen, K.K., Knudsen, M.F., Linge, H., 2014. Rapid early Holocene ice retreat in West Greenland. *Quaternary Science Reviews*, in press, <http://dx.doi.org/10.1016/j.quascirev.2013.05.027>.
- Levy, L.B., Kelly, M.A., Howley, J.A., Virginia, R.A., 2012. Age of the Ørkendalen moraines, Kangerlussuaq, Greenland: constraints on the extent of the southwestern margin of the Greenland Ice Sheet during the Holocene. *Quaternary Science Reviews*, 52, 1-5.
- Lifton, N., Bieber, J., Clem, J., Duldig, M., Evenson, P., Huble, J., and Pyle, R., 2005. Addressing solar modulation and long-term uncertainties in scaling secondary cosmic rays for in situ cosmogenic nuclide applications: *Earth and Planetary Science Letters*, 239, 140-161.
- Long, A.J., Roberts, D.H., and Wright, M.R., 1999, Isolation basin stratigraphy and Holocene relative sea-level change on Arveprinsen Ejland, Disko Bugt, West Greenland: *Journal of Quaternary Science*, v. 14, no. 4, p. 323-345.
- Long, A.J., Woodroffe, S.A., Roberts, D.H., and Dawson, S., 2011. Isolation basins, sea-level changes and the Holocene history of the Greenland Ice Sheet. *Quaternary Science Reviews*, 30, 3748-3768.

- Lucotte, M., Hilliare-Marcel, C., 1994. Identification and distribution of the main water masses in the Labrador and Irminger Seas: *Canadian Journal of Earth Science*, v. 31, p. 5-13, doi:10.1139/e94-002.
- Marcott, S.A., Shakun, J.D., Clark, P.U., Mix, A.C., 2013. A reconstruction of regional and global temperature for the past 11,300 years. *Science*, 339, 1198-1201.
- Mernild, S.H., Hanna, E., McConnell, J.R., Sigl, M., Beckerman, A.P., Yde, J.C., Cappelen, J., Malmros, J.K., and Steffen, K., 2014. Greenland precipitation trends in a long-term instrumental climate context (1980-2012): evaluation of coastal and ice core records: *International Journal of Climatology*, doi:10.1002/joc.3986.
- Møller, H.S., Jensen, K.G., Kuijpers, S., Aagaard-Sørensen, S., Seidenkrantz, M.-S., Prins, M., Endler, R., Mikkelsen, N., 2006. Late-Holocene environment and climatic changes in Ameralik Fjord, southwest Greenland: evidence from the sedimentary record: *Holocene*, v. 15, p. 685-695.
- Morlighem, M., Rignot, E., Mouginot, J., Seoussi, H., and Larour, E., 2014. Deeply incised submarine glacial valleys beneath the Greenland Ice Sheet: *Nature Geoscience*, v. 7, p. 418-422.
- Mortensen, J., Lennert, K., Bendtsen, J., Rysgaard, S., 2011. Heat sources for glacial melt in a sub-Arctic fjord (Godthåbsfjord) in contact with the Greenland Ice Sheet. *Journal of Geophysical Research* 116, C01013.
- Murray, T., Scharrer, K., James, T.D., Dye, S.R., Hanna, E., Booth, A.D., Selmes, N., Luckman, A., Hughes, A.L.C., Cook, S., Huybrechts, P., 2010. Ocean regulation hypothesis for glacier dynamics in southeast Greenland and implications for ice sheet mass changes: *Journal of Geophysical Research*, 115, F03026, doi:10.1029/2009JF001522.
- Nam, S.I., Stein, R., Grobe, H., and Hubberten, H., 1995. Late Quaternary glacial-interglacial changes in sediment composition at the East Greenland continental margin and their paleoceanographic implications. *Marine Geology*, 122, 243-262.
- Nelson, A.H., Bierman, P.R., Shakun, J.D., and Rood, D.H., (in press), Using *in situ* cosmogenic ^{10}Be to identify the source of sediment leaving Greenland: *Earth Surface Processes and Landforms*, doi: 10.1002/esp.3565.
- Nishiizumi, K., Elmore, D., Ma, X.Z., Arnold, J.R., 1984. ^{10}Be and ^{36}Cl profiles in an Apollo 15 drill core. *Earth and Planetary Science Letters*, 70, 157-163.
- Nishiizumi, K., Imamura, M., Caffee, M., Southon, J.R., Finkel, R.C., McAninch, J., 2007. Absolute calibration of ^{10}Be AMS standards. *Nuclear Instruments & Methods in Physics Research Section B: Beam Interactions with Materials and Atoms*, 258, 403-413.

- Nishiizumi, K., Kohl, C.P., Arnold, J.R., Klein, J., Fink, D., and Middleton, R., 1991, Cosmic ray produced ^{10}Be and ^{26}Al in Antarctic rocks: exposure and erosion history: *Earth and Planetary Science Letters*, v. 104, p. 440-454.
- Nishiizumi, K., Lal, D., Klein, J., Middleton, R., and Arnold, J.R., 1986, Production of ^{10}Be and ^{26}Al by cosmic rays in terrestrial quartz in situ and implications for erosion rates: *Nature*, v. 319, p. 134-136.
- Overpeck, J.T., Otto-Bliesner, B.L., Miller, G.H., Muhs, D.R., Alley, R.B., and Kiehl, J.T., 2006, Paleoclimatic evidence for future ice-sheet instability and rapid sea-level rise: *Science*, v. 311, p. 1747-1750.
- Pritchard, H.D., Arthern, R.J., Vaughan, D.G., Edwards, L.A., 2009. Extensive dynamic thinning on the margins of the Greenland and Antarctic ice sheets: *Nature*, v. 461, 971-975.
- Rignot, E., Kanagaratnam, P., 2006. Changes in the velocity structure of the Greenland Ice Sheet: *Science*, v. 311, p. 986-990.
- Rignot, E., Koppes, M., Velicogna, I., 2010. Rapid submarine melting of the calving faces of West Greenland glaciers: *Nature Geoscience*, v. 3, p. 187-191.
- Rignot, E., Mouginot, J., 2012. Ice flow in Greenland for the International Polar Year 2008-2009: *Geophysical Research Letters*, v. 39, L11501, doi:10.1029/2012GL051634.
- Rinterknecht, V.R., Clark, P.U., Raisbeck, G.M., Yiou, F., Bitinas, A., Brook, E.J., Marks, L., Zelcs, V., Lunkka, J.-P., Pavlovskaya, I.E., Piotrowski, J.A., and Raukas, A., The last deglaciation of the southeastern sector of the Scandinavian Ice Sheet: *Science*, v. 311, p. 1449-1452.
- Rinterknecht, V., Gorokhovich, Y., Schaeffer, J., and Caffee, M., 2009, Preliminary ^{10}Be chronology for the last deglaciation of the western margin of the Greenland Ice Sheet: *Journal of Quaternary Science*, v. 24, no. 3, p. 270-278, doi:10.1002/jqs.1226.
- Roberts, D.H., Long, A.J., Schnabel, C., Freeman, S., and Simpson, M.J.R., 2008, The deglacial history of southeast sector of the Greenland Ice Sheet during the Last Glacial Maximum: *Quaternary Science Reviews*, v. 27, p. 1505-1516.
- Roberts, D.H., Long, A.J., Schnabel, C., Davies, B., Xu, S., Simpson, M.J.R., and Huybrechts, P., 2009. Ice sheet extent and early deglacial history of the southwestern sector of the Greenland Ice Sheet: *Quaternary Science Reviews*, 28, 2760-2773.
- Roberts, D.H., Long, A.J., Davies, B.J., Simpson, M.J.R., and Schnabel, C., 2010. Ice stream influence on West Greenland Ice Sheet dynamics during the Last Glacial Maximum: *Journal of Quaternary Science*, doi:10.1002/jqs.1354.

- Roberts, D.H., Rea, B.R., Lane, P.T., Schnabel, C., and Rodés, A., 2013. New constraints on Greenland ice sheet dynamics during the last glacial cycle: evidence from the Uummannaq ice stream system: *Journal of Geophysical Research: Earth Surface*, 118, 1-12.
- Rood, D.H., Hall, S., Guilderson, T.P., Finkel, R.C., Brown, T.A., 2010. Challenges and opportunities in high-precision Be-10 measurements at CAMS. *Nuclear Instruments and Methods B: Beam Interactions with Materials and Atoms*, 268, 730-732.
- Schuenemann, K.C., Cassano, J.J., and Finnis, J., 2013. Synoptic forcing of precipitation over Greenland: Climatology for 1961-99: *Journal of Hydrometeorology*, v. 10, p. 60-78.
- Simpson, J.R.M., Milne, G.A., Huybrechts, P., and Long, A.J., 2009. Calibrating a glaciological model of the Greenland ice sheet from the Last Glacial Maximum to present-day using field observations of relative sea level and ice extent. *Quaternary Science Reviews*, 28, 1630-1656.
- Solignac, S., de Vernal, A., and Hillaire-Marcel, C., 2004. Holocene sea-surface conditions in the North Atlantic—contrasted trends and regimes in the western and eastern sectors (Labrador Sea vs. Iceland Basin): *Quaternary Science Reviews*, 23, 319-334.
- Sparrenbom, C.J., Bennike, O., Björck, S., and Lambeck, K., 2006a. Holocene relative sea-level changes in the Qaqortoq area, southern Greenland: *Boreas*, v. 35, p. 171-187.
- Sparrenbom, C.J., Bennike, O., Björck, S., Lambeck, K., 2006b. Relative sea-level changes since 15 000 cal. yr BP in the Nanortalik area, southern Greenland: *Journal of Quaternary Science*, v. 21, p. 29-48.
- Sparrenbom, C.J., Bennike, O., Fredh, D., Randsalu-Wendrup, L., Zwart, D., Ljung, K., Björck, S., Lambeck, K., 2013. Holocene relative sea-level changes in the inner Bredefjord area, southern Greenland: *Quaternary Science Reviews*, v. 69, p. 107-124.
- Steffen, K., and Box, J., 2001. Surface climatology of the Greenland ice sheet: Greenland Climate Network 1995-1999: *Journal of Geophysical Research*, v. 106, p. 33,951-33,964.
- Stone, J.O., 2000. Air pressure and cosmogenic isotope production: *Journal of Geophysical Research*, v. 105, p. 23,753-23,759.
- Storms, J.E.A., de Winter, I.L., Overeem, I., Drikkoningen, G.G., Lykke-Anders, H., 2012. The Holocene sedimentary history of the Kangerlussuaq Ford-valley fill, West Greenland: *Quaternary Science Reviews*, v. 35, p. 29-50.
- Straneo, F., Curry, R.G., Sutherland, D.A., Hamilton, G.S., Cenedese, C., Våge, K., Stearns, L.A., 2011. Impact of fjord dynamics and glacial runoff on the circulation near Helheim Glacier: *Nature Geoscience*, v. 4, p. 322-327.

- Straneo, F., Hamilton, G.S., Sutherland, D.A., Stearns, L.A., Davidson, F., Hammil, M.O., Stenson, G.B., Rosing-Asvid, A., 2010. Rapid circulation of warm subtropical waters in a major glacial fjord in East Greenland: *Nature Geoscience*, v. 3, 182-186.
- Straneo, F., Heimbach, P., 2013. North Atlantic warming and the retreat of Greenland's outlet glaciers: *Nature*, v. 504, p. 36-43.
- Tauber, H., 1968. Copenhagen radiocarbon dates IX: *Radiocarbon*, 10, 295-327.
- Vinther, B.M., Andersen, K.K., Jones, P.D., Briffa, K.R., and Cappelen, J., 2006. Extending Greenland temperature records into the late eighteenth century: *Journal of Geophysical Research*, 111, D11105, doi:10.1029/2005JD006810.
- Weidick, A., 1963. Ice margin features in the Julianehåb district, South Greenland. *Meddelelser om Grønland*, 165, 133 pp.
- Weidick, A., 1976. Glaciation and the Quaternary in Greenland. In Escher, A., and Watt, W.S., (eds.), *Geology of Greenland*, 430-460, Geological Survey of Greenland, Copenhagen.
- Weidick, A., Kelly, M., and Bennike, O., 2004. Late Quaternary development of the southern sector of the Greenland Ice Sheet, with particular reference to the Qassimiut lobe. *Boreas*, 33, 284-299.
- Winsor, K., Carlson, A.E., Klinkhammer, G.P., Stoner, J.S., Hatfield, R.G., 2012. Evolution of the northeast Labrador Sea during the last interglaciation: *Geochemistry, Geophysics, Geosystems*, 13, Q11006, doi:10.1029/2012GC004263.
- Woodroffe, S.A., Long, A.J., Lecavalier, B.S., Milne, G.A., Bryant, C.L., 2014. Using relative sea-level data to constrain the deglacial and Holocene history of southern Greenland: *Quaternary Science Reviews*, 92, 345-356.
- Young, N.E., Schaefer, J., Briner, J.P., Goehring, B., 2013. A ^{10}Be production-rate calibration for the Arctic, *Journal of Quaternary Science*, 28, 515-526.

Figure Captions:

Figure 1. Index map of Greenland study locales. Shown are: previous ^{10}Be exposure ages (yellow circles), ^{10}Be dates from this study (orange circles), GISP2 ice core location (blue square), and mapped modern elevations (m) above sea level (courtesy of G. Sinclair). Previous studies are numbered accordingly: ¹Carlson et al. (in press), ²Hughes et al. (2012), ³Kelly et al. (2008), ⁴Larsen et al. (2014), ⁵Levy et al. (2012), ⁶Roberts et al. (2013).

Figure 2. Close-up satellite imagery showing the study sites of A. Sisimiut, B. Nuuk, C. Paamiut, and D. Qaqortoq. Blue circles indicate sample locations for ^{10}Be dating published in Rinterknecht et al. (2009, medium blue), Roberts et al. (2009, light blue), and Larsen et al. (2014, medium blue). Orange circles mark our coastal locales, with nearby towns (pink circles), and yellow circles mark inland locales used to calculate retreat rates. Sites of relative sea level data are shown in green circles, with ages representing the start time of rapid deglacial sea level rise (Sparrenbom et al., 2006a; b; Woodroffe et al., 2014).

Figure 3. New ^{10}Be ages (circles) with internal errors for each boulder, with EWMs (orange squares) and EWM uncertainties for each elevation grouping. Outliers are included in this figure (gray circles), but pre-LGM Sisimiut dates are not. Bars indicate duration of coastal thinning as constrained by EWMs.

Figure 4. All ^{10}Be data from the Sisimiut region, including new ages from this study and data from Rinterknecht et al. (2009) and Roberts et al. (2009), recalculated using the Young et al. (2013) Arctic production rate for spallation.

Figure 5. Geomorphic difference between high-elevation Sisimiut and other coastal locales. (A) Highly weathered boulders in an environment resembling felsenmeer on the ridge-top sampling site at Sisimiut, and (B) glacially smoothed and exposed bedrock at the high elevation Nuuk site, exhibiting glacial scouring and little post-glaciation weathering.

Figure 6. Paleoclimate context for our ^{10}Be ages. (A-D) the EWM of our new coastal ^{10}Be dates (squares) and published inland ^{10}Be dates (open circles) (Carlson et al., in press; Larsen et al., 2014), (E) June insolation at 60°N (Berger and Loutre, 1991), (F) Ca-corrected Ti concentrations from the northeastern Labrador Sea representing GrIS runoff (Carlson et al., 2008), (G) Mg/Ca-derived calcification temperatures of *Neogloboquadrina pachyderma* (s) from the northeastern Labrador Sea (Winsor et al., 2012), and (H) Greenland ice core GISP2 $\delta^{18}\text{O}$ (Grootes and Stuiver, 1997).

Figure 7. Summary of ^{10}Be exposure ages from this study and from Levy et al. (2012)⁵, Larsen et al. (2014)⁴, Carlson et al. (in press)¹. Image is from Figure 1.

Table 1. Sampling and lab processing data for ^{10}Be surface exposure dating.

Sample Name	Latitude (N)	Longitude (E)	Elevation (m asl)	Shielding correction	Sample Thickness (cm)	Quartz mass (g)	9Be Carrier Added (g)
QAQORTOQ							
QQ-1-08	60.736	-46.033	313	1.000	2.0	12.002	0.502
QQ-2b-08	60.735	-46.033	326	1.000	2.0	46.976	0.508
QQ-3-08	60.735	-46.031	305	1.000	2.0	21.299	0.497
QQ-4-08	60.735	-46.031	305	1.000	1.0	11.220	0.502
QQ-5-08	60.732	-46.022	176	0.994	2.5	35.946	0.494
QQ-6-08	60.733	-46.018	97	0.991	1.0	28.401	0.511
QQ-7-08	60.733	-46.018	97	0.991	2.0	24.585	0.506
QQ-8-08	60.733	-46.018	97	0.991	2.0	26.268	0.506
QQ-1-10	60.744	46.046	399	1.000	1.0	21.769	0.251
QQ-2-10	60.744	-46.046	399	1.000	1.0	28.246	0.248
QQ-3-10	60.744	-46.046	399	1.000	1.0	28.937	0.248
QQ-4-10	60.731	-46.023	175	0.997	1.0	28.303	0.247
QQ-5-10	60.732	-46.023	185	0.996	2.0	27.219	0.248
PAAMIUT							
PA-1-10	62.004	-49.550	65	0.997	3.0	29.041	0.233
PA-2-10	62.004	-49.550	65	0.997	1.8	28.777	0.247
PA-3-10	62.004	-49.550	66	0.997	1.0	22.805	0.249
PA-4-10	62.005	-49.554	57	0.999	2.3	20.126	0.250
PA-5-10	62.005	-49.553	59	0.998	2.8	29.977	0.252
PA-6-10	62.012	-49.528	515	0.959	2.0	30.233	0.247
PA-7-10	62.012	-49.528	499	0.985	2.0	29.481	0.252
PA-8-10	62.011	-49.530	448	0.990	2.3	28.774	0.252
PA-9-10	62.011	-49.530	448	0.990	3.4	29.376	0.250
PA-10-10	62.011	-49.529	439	0.988	3.3	32.242	0.250
PA-11-10	62.007	-49.538	257	0.994	1.5	23.717	0.248
PA-12-10	62.007	-49.540	251	0.994	3.5	26.043	0.248
NUUK							
NU-1-10	64.178	-51.674	126	0.995	2.6	20.824	0.248
NU-2-10	64.178	-51.672	149	0.997	2.0	17.984	0.249
NU-3-10	64.178	-51.673	144	0.996	1.9	20.113	0.250
NU-4-10	64.187	-51.645	427	1.000	2.7	23.071	0.249
NU-5-10	64.187	-51.645	427	1.000	3.8	20.305	0.250
NU-1-2008	64.187	-51.646	419	1.000	2.5	22.578	0.249
NU-2-2008	64.187	-51.646	422	1.000	2.0	19.258	0.248
NU-4-2008	64.183	-51.657	334	0.998	1.5	23.837	0.248
NU-5-2008	64.182	-51.657	333	0.998	2.0	21.456	0.248
NU-7-2008	64.178	-51.672	146	0.997	1.5	22.739	0.251
SISIMIUT							
SM-1-2009	66.928	-53.577	588	1.000	1.5	20.855	0.248
SM-2-2009	66.928	-53.577	592	1.000	2.5	20.558	0.248
SM-3-2009	66.928	-53.577	592	1.000	2.0	51.703	0.483
SM-4-2009	66.928	-53.578	591	1.000	3.0	19.406	0.248
SM-5-2009	66.928	-53.578	591	1.000	2.0	40.226	0.510
SM-6-2009	66.937	-53.560	158	0.985	2.0	20.107	0.249
SM-7-2009	66.937	-53.559	149	0.990	2.0	46.298	0.511
SM-8-2009	66.937	-53.559	149	0.990	3.5	22.076	0.250
SM-9-2009	66.937	-53.560	158	0.990	2.0	46.260	0.511

Table 2. AMS results and age calculation of boulder samples using the CRONUS online calculator (Balco et al., 2009). All ages calculated with the Arctic high latitude/sea level production rate (Young et al., 2013b), zero erosion, a rock density of 2.65 g cm^{-3} , and the Lal/Stone time-varying spallation scaling scheme (Lal, 1991; Stone, 2000).

Sample Name	Elevation (m asl)	Measured ^{10}Be (10^{-15})	Measured ^{10}Be Error (10^{-15})	^{10}Be (atoms/g) (10^{-4})	^{10}Be uncertainty (atoms/g) (10^{-3})	Production Rate (muons) (atoms/g/yr)	Production Rate (spallation) (atoms/g/yr)	Exposure Age (ka)	Internal Uncertainty (ka)	External Uncertainty (ka)
QAQORTOQ										
QQ-1-08	313	43	6	8.12	2.5	0.206	5.74	13.7	4.2	4.2
QQ-2b-08	326	118	9	7.54	8.3	0.207	5.81	12.6	1.4	1.5
QQ-3-08	305	48	7	5.20	15.3	0.206	5.69	8.8	2.6	2.6
QQ-4-08	305	38	3	7.19	23.0	0.206	5.74	12.1	3.9	3.9
QQ-5-08	176	74	6	5.38	5.8	0.196	4.94	10.5	1.1	1.2
QQ-6-08	97	52	4	4.41	5.9	0.191	4.59	9.3	1.2	1.3
QQ-7-08	97	40	2	3.43	4.5	0.191	4.55	7.2	0.9	1.0
QQ-8-08	97	47	2	4.14	4.3	0.191	4.55	8.8	0.9	1.0
QQ-1-10	399	81	14	5.99	13.1	0.208	5.94	9.8	2.1	2.2
QQ-2-10	399	133	9	7.69	5.4	0.213	6.29	11.9	0.8	1.0
QQ-3-10	399	135	7	7.61	3.9	0.213	6.29	11.7	0.6	0.8
QQ-4-10	175	115	5	6.62	3.0	0.196	5.01	12.7	0.6	0.8
QQ-5-10	185	110	6	6.56	3.5	0.197	5.02	12.6	0.7	0.8
PAAMIUT										
PA-1-10	65	104	8	5.45	4.4	0.188	4.37	12.0	1.0	1.1
PA-2-10	65	85	6	4.78	3.4	0.188	4.42	10.4	0.7	0.8
PA-3-10	66	79	13	5.67	9.9	0.189	4.45	12.3	2.1	2.2
PA-4-10	57	79	18	6.48	14.8	0.188	4.37	14.3	3.3	3.3
PA-5-10	59	82	7	4.40	6.7	0.188	4.36	9.7	1.5	1.5
PA-6-10	515	150	8	8.05	4.3	0.221	6.69	11.7	0.6	0.8
PA-7-10	499	112	11	6.18	8.5	0.22	6.77	8.9	1.2	1.3
PA-8-10	448	129	21	7.32	13.5	0.216	6.46	11.0	2.0	2.1
PA-9-10	448	122	14	6.75	9.9	0.216	6.4	10.2	1.5	1.6
PA-10-10	439	138	18	6.94	10.4	0.215	6.34	10.6	1.6	1.6
PA-11-10	257	81	4	5.54	3.2	0.202	5.41	9.9	0.6	0.7
PA-12-10	251	87	4	5.44	2.4	0.201	5.28	10.0	0.5	0.6
NUUK										
NU-1-10	126	66	7	5.15	5.4	0.193	4.68	10.6	1.1	1.2
NU-2-10	149	82	14	7.46	12.8	0.194	4.83	14.9	2.6	2.6
NU-3-10	144	71	11	5.85	9.2	0.194	4.81	11.7	1.9	1.9
NU-4-10	427	106	23	7.53	16.9	0.215	6.4	11.4	2.6	2.6
NU-5-10	427	78	11	6.32	9.4	0.214	6.34	9.7	1.4	1.5
NU-1-2008	419	97	8	7.15	6.0	0.214	6.36	10.9	0.9	1.0
NU-2-2008	422	82	8	7.04	6.6	0.215	6.4	10.7	1.0	1.1
NU-4-2008	334	83	5	5.81	3.8	0.208	5.88	9.6	0.6	0.7
NU-5-2008	333	78	7	5.99	5.2	0.208	5.85	9.9	0.9	0.9
NU-7-2008	146	66	7	4.85	5.3	0.194	4.84	9.7	1.1	1.1
SISMIUT										
SM-1-2009	588	362	16	28.80	13.4	0.228	7.53	37.4	1.8	2.3
SM-2-2009	592	170	7	13.73	6.1	0.228	7.5	17.8	0.8	1.1
SM-3-2009	592	463	18	28.88	11.3	0.228	7.53	37.6	1.5	2.1
SM-4-2009	591	328	16	28.02	13.6	0.228	7.46	36.8	1.8	2.3
SM-5-2009	591	301	16	25.52	13.6	0.228	7.53	33.2	1.8	2.2
SM-6-2009	158	91	5	7.55	4.3	0.195	4.79	15.2	0.9	1.1
SM-7-2009	149	97	10	7.12	7.2	0.194	4.77	14.4	1.5	1.6
SM-8-2009	149	66	4	4.96	2.9	0.194	4.71	10.1	0.6	0.7
SM-9-2009	158	91	7	6.74	5.0	0.195	4.82	13.5	1.0	1.1

Table 3. Maximum and minimum calculated thinning (this study) and retreat (this study, Carlson et al., in press; Larsen et al., 2014) rates. Elevation change between high and low elevation sites, and distance between coastal and inland sites, is also listed. Dates are error-weighted means of individual ages, with associated error-weighted mean uncertainties.

Coastal Site	High Elevation		EWM Uncertainties		Low Elevation		EWM Uncertainties		Coastal Change in Elevation		Max Thinning		Min Thinning		Inland Site		EWM Uncertainties		Coastal to Inland Along-fjord Distance		Maximum Retreat		Minimum Retreat	
	EWM (ka)	(ka)	EWM (ka)	(ka)	EWM (ka)	(ka)	EWM (ka)	(ka)	(m)	Rate (m/yr)	Rate (m/yr)	Rate (m/yr)	Rate (m/yr)	Inland Site	EWM (ka)	(ka)	EWM (ka)	(ka)	(km)	Rate (m/yr)	Rate (m/yr)	Rate (m/yr)	Rate (m/yr)	
Qaqortoq	11.7	0.5	12.5	0.4	219	infinite	2	Narsarsuaq ¹	11.1	0.2	70	95	35											
Paamiut	11.7	0.6	11.2	0.5	451	infinite	0.3	Inland Paamiut ¹	10.4	0.4	43	infinite	25											
Nuuk	10.7	0.6	11.0	0.7	284	infinite	0.3	Inland Nuuk ²	10.1	0.3	120	infinite	65											
Sisimiut	17.8	1.1	14.5	0.6	437	0.3	0.1	Kangerlussuaq ^{1,3}	6.7	0.2	147	20	15											

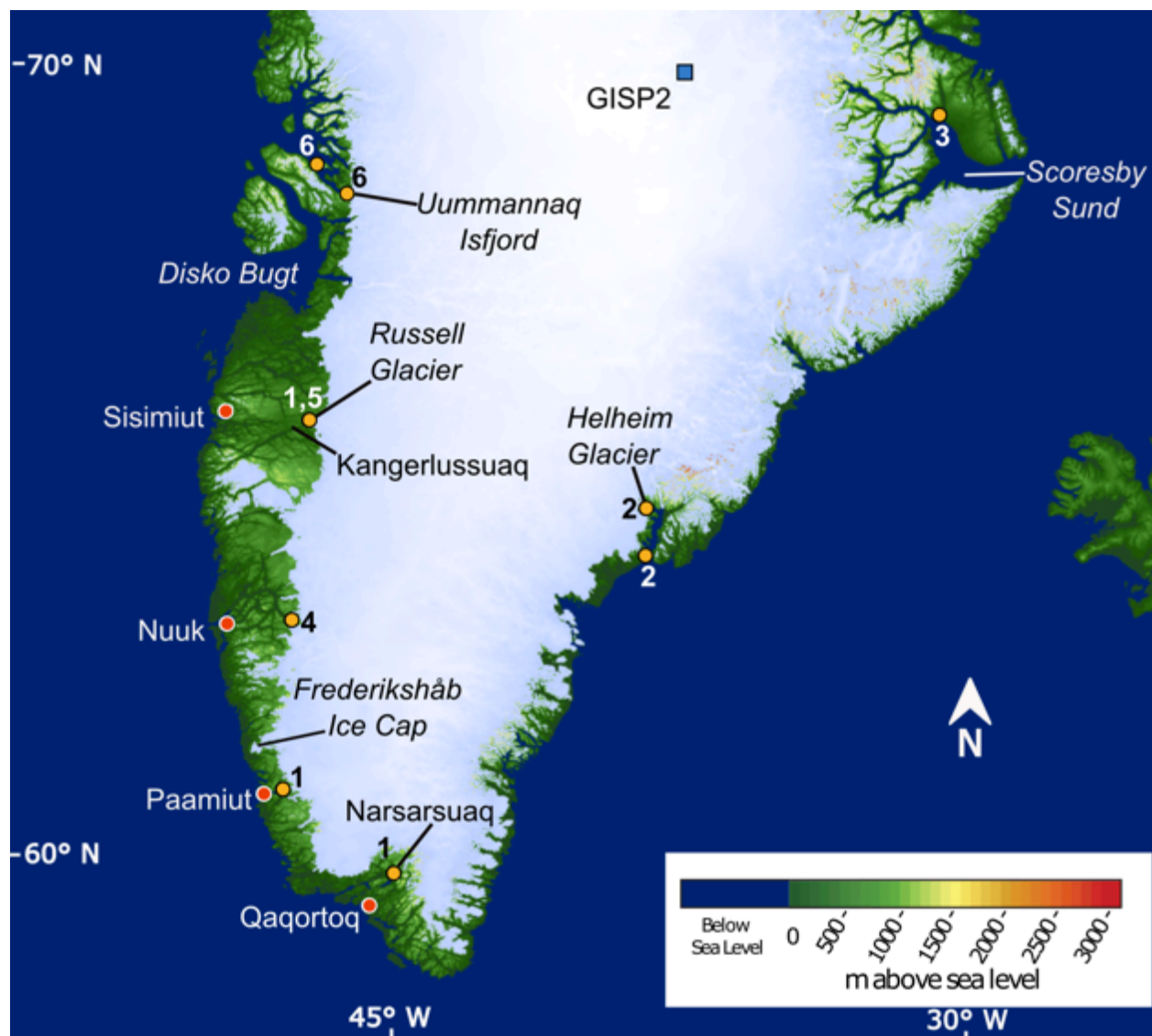


Figure 3-1.

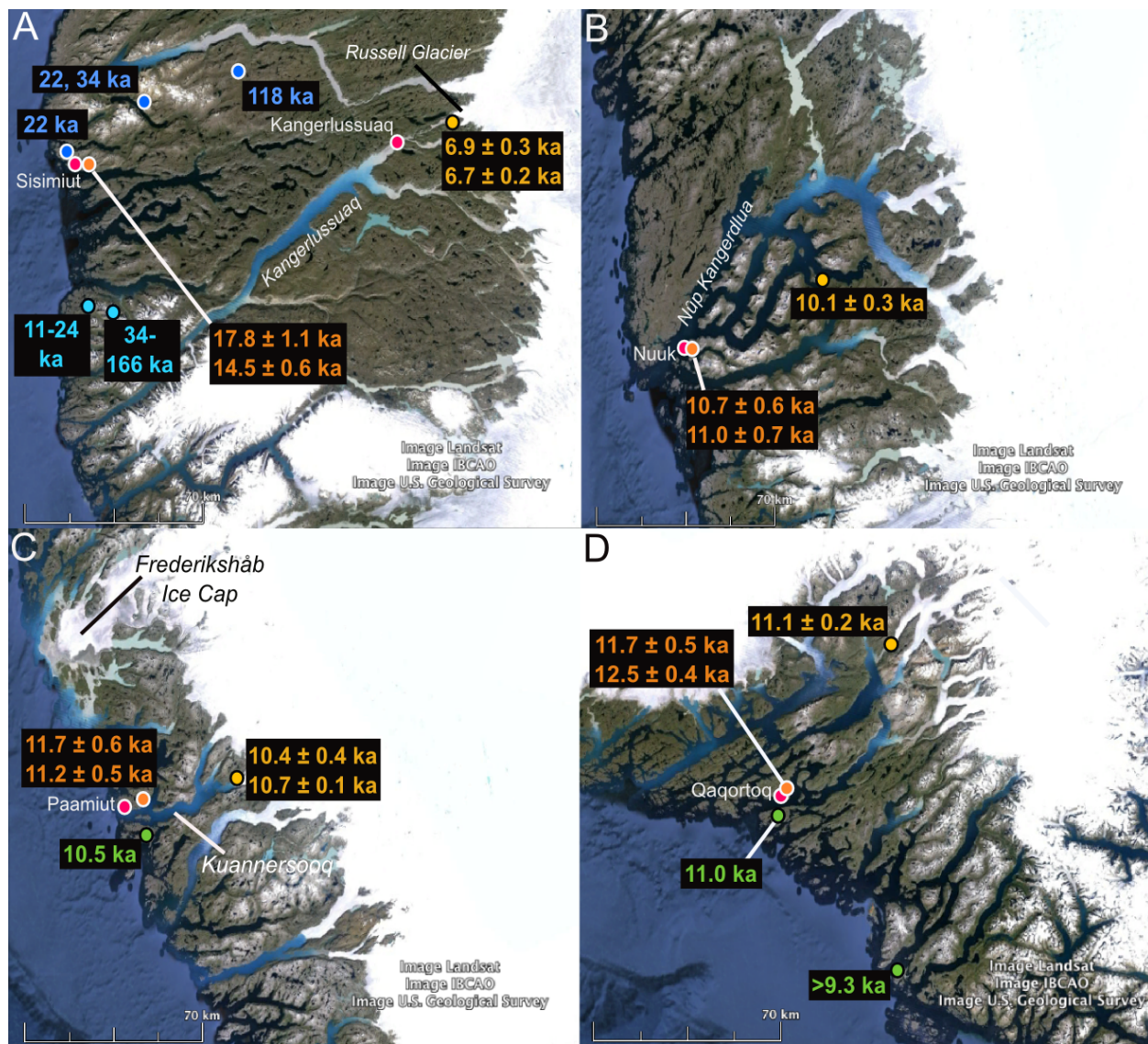


Figure 3-2.

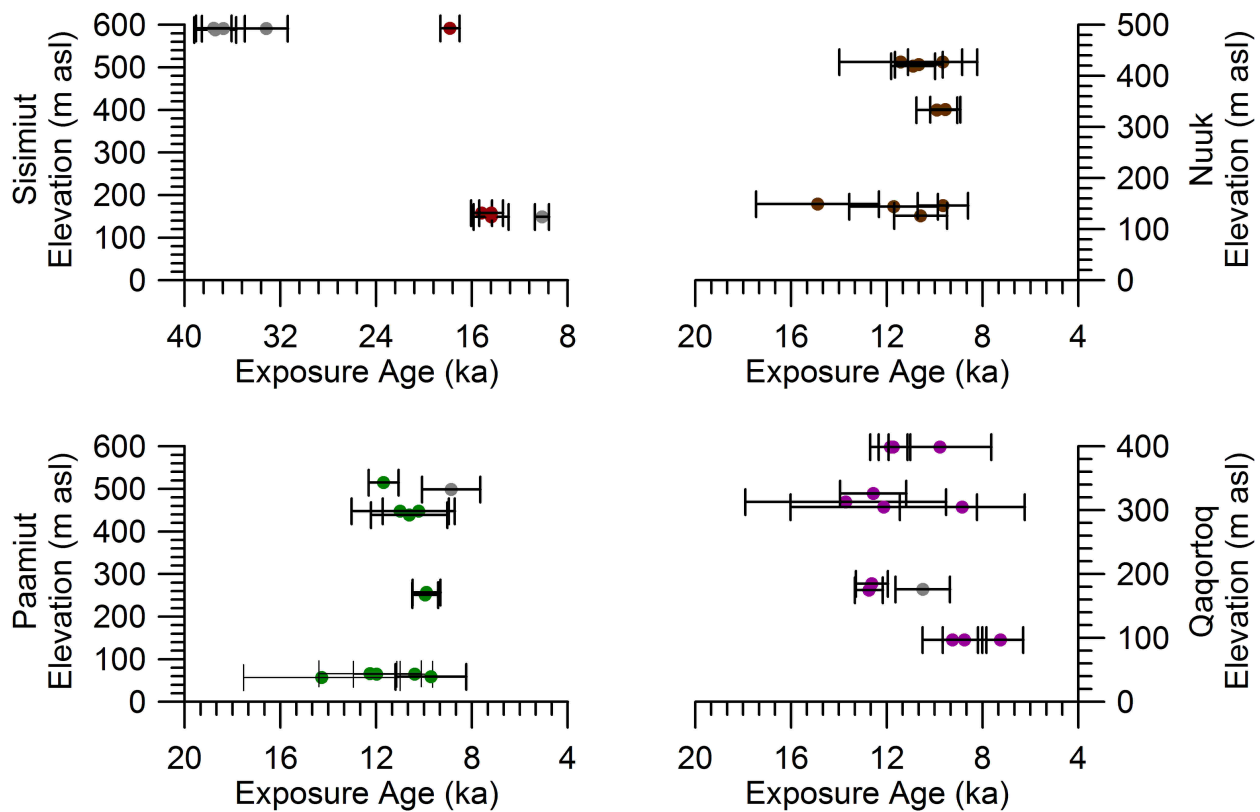


Figure 3-3.

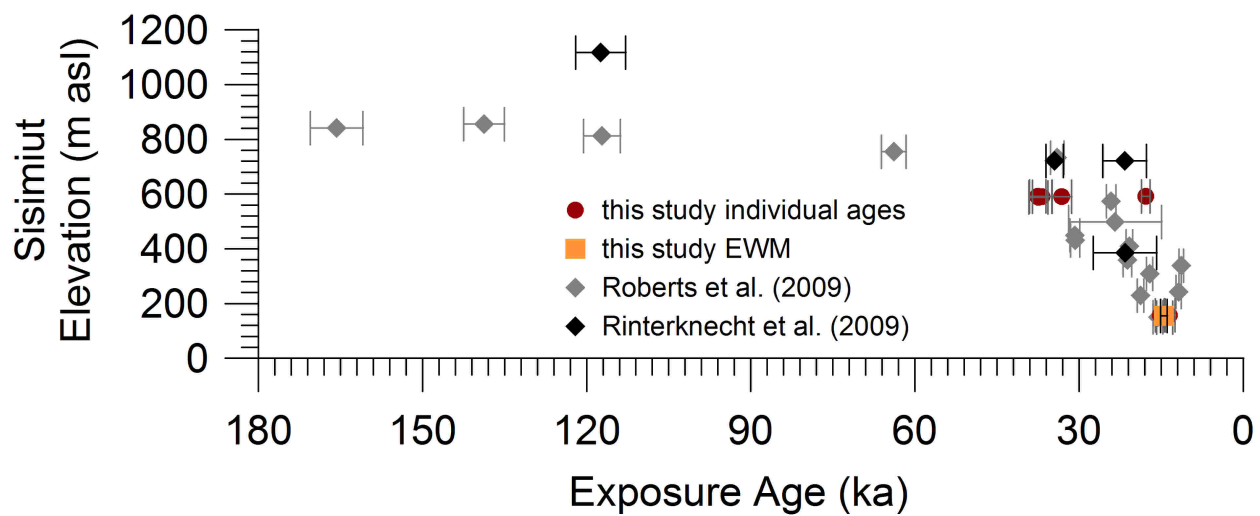


Figure 3-4.

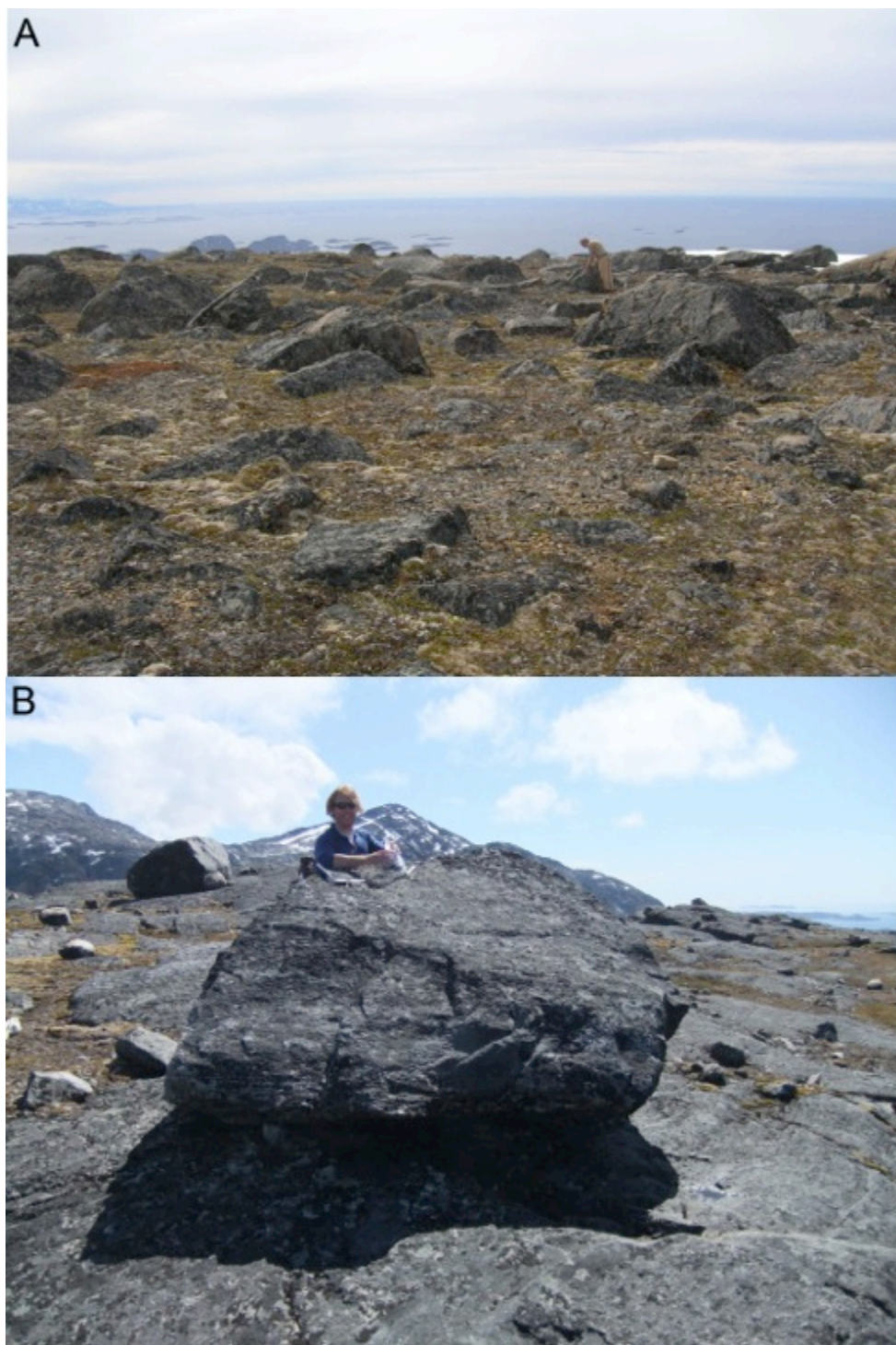


Figure 3-5

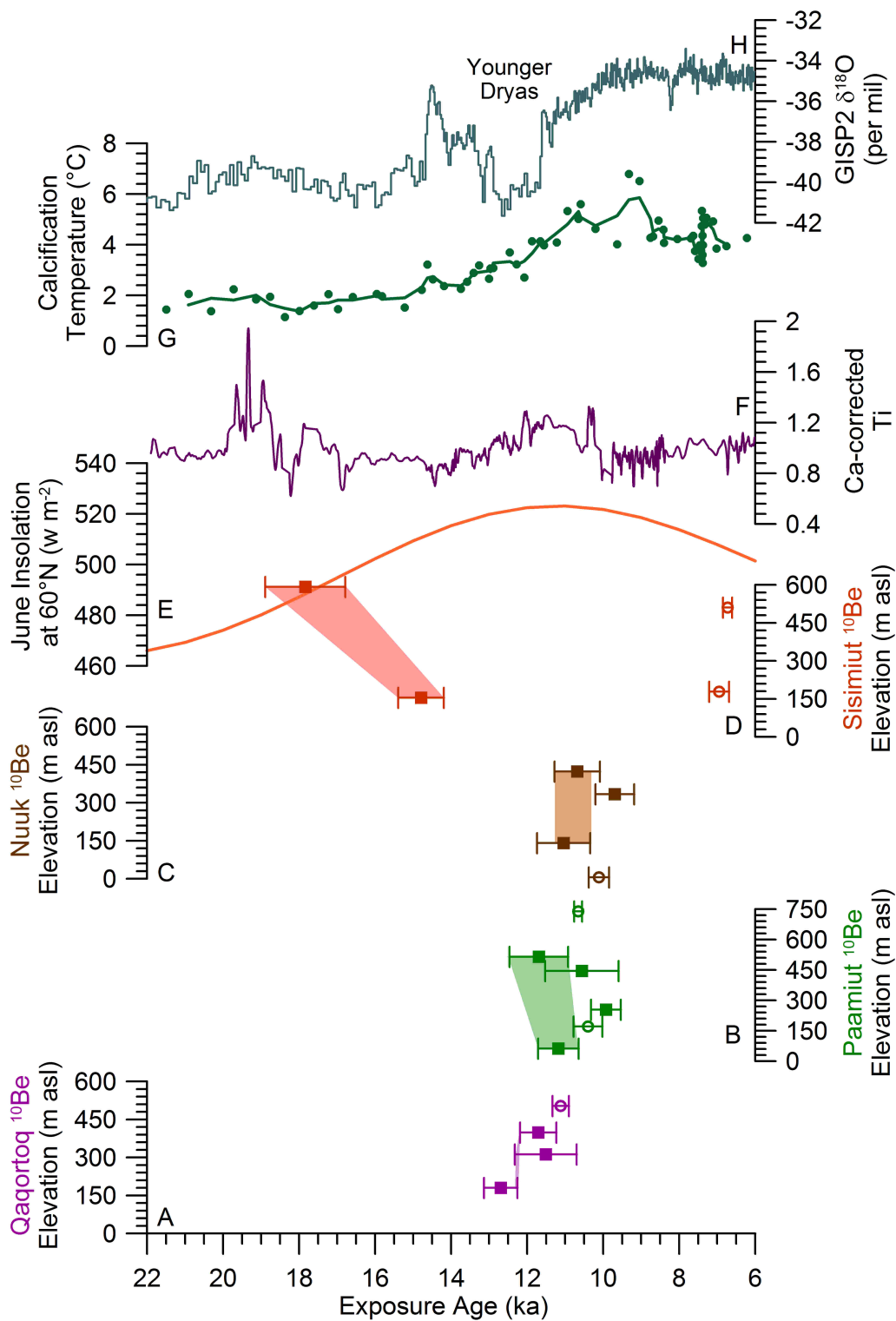


Figure 3-6

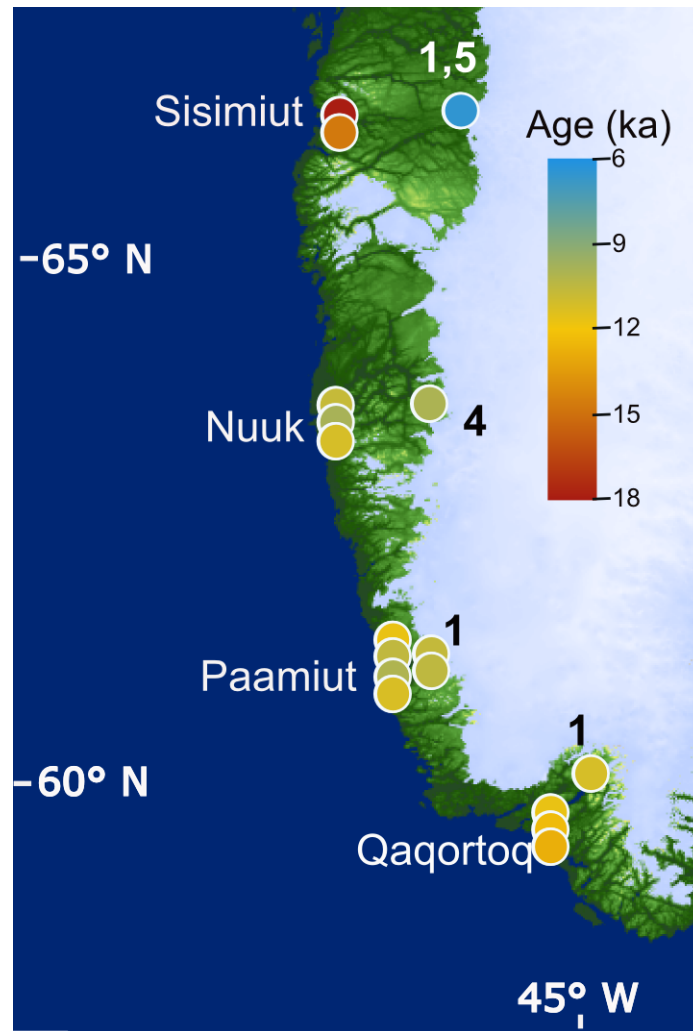


Figure 3-7.

Appendix A3-1. Calculating uncertainty in ^{10}Be exposure ages.

In our discussion of ^{10}Be exposure ages, we refer to internal and external uncertainties, which are both outputs of the CRONUS online calculator (Balco et al., 2008) and explained in the MATLAB documentation on <http://hess.ess.washington.edu/>. Here, we briefly describe the sources of uncertainty in stated internal and external uncertainties. A very thorough description of sources of uncertainty, and the associated percent errors at the date of publication, is provided in Gosse and Phillips (2001).

Internal Uncertainty

The internal uncertainty ($\sigma_{\text{int}} \times t_{\text{Xx}}$) is calculated by:

$$(\sigma_{\text{int}} \times t_{\text{Xx}})^2 = ((\partial t_{\text{Xx}})/(\partial N))^2 \times \sigma N^2$$

where:

$$(\partial t_{\text{Xx}})/(\partial N) = (P_{\text{eff, Xx}} - N(\lambda + (\rho\varepsilon)/\Lambda_{\text{sp}}))^{-1}$$

Scaling scheme is represented by Xx, N is the concentration of the ^{10}Be nuclide, σN is the standard error associated with the measured N, ε is the erosion rate, λ is the ^{10}Be decay constant, Λ_{sp} is the effective attenuation length for production for neutron spallation, ρ is the sample density, and the effective production rate is P_{eff} , where:

$$P_{\text{eff}} = P_{\text{ref, Xx}} \times S_{\text{eff, Xx}} \times S_{\text{thick}} \times S_{\text{g}}$$

S_{thick} is the thickness scaling factor, $S_{\text{eff, Xx}}$ is the effective scaling factor for a given scaling scheme and S_{g} is the geometric shielding correction.

External Uncertainty

The external uncertainty in ^{10}Be exposure ages for the CRONUS online calculator are calculated as follows:

$$(\sigma_{\text{ext}} \times t_{\text{Xx}})^2 = ((\partial t_{\text{Xx}})/(\partial N))^2 \times \sigma N^2 + ((\partial t_{\text{Xx}})/(\partial P_{\text{eff, Xx}}))^2 \times \sigma P_{\text{eff, Xx}}^2$$

where

$$(\partial t_{\text{Xx}} \sigma)/(\partial P_{\text{eff, Xx}}^2) = -N(P_{\text{eff, Xx}} - N \times P_{\text{ref, Xx}} (\lambda + (\rho\varepsilon)/\Lambda_{\text{sp}}))^{-1}$$

and

$$\sigma \times P_{\text{eff, Xx}} = \sigma \times P_{\text{ref, Xx}} \times S_{\text{eff, Xx}} \times S_{\text{thick}} \times S_{\text{g}}$$

and $P_{\text{ref, Xx}}$ is the reference production rate standard error for a given scaling scheme.

CHAPTER IV:**¹⁰BE DATING OF THE NARSARSUAQ MORaine IN SOUTHERNMOST GREENLAND: EVIDENCE FOR
A LATE-HOLOCENE ICE ADVANCE EXCEEDING THE LITTLE ICE AGE MAXIMUM**

Winsor, K.¹
Carlson, A.E.^{1,2}
Rood, D.H.^{3,4}

¹Department of Geoscience, University of Wisconsin-Madison, Wisconsin, Madison, 53706,
USA

²College of Earth, Ocean, and Atmospheric Sciences, Oregon State University, Corvallis,
Oregon, 97331, USA

³Scottish Universities Environmental Research Centre (SUERC), University of Glasgow, East
Kilbride, G75 0QF, UK

⁴Earth Research Institute, University of California-Santa Barbara, Santa Barbara, CA, 93106,
USA

This manuscript is published in Quaternary Science Reviews and is therefore formatted to fit the specifications of that journal.

Winsor, K., Carlson, A.E., and Rood, D.H., 2014, ¹⁰Be dating of the Narsarsuaq moraine in southernmost Greenland: evidence for a late-Holocene ice advance exceeding the Little Ice Age maximum. Quaternary Science Reviews, 98, 135-143, 10.1016/j.quascirev.2014.04.026.

Abstract

In southernmost Greenland near Narsarsuaq, the terminal Narsarsuaq moraine was deposited well outside of a historical Little Ice Age (LIA) moraine adjacent to the modern ice margin. Using ^{10}Be surface exposure dating, we determine Narsarsuaq moraine abandonment at 1.51 ± 0.11 ka. A second set of ^{10}Be ages from a more ice-proximal position shows that ice has been within or at its historical (i.e., LIA) extent since 1.34 ± 0.15 ka. Notably, Narsarsuaq moraine abandonment was coincident with climate amelioration in southern Greenland. Southern Greenland warming at ~ 1.5 ka was also concurrent with the end of the Roman Warm Period as climate along the northern North Atlantic sector of Europe cooled into the Dark Ages. The warming of southern Greenland and retreat of ice from the Narsarsuaq moraine is consistent with studies suggesting possible anti-phase centennial-scale climate variability between northwestern Europe and southern Greenland. Other southernmost Greenland ice-margin records do not preclude a pre-LIA ice-margin maximum, potentially concurrent with a Narsarsuaq advance prior to ~ 1.51 ka, but also lack sufficient ice-margin control to confirm such a correlation. We conclude that there is a clear need to further determine whether a late-Holocene pre-LIA maximum was a local phenomenon or a regional southern Greenland ice maximum, and if this advance and retreat reflects a regional fluctuation in climate.

4.1. Introduction

Over the Holocene, boreal climate generally cooled in response to declining high northern latitude summer insolation, culminating in the Little Ice Age (LIA) of the last several centuries (Kaufman et al., 2009; Marcott et al., 2013). In Greenland, valley glaciers and the Greenland ice sheet advanced across the Neoglacial interval (the last 4 ka), with their maximum extents

generally occurring during the LIA (Weidick, 1963; Kelly, 1980; Weidick et al., 2004; 2012; Kelly et al., 2008; Kelly & Lowell, 2009; Alley et al., 2010; Briner et al., 2011; Funder et al., 2011; Levy et al., 2012; 2013; Lowell et al., 2013). The timing and extent of these late-Holocene glacier maxima are often used as baselines for assessing the cause of present and future ice volume changes on the island (Oerlemans, 2005; Jansen et al., 2007). It is therefore societally relevant to determine the timings of Greenland ice margin maximum late-Holocene extents and to constrain the geographic variability of these maxima (Seidenkrantz et al., 2008).

Ice margin records from across Greenland suggest that general global cooling resulted in glacial maxima at different times during the late Holocene. Jakobshavn Isbræ, which is the largest single source of modern ice loss in Greenland, advanced throughout the LIA, surpassing older late Holocene extents (Weidick & Bennike, 2007; Briner et al., 2011). However, just to the south of Jakobshavn, ^{14}C dating of land-terminating ice margins indicates a late-Holocene maximum post-dating the LIA in the last century (Kelley et al., 2012). Ice-marginal records from east Greenland also show a nuanced response to late-Holocene climate change, with one valley glacier reaching its maximum extent early in the LIA (Kelly et al., 2008), while two ice caps neared their late-Holocene maximum prior to the LIA (Levy et al., 2013; Lowell et al., 2013). In southwest and southeast Greenland, ice-marginal records are more limited and do not provide a close constraint on late-Holocene Greenland ice sheet and valley glacier behavior (e.g., Roberts et al., 2008; Hughes et al., 2012; Weidick et al., 2012; Larsen et al., 2013).

In southernmost Greenland, the prominent Narsarsuaq moraine was deposited outside of the LIA/historical extent of the outlet glacier Kiagtût sermiat, and is indirectly inferred to be late Holocene in age, although an early or middle Holocene age is also plausible given available chronologic constraints (Weidick, 1963; Kelly, 1980; Dawson, 1983; Bennike & Sparrenbom,

2007). Analysis of sediments originating from a combination of glaciated and unglaciated terrain downstream of Kiagtût sermiat yielded an average age of 3.5 ka (Nelson et al., 2014). Existing records from other southern Greenland ice margins are somewhat contradictory, and are interpreted to show either ice-margin late-Holocene maxima during the LIA (Kaplan et al., 2002) or an earlier maximum (Larsen et al., 2011). Here, we use ^{10}Be surface exposure ages to directly date ice retreat from the Narsarsuaq moraine and to determine if this moraine represents a pre-LIA late-Holocene maximum ice-margin advance.

4.2. Kiagtût Sermiat setting & methodology

Northeast of Narsarsuaq [61.15°N, 45.43°W] (Figure 1), the Kiagtût sermiat outlet glacier flows to the southwest. The outlet glacier is sourced from the southern dome of the Greenland ice sheet as part of a larger outlet glacier that splits into Kiagtût sermiat and Qôrqup sermia glaciers (Figure 2) (Weidick et al., 2004; Larsen et al., 2011). The modern glacier is land-terminating, with the mouth of Tunugliarfik fjord located ~8 km down valley to the southwest of the present ice margin. Kiagtût sermiat glacier is sometimes referred to as Kiattut sermiat or Kiatuut sermia (e.g., Weidick et al., 2004; Nelson et al., 2014).

The Narsarsuaq moraine of Kiagtût sermiat is clast-supported and consists of a prominent ridge extending from the valley mouth up onto the plateau (Figure 2) (Weidick, 1963; Larsen et al., 2011). Several recessional moraines are up-valley of the terminal moraine, but these as well as the terminal moraine have been heavily reworked by human activity, particularly during and shortly after World War II. Weidick (1963) first suggested a late-Holocene age for the Narsarsuaq moraine based on its elevation relative to the marine limit, although marine limit deposits also experienced significant human impact from World War II activity. Organic

materials recovered from Cedar Lake within the moraine date (calibrated) to ~1.2 ka (Bennike & Sparrenbom, 2007), but these are minimum-limiting radiocarbon dates and therefore do not preclude an age for the moraine ranging from the last deglaciation to the late Holocene.

Similarly, lichenometry has been interpreted to suggest a moraine age of ~2.4 ka, but this age is an extrapolation of the lichen growth curve well beyond its calibration period of the last several centuries, and only constrains the moraine as older than the latest-Holocene lichen-calibration period (Dawson, 1983; Loso & Doak, 2006).

For this study, we sampled 17 boulders for ^{10}Be surface exposure dating from within the innermost recessional segments of the Narsarsuaq moraine (Figure 2). Eleven samples were from just within the last recessional moraine segment and thus date the onset of Kiagtût sermiat retreat from the Narsarsuaq moraine. Another six samples are just ice-distal of the historical ice limit—which also is the LIA ice limit—and therefore constrain the last time Kiagtût sermiat was more advanced than its 20th century extent (Weidick, 1963). We chose large (>1 m tall) granitoid or gneissic boulders with relatively even and horizontal tops. Samples showed no sign of post-depositional rolling or of being reworked, and their topographic shielding was recorded. We avoided boulders on the moraine itself because of human impact on the end-moraine segments and clear evidence for downhill deflation of the lateral moraines. We note that our samples are likely not noticeably impacted by inheritance, as evidenced by low concentrations of ^{10}Be found in sediments released from the GIS in this region (Nelson et al., 2014).

Laboratory preparation of ^{10}Be targets was performed in the University of Wisconsin-Madison Cosmogenic Nuclide Laboratory. Processing included the isolation of pure quartz and removal of meteoric ^{10}Be using successive HF/HNO₃ acid leaches, chemical separation and purification of Be(OH)₂ via anion and cation chromatography and selective hydroxide

precipitation, ignition to BeO, and mixture with Nb powder prior to loading into cathodes (Nishiizumi et al., 1984; Kohl & Nishiizumi, 1992). Samples were analyzed by Accelerator Mass Spectrometry (AMS) for $^{10}\text{Be}/^9\text{Be}$ (online data repository) at Lawrence Livermore National Laboratory (LLNL) and the Scottish Universities Environmental Research Centre (SUERC) (Rood et al., 2010; 2013; Xu et al., 2010). At LLNL, samples were normalized to standard 07KNSTD3110 with a reported ratio of 2.85×10^{-12} (Nishiizumi et al., 2007). At SUERC, samples were normalized to the NIST standard with an assumed ratio of 2.79×10^{-11} . All samples were blank corrected (online data repository).

We calculated surface exposure ages with the CRONUS online calculator (version 2.2, with constants version 2.2) using the Arctic reference sea-level high-latitude production rate due to spallation of 3.96 ± 0.15 ^{10}Be atoms $\text{g}^{-1} \text{yr}^{-1}$ (Young et al., 2013), the muonogenic production rate from Heisinger et al. (2002a; b), and the time-dependent Lal/Stone scaling scheme (Table 1 and online data repository) (Lal, 1991; Stone, 2000; Balco et al., 2008). Use of other scaling schemes provided by the CRONUS calculator yield maximum age differences of 4-7 % (online data repository). No corrections were made for snow cover or erosion, considering the height of the boulders and their young age, respectively.

4.3. Results

The five samples from just ice-distal of the historical extent of Kiagtût sermiat yield exposure ages between 0.91 ± 0.06 ka and 1.82 ± 0.09 ka, after excluding one outlier based on Chauvenet's criterion (NA08-03; 3.49 ± 0.34 ka) (Table 1, Figure 2, 3). Because the five ages are normally distributed, as determined by a Shapiro-Wilk normality test, we calculate an arithmetic mean of 1.34 ± 0.15 ka (all ages are presented with one standard error uncertainty). After excluding one

outlier based on Chauvenet's criterion (NA08-05; 4.85 ± 0.39 ka), the remaining ten samples from just within the Narsarsuaq moraine are normally distributed according to a Shapiro-Wilk test and have exposure ages between 1.04 ± 0.26 and 2.12 ± 0.18 ka (Table 1, Figure 2, 3), with an arithmetic mean of 1.51 ± 0.11 ka for ice retreat from the Narsarsuaq moraine. Our mean ages for the two sample locations overlap within the standard errors of the sample sets, but due to their different geographic settings are separate glacial deposits from Kiagtût sermiat retreat.

4.4. Discussion

Our new ^{10}Be exposure ages suggest that the Narsarsuaq moraine is from a pre-LIA, late-Holocene advance of Kiagtût sermiat. It is unlikely that the moraine is a recessional deposit from an early to middle Holocene ice advance, as abundant evidence points to a smaller-than-present early- to mid-Holocene ice margin extent (e.g., Weidick et al., 2004; Sparrenbom et al., 2006a; b; Long et al., 2011), with Neoglacial advance occurring after ~ 3 ka (e.g., Weidick et al., 2004; Larsen et al., 2011). Additionally, the only moraine that lies in front of these ^{10}Be sample locations is the Narsarsuaq moraine, thus suggesting that they provide a close age constraint on ice retreat after moraine deposition. Our data is in agreement with previous inferences from the marine limit, minimum-limiting ^{14}C dates, and new ^{10}Be data (Weidick, 1963; Kelly, 1980; Bennike & Sparrenbom, 2007; Nelson et al., 2014). We now precisely date moraine abandonment at 1.51 ± 0.11 ka, several hundred years earlier than the oldest minimum-limiting AMS ^{14}C date from within the moraine (Bennike & Sparrenbom, 2007). Our ice-proximal ^{10}Be ages show that up-valley retreat to near the present ice margin occurred by 1.34 ± 0.15 ka, and that ice did not subsequently exceed its historical extent. These ^{10}Be ages suggest that Kiagtût sermiat retreated from the Narsarsuaq moraine to its historical/LIA extent at a rate of greater than

15 m yr⁻¹ (maximum age difference between the two sampling sites).

4.4.1. Comparison to other Greenland ice margins

Our results raise the question as to whether the Narsarsuaq-moraine maximum prior to the LIA was a local phenomenon or part of a more regional-scale ice-margin fluctuation. We therefore compare our Narsarsuaq ¹⁰Be ages against other Greenland ice-margin constraints on when glaciers and the ice-sheet margin reached their late-Holocene maximum extent (Figure 4).

No direct ages or indirect ¹⁴C dates confirm correlative mapping of the Narsarsuaq moraine outside the terminal region of Kiagtût sermiat (Figure 2) (Weidick, 1963; Weidick et al., 2004; Larsen et al., 2011). However, Larsen et al. (2011) used a sediment sequence from a nearby threshold lake of Nordbo Glacier (Figure 1, 2), Lower Nordbosø, to constrain Nordbo Glacier behavior during the Holocene. Larsen et al. (2011) documented minerogenic sedimentation at ~3 to 2.8 ka and in the last ~0.5 ka, probably resulting from ice-margin advance into the catchment. We show in Figure 4A the ¹⁴C dates from Lower Nordbosø that are unambiguously from intervals of organic deposition in the lake and firmly constrain a retracted ice margin. Like Larsen et al. (2011), we suggest that the Nordbo Glacier margin was at least near its late Holocene maximum by ~3 ka. We note, however, that Nordbosø Lake lies above Lower Nordbosø and could buffer the Lower Nordbosø sediment sequence from recording more subtle changes in the sediment discharge from Nordbo Glacier (Figure 2).

Another sediment record from Qipisarqo Lake may constrain the behavior of the Qassimiut lobe in southern Greenland (Figure 1). Kaplan et al. (2002) interpreted the sediment record as indicating maximum extent of the Qassimiut lobe during the LIA. However, multiple radiocarbon date reversals occur in the upper 50 cm (late Holocene) portion of the core,

particularly in the sequence attributed to the LIA period (Kaplan et al., 2002). Because these are ^{14}C dates on humic acid extractions, not macrofossils, the cause of the reversals is not unequivocally reworking of plant remains. We thus only show the ^{14}C dates from portions of the lake record that are clearly intervals of organic sedimentation >2 ka (Figure 4A), which document the Qassimiut lobe as being smaller than present prior to the Neoglacial advance. It is therefore unclear from the Qipisarqo Lake record as to when the Qassimiut lobe reached its maximum late-Holocene extent, which could have occurred prior to the LIA. In agreement with our interpretation of the Qipisarqo Lake record, ^{14}C dates on samples reworked in historical moraines of southern Greenland outlet glaciers and the Qassimiut lobe have yet to be found younger than ~ 3 ka (Figure 1, 4A) (Weidick et al., 2004; 2012). These maximum-limiting, indirect ^{14}C dates on ice-margin advance in southern Greenland are consistent with our direct ^{10}Be ages on Kiagtût sermiat retreat.

A single marine ice-rafted debris (IRD) record from a southern Greenland fjord near Kiagtût sermiat (Figure 1, 2) shows a peak in iceberg sedimentation 2.3-1.8 ka, with a decrease at ~ 1.5 ka (Figure 4B) (Nørgaard-Pedersen & Mikkelsen, 2009). Increased IRD deposition is, however, ambiguous with respect to ice-margin position. This late Holocene peak and subsequent diminution at ~ 1.5 ka could reflect either an ice-margin maximum (more icebergs and IRD from closer ice proximity) and later retreat at ~ 1.5 ka (fewer icebergs/IRD), or ice retreat 2.3 to 1.8 ka (more icebergs/IRD from increased calving) and subsequent advance at ~ 1.5 ka (reduced calving/IRD) (Nørgaard-Pedersen & Mikkelsen, 2009).

In southwest Greenland, there are fewer chronologic constraints on when ice margins reached their late-Holocene maxima (Figure 1, 4A) (Weidick et al., 1990; 2012; Larsen et al., 2013). Radiocarbon dates on marine shells underlying late-Holocene glacial outwash from inland

of Nuuk document local outlet glacier advance after ~ 4.7 ka (Figure 1) (Weidick et al., 1990; 2012). Larsen et al. (2013) produced ^{10}Be boulder and bedrock surface exposure ages outside of the historical extent of the southwest Greenland ice-sheet margin (Figure 1). These ^{10}Be samples date to the early Holocene and thus preclude a late-Holocene advance of the ice margin to their position, consistent with continuous organic sedimentation in a lake ~ 4 km from the ice margin since ~ 8.7 ka (Larsen et al., 2013). Nevertheless, they are >500 m above the present historical ice limit, or ~ 1 km in front of the historical ice limit, and therefore do not provide a constraint on margin behavior within this distance. Indeed, Weidick et al. (2012) noted that the late-Holocene history of this portion of Greenland was not well constrained before ~ 0.3 ka.

Southwest and west Greenland ice margins near Kangerlussuaq and in the Disko Bugt, Uummannaq Fjord, and Upernavik regions are well-constrained by ^{10}Be ages, reworked ^{14}C dates in historically deposited moraines, and ice-marginal lake records. Most of these records show that ice margins reached their maximum extent during the LIA (Figure 1, 4A) (Briner et al., 2010; 2011; 2013; 2014; Corbett et al., 2011; 2013; Young et al., 2011; 2013; Kelley et al., 2012).

The timings of southeast Greenland late-Holocene ice maxima are poorly constrained. ^{10}Be ages from Sermilik Fjord only constrain the Helheim Glacier Holocene history to within ~ 40 km of its present calving margin (Hughes et al., 2012). Roberts et al. (2008) produced bedrock ^{10}Be and ^{26}Al ages that constrain the Greenland ice-sheet margin just south of Sermilik Fjord to have not advanced beyond its LIA extent since ~ 11 - 12.5 ka (we recalculate this published data on samples T11 and T15 using the new Arctic ^{10}Be production rate and updated CRONUS versions; Young et al., 2013). However, these concordant ^{10}Be - ^{26}Al bedrock ages do not necessarily rule out brief periods of ice cover given the uncertainties in both measurements.

Ice-sheet margins have not been directly dated in east Greenland, but four ^{10}Be dates on a moraine in the Scoresby Sund region have two different populations (ages calculated with the Arctic ^{10}Be production rate; Young et al., 2013). One population suggests moraine deposition during the LIA, the other several hundred years prior to the LIA (Kelly et al., 2008). Threshold lake records for two other ice caps in the Scoresby Sund region show that these ice margins neared their maximum late-Holocene extents prior to the LIA, but do not constrain precisely when this maximum occurred (Levy et al., 2013; Lowell et al., 2013).

We have summarized an emerging picture of Greenland ice-sheet and glacier margin advance in the late Holocene. In west and east Greenland, it is clear that most ice margins were at their maximum extents during the LIA, although in east Greenland the advance to this maximum could have occurred prior to the LIA. In southwest and southeast Greenland, records are more tentative, and in only one location in southeast Greenland is the ice-margin maximum confirmed as likely occurring during the LIA (Roberts et al., 2008). In contrast, in south Greenland, the only record that suggests an LIA maximum, the Qipisarqo Lake sediment sequence (Kaplan et al., 2002), has issues with age reversals during the most critical part of the record.

Other south Greenland ice-margin constraints from reworked ^{14}C dates and IRD, as well as a more conservative interpretation of the Qipisarqo Lake record, are not inconsistent with our Narsarsuaq ^{10}Be ages for a pre-LIA maximum that terminated at ~ 1.5 ka. The Larsen et al. (2011) Lower Nordbosø sediment record does suggest an earlier timing for the end of the first late-Holocene maximum extent of Nordbo Glacier, but the onset of this maximum still could have been coincident with the advance of Kiagtût sermiat. The role of upstream Nordbosø in buffering the Lower Nordbosø sediment record has also yet to be resolved. We suggest that direct dating of Nordbo Glacier margin deposits and coring of Nordbosø would help to determine

if Nordbo Glacier behaved differently than the adjacent Kiagtût sermiat. This comparison of records across the southern half of Greenland implies that southern Greenland ice margins may have behaved differently from their northern counterparts. Therefore, an inspection of regional climate (and the forcings behind this climate) is warranted to help understand potential spatial variability in late-Holocene Greenland ice margins.

4.4.2. Late Holocene Greenland climate change

We now assess the records of climate change across the southern half of Greenland to determine if a climatic forcing underlies Kiagtût sermiat advance to and later abandonment of the Narsarsuaq moraine, and if spatially variable climate change could explain ice-margin variability. We note that observations and glacier modeling suggests that marine-terminating ice margins can respond to climate change within a decade while land-terminating ice margins can respond to climate change within a century (Andresen et al., 2012; Kelley et al., 2012; Nick et al., 2013). As such, we limit our discussion of paleoclimate records to the century or longer time scale to reduce the potential for associating climate variations to local non-climatic ice-margin variations. There is no evidence for centennial scale variations in snow accumulation over Greenland during the late Holocene (Cuffey & Clow, 1997), implying that temperature was the primary forcing of late-Holocene Greenland glacier variations. A climatically driven pre-LIA maximum in southern Greenland is conceivable, as the Mann et al. (2009) hemispheric climate reconstruction for the last 1.5 ka shows southern Greenland to be anomalously warm during both the LIA and the preceding Medieval Climate Anomaly, relative to the mid-last century and the general Arctic temperature pattern (Figure 4G) (Kaufman et al., 2009; PAGES 2k Network, 2013).

One pollen-based record exists from Qipisarqo Lake in southern Greenland (Fréchette & de Vernal, 2009), but its interpreted surface air temperature (SAT) record has uncertainties large enough to preclude any assessment of relative temperature change within the late Holocene. The aforementioned humic ^{14}C age reversals from the same core question its late-Holocene stratigraphic integrity. The SAT estimate of the Qipisarqo Lake pollen record may also have biases introduced from far traveled pollen sourced from Canada (Jessen et al., 2011).

Two biogenic silica records, which are proxies of lake biological productivity potentially related to temperature and/or precipitation, exist in south Greenland but are in disagreement. The record from Lake N14 (Figure 1) suggests cooler/drier conditions during the Narsarsuaq ice maximum and warmer/wetter conditions around the time of ice retreat (Figure 4F) (Andresen et al., 2004). The Lake N14 record ends at ~ 0.5 ka, precluding an assessment of whether the LIA was actually a cool/dry period in southern Greenland. The other record is from Qipisarqo Lake (Figure 1) (Kaplan et al., 2002) and has the aforementioned issues with humic acid ^{14}C date reversals that question the stratigraphic integrity of the record.

Southern Greenland's fjord benthic faunal records do show consistent late-Holocene subsurface water source variability (Arctic vs. Atlantic, i.e., temperature). The best-resolved and dated record, however, comes from southern southwest Greenland. Core 248260-2 in Amerilik Fjord near Nuuk documents the first late-Holocene arrival of cold Arctic waters at ~ 2.8 ka and the return of warm Atlantic waters at ~ 1.5 ka (Figure 4C) (Møller et al., 2006; Seidenkrantz et al., 2007), which also occurred in southernmost Greenland fjords near Narsarsuaq (Jensen et al., 2004; Lassen et al., 2004). The return of warm Atlantic waters at ~ 1.5 ka is concurrent with Kiagtût sermiat retreat from the Narsarsuaq moraine (Figure 4A).

Two lake alkenone-SAT records from near Kangerlussuaq in southwest Greenland also show

a decrease to generally colder temperatures between ~2.8 and 1.8 ka, with rapid warming centered at ~1.6 ka followed by cooling to a non-trending but variable SAT (Figure 4E) (D'Andrea et al., 2011). No SAT proxy records exist at present from southeast or east Greenland ice margins. Although the Dye 3 mean-annual borehole SAT records the coldest late-Holocene interval as occurring during the LIA (Figure 4E) (Dahl-Jensen et al., 1998), such high-elevation observations should not necessarily be extrapolated to Greenland ice-sheet margins due to the thermal inversion over the Greenland ice sheet (e.g., Cuffey & Clow, 1997; Severinghaus et al., 1998).

In west Greenland's Disko Bugt, lake and marine records show that the LIA interval was the coldest period of the late Holocene on land and in the adjacent fjords (Figure 4D, 4E) (Seidenkrantz et al., 2008; Briner et al., 2011; Perner et al., 2011; Axford et al., 2013). Most of the existing ice-marginal constraints document that the west Greenland ice margin maximum extent occurred during this late-Holocene temperature minimum (Briner et al., 2011; 2013; Kelley et al., 2012).

The paleoclimate records from southern Greenland could therefore suggest an underlying climate forcing of the Kiagtût sermiat advance to and retreat from the Narsarsuaq moraine. Cold/dry atmospheric conditions existed in southernmost Greenland and Arctic-sourced waters occupied its fjords when Kiagtût sermiat was presumably advancing to the Narsarsuaq maximum. Likewise, abandonment of the Narsarsuaq moraine corresponds with warm/wet conditions in southernmost Greenland and the arrival of warm Atlantic-sourced waters in its fjords. Similarly, the LIA maximum in west Greenland is concurrent with the coldest late-Holocene temperatures. This spatially variable Greenland climate could be the underlying cause of the different timing of ice-margin maximum extent between south and west Greenland.

Andresen et al. (2004) and Seidenkrantz et al. (2007) both noted that the period of relatively cold conditions in southern Greenland prior to 1.5-1.6 ka corresponded with the Roman Warm Period in northwestern Europe, while the return to relatively warm conditions in southern Greenland corresponded with cooling of northwestern Europe into the Dark Ages. Glacier records from northern Europe are consistent with this regional pattern of climate change as they show retracted ice during the Roman Warm Period with ice advance during the Dark Ages (Denton & Karlen, 1973; Nesje, 2009). The contrast between southern Greenland and northwestern European climate fits with the analogy that late-Holocene centennial-scale climate variability in the North Atlantic region had a footprint similar to the modern North Atlantic Oscillation (Keigwin and Pickart, 1999; Andresen et al., 2004; Seidenkrantz et al., 2007; Mann et al., 2009; Trouet et al., 2009; D'Andrea et al., 2011; Ribeiro et al., 2011). The North Atlantic Oscillation is defined as the pressure difference between the Azores high and the Icelandic low over the last century (Marshall et al., 2001), and the resulting climate pattern shows an anti-phase behavior between southern Greenland SAT and northwestern European SAT (Hanna & Cappelen, 2003).

This North Atlantic Oscillation analogy has usually been made when comparing the Medieval Climate Anomaly to the LIA (e.g., Keigwin and Pickart, 1999; Mann et al., 2009; Trouet et al., 2009), but it may also have extended to earlier centennial climate events like the Roman Warm Period and the Dark Ages (e.g., Keigwin, 1996; Keigwin and Pickart, 1999; Andresen et al., 2004; Seidenkrantz et al., 2007; D'Andrea et al., 2011; Ribeiro et al., 2011). If this is the case, the Narsarsuaq moraine could indicate that at least one southern Greenland ice margin responded to late-Holocene century-scale climate variability. This speculation does, however, require further dating of other southern Greenland ice margins, because a regional

advance would be predicted if southern Greenland was generally cooler during the Roman Warm Period relative to the LIA.

4.5. Conclusions

We have used ^{10}Be surface exposure ages to date the retreat of Kiagtût sermiat from the Narsarsuaq moraine in southernmost Greenland at 1.51 ± 0.11 ka, and determined that ice reached its historical/LIA position at 1.34 ± 0.15 ka. Thus, high-precision dating confirms a pre-LIA late-Holocene glacier maximum extent in southernmost Greenland. We show that the Kiagtût sermiat occupied the Narsarsuaq moraine during cool/dry climate conditions in southern Greenland when cold Arctic waters filled nearby fjords, with retreat of Kiagtût sermiat from the moraine coincident with warming of southern Greenland. This transition from colder to warmer conditions in southern Greenland and the contemporary retreat of ice from the Narsarsuaq moraine are concurrent with northwestern European cooling from the Roman Warm Period into the Dark Ages, which would lend support to the hypothesis that late Holocene climate variability in southern Greenland did not necessarily track that of northwestern Europe (Andresen et al., 2004; Seidenkrantz et al., 2007; Mann et al., 2009; D'Andrea et al., 2011). At present, records for other southern Greenland ice margins are not necessarily inconsistent with the Narsarsuaq advance being regional in extent, but they also do not confirm such a correlation. We conclude that future research should focus on directly dating the late-Holocene extent of southern Greenland ice margins and quantitatively reconstructing the parallel climate conditions.

Acknowledgements

We thank E. Colville, E. Obbink, M. Reusche, E. Siewert, and D. Ullman for assistance in the

field and the laboratory. G. Sinclair provided our base map of Greenland. N. Larsen, N. Glasser, and an anonymous reviewer provided valuable suggestions on an early version of this manuscript. The National Geographic Society (8687-09), University of Wisconsin Climate, People and Environment Program and Wisconsin Alumni Research Foundation (AEC), and National Science Foundation Graduate Fellowship Program (KW) supported this research.

Online repository

Contains sample information, CRONUS online calculator input, and resulting ^{10}Be surface exposure ages for different production rate scaling schemes.

References

- Alley, R.B., Andrews, J.T., Brigham-Grette, J., Clarke, G.K.C., Cuffey, K.M., Fitzpatrick, J.J., Funder, S., Marshall, S.J., Miller, G.H., Mitrovica, J.X., Muhs, D.R., Otto-Bliesner, B.L., Polyak, L., White, J.W.C., 2010. History of the Greenland Ice Sheet: paleoclimatic insights. *Quaternary Science Reviews*, 29, 1728-1756.
- Andresen, C.S., Björck, S., Bennike, O., Bond, G., 2004. Holocene climate changes in southern Greenland. *Journal of Quaternary Science*, 18, 783-795.
- Andresen, C.S., Straneo, F., Ribergaard, M.H., Björk, A.A., Andersen, T.J., Kuijpers, A., Nørgaard-Pedersen, N., Kjær, K.H., Schjøth, F., Weckström, K., Ahlstrom, A.P., 2012. Rapid response of Helheim Glacier in Greenland to climate variability over the past century. *Nature Geoscience*, 5, 37-41.
- Axford, Y., Lose, S., Briner, J.P., Francis, D.R., Langdon, P.G., Walker, I.R., 2013. Holocene temperature history at the western Greenland Ice Sheet margin. *Quaternary Science Reviews*, 59, 87-100.
- Balco, G., Stone, J.O., Lifton, N.A., Dunai, T.J., 2008. A complete and easily accessible means of calculating surface exposure ages or erosion rates from ^{10}Be and ^{26}Al measurements. *Quaternary Geochronology*, 3, 174-195.
- Bennike, O., Sparrenbom, C.J., 2007. Dating of the Narssarsuaq stade in southern Greenland. *The Holocene*, 17, 279-282.
- Briner, J.P., Stewart, H.A.M., Young, N.E., Philipps, W., Losee, S., 2010. Using proglacial-threshold lakes to constrain fluctuations of the Jakobshavn Isbrae ice margin, western Greenland, during the Holocene. *Quaternary Science Reviews*, 29, 3861-3874.
- Briner, J.P., Young, N.E., Thomas, E.K., Stewart, H.A.M., Losee, S., Truex, S., 2011. Varve and radiocarbon dating support the rapid advance of Jakobshavn Isbrae during the Little Ice Age. *Quaternary Science Reviews*, 30, 2476-2486.
- Briner, J.P., Håkansson, L., Bennike, O., 2013. The deglaciation and Neoglaciation of Upernavik Isstrøm, Greenland. *Quaternary Research*, 80, 459-467.
- Briner, J.P., Kaufman, D.S., Bennike, O., Kosnik, M.A., 2014. Amino acid ratios in reworked marine bivalve shells constrain Greenland Ice Sheet history during the Holocene. *Geology*, 42, 75-78.
- Corbett, L.B., Young, N.E., Bierman, P.R., Briner, J.P., Neumann, T.A., Rood, D.H., Graly, J.A., 2011. Paired bedrock and boulder ^{10}Be concentrations resulting from early Holocene ice retreat near Jakobshavn Isfjord, western Greenland. *Quaternary Science Reviews*, 30, 1739-1749.

- Corbett, L.B., Bierman, P.R., Graly, J.A., Neumann, T.A., Rood, D.H., 2013. Constraining landscape history and glacial erosivity using paired cosmogenic nuclides in Upernavik, northwest Greenland. *Geological Society of America Bulletin*, doi:10.1130/B30813.1.
- Cuffey, K.M., Clow, G.D., 1997. Temperature, accumulation, and ice sheet elevation in central Greenland through the last deglacial transition. *Journal of Geophysical Research*, 102, 26,383-26,396.
- D'Andrea, W.J., Huang, Y., Fritz, C.S., Anderson, N.J., 2011. Abrupt Holocene climate change as an important factor for human migration in West Greenland. *Proceedings of the National Academies of Science*, 108, 9765-9769.
- Dahl-Jensen, D., Mosegaard, K., Gundestrup, N., Clow, G.D., Johnsen, S.J., Hansen, A.W., Balling, N., 1998. Past temperatures directly from the Greenland ice sheet. *Science*, 282, 268-271.
- Dawson, A.G., 1983. Glacier-dammed lake investigations in the Hullet lake area, South Greenland. *Meddelelser om Grønland, Geoscience*, 11, 24 pp.
- Denton, G.H., Karlen, W., 1973. Holocene climate variations—their pattern and possible cause. *Quaternary Research*, 3, 155-205.
- Fréchette, B., de Vernal, A., 2009. Relationship between Holocene climate variations over southern Greenland and eastern Baffin Island and synoptic circulation pattern. *Climate of the Past*, 5, 347-359.
- Funder, S., Kjeldsen, K.K., Kjær, Ó Cofaigh, C., 2011. The Greenland Ice Sheet during the past 300,000 years: a review. In: Ehlers, J., Gibbard, P.L., and Hughes, P.D., (Eds.) *Developments in Quaternary Science*, v. 15, Amsterdam, The Netherlands, pp. 699-713.
- Hanna, E., Cappelen, J., 2003. Recent cooling in coastal southern Greenland and relation with the North Atlantic Oscillation. *Geophysical Research Letters*, 30, 1132, doi:10.1029/2002GL015797.
- Heisinger, B., Lal, D., Jull, A.J.T., Kubik, P., Ivy-Ochs, S., Neumaier, S., Knie, K., Lazarev, V., Nolte, E., 2002a. Production of selected cosmogenic radionuclides by muons: 1. Fast muons. *Earth and Planetary Science Letters*, 200, 345-355.
- Heisinger, B., Lal, D., Jull, A.J.T., Kubik, P., Ivy-Ochs, S., Knie, K., Nolte, E., 2002b. Production of selected cosmogenic radionuclides by muons: 2. Capture of negative muons. *Earth and Planetary Science Letters*, 200, 357-369.
- Hughes, A.L.C., Rainsley, E., Murray, T., Fogwill, C.J., Schnabel, C., Xu, S., 2012. Rapid response of Helheim Glacier, southeast Greenland, to early Holocene climate warming. *Geology*, 40, 427-430.

- Jansen, E., Overpeck, J., Briffa, K.R., Duplessy, J.-C., Joos, F., Masson-Delmotte, V., Olago, D., Otto-Bliesner, B., Peltier, W.R., Rahmstorf, S., Ramesh, R., Raynaud, D., Rind, D., Solomina, O., Villalba, R., Zhange, D., 2007. Paleoclimate. In: Solomon, S., Qin, D., Manning, M., Chen, Z., Marquis, M., Averyt, K.B., Tignor, M., Miller, H.L. (Eds.), *Climate Change 2007: the Physical Science Basis. Contribution of Working Group I to the Fourth Assessment Report of the Intergovernmental Panel on Climate Change*. Cambridge University Press, Cambridge, United Kingdom and New York, NY, USA.
- Jensen, K.G., Kuijpers, A., Koç, N., Heinemeier, J., 2004. Diatom evidence of hydrographic changes and ice conditions in Igaliku Fjord, South Greenland, during the past 1500 years. *The Holocene*, 14, 152-164.
- Jessen, C.A., Solignac, S., Nørgaard-Pedersen, N., Mikkelsen, N., Kuijpers, A., Seidenkrantz, M.-S., 2011. Exotic pollen as an indicator of variable atmospheric circulation over the Labrador Sea region during the mid to late Holocene. *Journal of Quaternary Science*, 26, 286-296.
- Kaplan, M.R., Wolfe, A.P., Miller, G.H., 2002. Holocene environmental variability in southern Greenland inferred from lake sediments. *Quaternary Research*, 58, 149-159.
- Kaufman, D.S., Schneider, D.P., McKay, N.P., Ammann, C.M., Bradley, R.S., Briffa, K.R., Miller, G.H., Otto-Bliesner, B.L., Overpeck, J.T., Vinther, B.M., Arctic Lakes 2k Project Members, 2009. Recent warming reverses long-term Arctic cooling. *Science*, 325, 1236-1239.
- Keigwin, L.D., 1996. The Little Ice Age and Medieval Warm Period in the Sargasso Sea. *Science*, 274, 1504-1508.
- Keigwin, L.D., Pickart, R.S., 1999. Slope water current over the Laurentian Fan on interannual to millennial time scales. *Science*, 286, 520-523.
- Kelley, S.E., Briner, J.P., Young, N.E., Babonis, G.S., Csatho, B., 2012. Maximum late Holocene extent of the western Greenland Ice Sheet during the late 20th century. *Quaternary Science Reviews*, 56, 89-98.
- Kelly, M., 1980. The status of the Quaternary geology of western Greenland. *Rapport Grønlands Geologiske Undersøgelse*, 96, 24 pp.
- Kelly, M.A., Lowell, T.V., 2009. Fluctuations of local glaciers in Greenland during latest Pleistocene and Holocene time. *Quaternary Science Reviews*, 28, 2088-2106.
- Kelly, M.A., Lowell, T.V., Hall, B.L., Schaefer, J.M., Finkel, R.C., Goehring, B.M., Alley, R.B., Denton, G.H., 2008. A ¹⁰Be chronology of lateglacial and Holocene mountain glaciation in the Scoresby Sund region, east Greenland: implication for seasonality during lateglacial time. *Quaternary Science Reviews*, 27, 2273-2282.

- Kohl, C.P., Nishiizumi, K., 1992. Chemical isolation of quartz measurement of *in-situ*-produced cosmogenic nuclides. *Geochimica et Cosmochimica Acta*, 56, 3583-3587.
- Lal, D., 1991. Cosmic ray labeling of erosion surfaces: *in situ* nuclide production rates and erosion models. *Earth and Planetary Science Letters*, 104, 424-439.
- Lane, T.P., Roberts, D.H., Rea, B.R., Ó Cofaigh, C., Vieli, A., Ródes, A., 2013. Controls upon the Last Glacial Maximum deglaciation of the northern Uummannaq Ice Stream System, West Greenland. *Quaternary Science Reviews*, *in press*.
- Larsen, N.K., Kjær, K.H., Olsen, J., Funder, S., Kjeldsen, K.K., Nørgaard-Pedersen, N., 2011. Restricted impact of Holocene climate variations on the southern Greenland Ice Sheet. *Quaternary Science Reviews*, 30, 3171-3180.
- Larsen, N.K., Funder, S., Kjær, K.H., Kjeldsen, K.K., Knudsen, M.F., Linge, H., 2013. Rapid early Holocene ice retreat in West Greenland. *Quaternary Science Reviews*, *in press*, <http://dx.doi.org/10.1016/j.quascirev.2013.05.027>.
- Lassen, S.J., Kuijpers, A., Kunzendorf, H., Hoffmann-Wieck, G., Mikkelsen, N., Konradi, P., 2004. Late-Holocene Atlantic bottom-water variability in Igaliku Fjord, South Greenland, reconstructed from foraminifera faunas. *The Holocene*, 14, 165-171.
- Levy, L.B., Kelly, M.A., Howley, J.A., Virginia, R.A., 2012. Age of the Ørkendalen moraines, Kangerlussuaq, Greenland: constraints on the extent of the southwestern margin of the Greenland Ice Sheet during the Holocene. *Quaternary Science Reviews*, 52, 1-5.
- Levy, L.B., Kelly, M.A., Lowell, T.V., Hall, B.L., Hempel, L.A., Honsaker, W.M., Lusas, A.R., Howley, J.A., Axford, Y.L., 2013. Holocene fluctuations of Bregne ice cap, Scoresby Sund, east Greenland: a proxy for climate along the Greenland Ice Sheet margin. *Quaternary Science Reviews*, *in press*.
- Long, A.J., Woodroffe, S.A., Roberts, D.H., Dawson, S., 2011. Isolation basins, sea-level changes and the Holocene history of the Greenland Ice Sheet. *Quaternary Science Reviews*, 30, 3748-3768.
- Loso, M.G., Doak, D.F., 2006. The biology behind lichenometric dating curves. *Oecologia*, 147, 223-229.
- Lowell, T.V., Hall, B.L., Kelly, M.A., Bennike, O., Lusas, A.R., Honsaker, W., Smith, C.A., Levy, L.B., Travis, S., Denton, G.H., 2013. Late Holocene expansion of Istovet ice cap, Liverpool Land, east Greenland. *Quaternary Science Reviews*, 63, 128-140.
- Mann, M.E., Zhang, Z., Rutherford, S., Bradley, R.S., Hughes, M.K., Shindell, D., Ammann, C., Faluvegi, G., Ni, F., 2009. Global signatures and dynamical origins of the Little Ice Age and Medieval Climate Anomaly. *Science*, 326, 1256-1260.

- Marcott, S.A., Shakun, J.D., Clark, P.U., Mix, A.C., 2013. A reconstruction of regional and global temperature for the past 11,300 years. *Science*, 339, 1198-1201.
- Marshall, J., Johnson, H., Goodman, J., 2001. A study of the interaction of the North Atlantic Oscillation with ocean circulation. *Journal of Climate*, 14, 1399-1421.
- Møller, H.S., Jensen, K.G., Kuijpers, A., Aagaard-Sørensen, S., Seidenkrantz, M.-S., Prins, M., Endler, R., Mikkelsen, N., 2006. Late-Holocene environment and climatic changes in Ameralik Fjord, southwest Greenland: evidence from the sedimentary record. *The Holocene*, 16, 685-695.
- Nelson, A.H., Bierman, P.R., Shakun, J.D., Rood, D.H., 2014, in press. Using *in situ* cosmogenic ^{10}Be to identify the source of sediment leaving Greenland. *Earth Surface Processes and Landforms*, doi:10.1002/esp.356574.
- Nesje, A., 2009. Latest Pleistocene and Holocene alpine glacier fluctuations in Scandinavia. *Quaternary Science Reviews*, 28, 2119-2136.
- Nick, F.M., Vieli, A., Andersen, M.L., Joughin, I., Payne, A., Edwards, T.L., Pattyn, F., van de Wal, R.S.W., 2013. Future sea-level rise from Greenland's main outlet glaciers in a warming climate. *Nature*, 497, 235-238.
- Nishiizumi, K., Elmore, D., Ma, X.Z., Arnold, J.R., 1984. ^{10}Be and ^{36}Cl profiles in an Apollo 15 drill core. *Earth and Planetary Science Letters*, 70, 157-163.
- Nishiizumi, K., Imamura, M., Caffee, M., Southon, J.R., Finkel, R.C., McAninch, J., 2007. Absolute calibration of ^{10}Be AMS standards. *Nuclear Instruments & Methods in Physics Research Section B: Beam Interactions with Materials and Atoms*, 258, 403-413.
- Nørgaard-Pedersen, N., Mikkelsen, 2009. 8000 year record of climate variability and fjord dynamics from Southern Greenland. *Marine Geology*, 264, 177-189.
- Oerlemans, J., 2005. Extracting a climate signal from 169 glacier records. *Science*, 308, 675-677.
- PAGES 2k Network, 2013. Continental-scale temperature variability during the past two millennia. *Nature Geoscience*, 6, 339-346.
- Perner, K., Moros, M., Lloyd, J.M., Kuijpers, A., Telford, R.J., Harff, J., 2011. Centennial scale benthic foraminiferal record of late Holocene oceanographic variability in Disko Bugt, West Greenland. *Quaternary Science Reviews*, 30, 2815-2826.
- Ribeiro, S., Moros, M., Ellegaard, M., Kuijpers, A., 2011. Climate variability in West Greenland during the past 1500 years: evidence from a high-resolution marine palynological record from Disko Bay. *Boreas*, 10.1111/j.1502-3885.2011.00216.x.

- Roberts, D.H., Long, A.J., Schnabel, C., Freeman, S., Simpson, M.J.R., 2008. The deglacial history of southeast sector of the Greenland Ice Sheet during the Last Glacial Maximum. *Quaternary Science Reviews*, 27, 1505-1516.
- Roberts, D.H., Rea, B.R., Lane, T.P., Schnabel, C., Rodés, 2013. New constraints on Greenland ice sheet dynamics during the last glacial cycle: Evidence from the Uummannaq ice stream system. *Journal of Geophysical Research: Earth Surface*, 118, 1-23, doi:10.1002/jgrf.20032.
- Rood, D.H., Hall, S., Guilderson, T.P., Finkel, R.C., Brown, T.A., 2010. Challenges and opportunities in high-precision Be-10 measurements at CAMS. *Nuclear Instruments and Methods B: Beam Interactions with Materials and Atoms*, 268, 730-732.
- Rood, D.H., Brown, T.A., Finkel, R.C., Guilderson, T.P., 2013. Poisson and non-Poisson uncertainty estimations of $^{10}\text{Be}/^9\text{Be}$ measurements at LLNL-CAMS. *Nuclear Instruments and Methods B: Beam Interactions with Materials and Atoms*, 294, 426-429.
- Seidenkrantz, M.-S., Aagaard-Sørensen, S., Sulsbrück, H., Kuijpers, A., Jensen, K.G., Kunzendorf, H., 2007. Hydrography and climate of the last 4400 years in a SW Greenland fjord: implications for Labrador Sea palaeoceanography. *The Holocene*, 17, 387-401.
- Seidenkrantz, M.-S., Roncaglia, L., Fischel, A., Heilmann-Clausen, C., Kuijpers, A., Moros, M., 2008. Variable North Atlantic climate seesaw patterns documented by a late Holocene marine record from Disko Bugt, West Greenland. *Marine Micropaleontology*, 68, 66-83.
- Severinghaus, J.P., Sowers, T., Brook, E.J., Alley, R.B., Benders, M.L., 1998. Timing of abrupt climate change at the end of the Younger Dryas interval from thermally fractionated gases in polar ice. *Nature*, 39, 141-146.
- Sparrenbom, C.J., Bennike, O., Björck, S., Lambeck, K., 2006a. Relative sea-level changes since 15 000 cal. yr BP in the Nanortalik area, southern Greenland. *Journal of Quaternary Science*, 21, 29-48.
- Sparrenbom, C.J., Bennike, O., Björck, S., Lambeck, K., 2006b. Holocene relative sea-level changes in the Qaqortoq area, southern Greenland. *Boreas*, 35, 171-187.
- Stone, J.O., 2000. Air pressure and cosmogenic isotope production. *Journal of Geophysical Research*, 105, 23,753-23,759.
- Trouet, V., Esper, J., Graham, N.E., Baker, A., Scourse, J.D., Frank, D.C., 2009. Persistent positive North Atlantic Oscillation mode dominated the Medieval Climate Anomaly. *Science*, 324, 78-80.
- Weidick, A., 1963. Ice margin features in the Julianehåb district, South Greenland. *Meddelelser*

om Grønland, 165, 133 pp.

- Weidick, A., Oerter, H., Reeh, N., Thomsen, H.H., Thorning, L., 1990. The recession of the Inland Ice margin during the Holocene climatic optimum in the Jakobshavn Isfjord area of West Greenland. *Palaeoceanography, Palaeoclimatology, Palaeoecology*, 82, 389-399.
- Weidick, A., Kelly, M., and Bennike, O., 2004. Late Quaternary development of the southern sector of the Greenland Ice Sheet, with particular reference to the Qassimiut lobe. *Boreas*, 33, 284-299.
- Weidick, A., Bennike, O., 2007. Quaternary glaciation history of Jakobshavn Isbræ and the Disko Bugt region, west Greenland: a review. *Geological Survey of Denmark and Greenland Bulletin*, 14, 78.
- Weidick, A., Bennike, O., Citterio, M., Nørgaard-Pedersen, 2012. Neoglacial and historical glacier changes around Kangersuneq fjord in southern West Greenland. *Geological Survey of Denmark and Greenland Bulletin*, 27, 68 pp.
- Xu, S., Dognas, A.B., Freeman, S.P.H.T., Schnabel, C., Wilcken, K.M., 2010. Improved ^{10}Be and ^{26}Al -AMS with a 5 M V spectrometer. *Nuclear Instruments and Methods in Physics Research B*, 268, 736-738.
- Young, N.E., Briner, J.P., Stewart, H.A.M., Axford, Y., Csatho, B., Rood, D.H., Finkel, R.C., 2011. Response of Jakobshavn Isbræ, Greenland, to Holocene climate change. *Geology*, 39, 131-134.
- Young, N.E., Schaefer, J., Briner, J.P., Goehring, B., 2013. A ^{10}Be production-rate calibration for the Arctic, *Journal of Quaternary Science*, 28, 515-526.

Figure Captions.

Figure 4.1. Location of Holocene records from southern to central Greenland. Figure 2 location is indicated by the dashed-line box. Also shown are early and late Holocene ^{10}Be dates, ice-marginal lake records, reworked ^{14}C dates in historical moraines, surface-air temperature (SAT) records, lake biogenic silica records, marine ice-rafted debris, and benthic faunal records. In counter-clockwise order around the island are represented sites from ¹Briner et al. (2011), ²Briner et al. (2014), ³Briner et al. (2013), ⁴Corbett et al. (2013), ⁵Lane et al. (2013), ⁶Roberts et al. (2013), ⁷Perner et al. (2011), ⁸Corbett et al. (2011), ⁹Axford et al. (2013), ¹⁰Weidick et al. (1990), ¹¹Briner et al. (2010), ¹²Kelley et al. (2012), ¹³Young et al. (2011), ¹⁴Levy et al. (2012), ¹⁵D'Andrea et al. (2011), ¹⁶Kelly (1980), ¹⁷Seidenkrantz et al. (2007), ¹⁸Weidick et al. (2004), ¹⁹Kaplan et al. (2002), ²⁰Nørgaard-Pedersen & Mikkelsen (2009), ²¹Larsen et al. (2011), ²²this study, ²³Andresen et al. (2004), ²⁴Dahl-Jensen et al. (1998), ²⁵Hughes et al. (2012), ²⁶Levy et al. (2013), ²⁷Kelly et al. (2008), and ²⁸Lowell et al. (2013).

Figure 4.2. The Narsarsuaq region, its three main outlet glaciers—Eqalorutsit kangigdlît sermiat, Kiagtût sermiat, and Qôrqp sermia, early Holocene moraines (orange lines), Narsarsuaq moraine (yellow lines), and historical moraine (blue lines). (Modified from Larsen et al., 2011.) ^{10}Be sample sites of this study indicated by the red circles, and ^{14}C sample sites of previous studies by the green circles. Note the locations of Nordbo Glacier, Nordbosø, and Lower Nordbosø (the Larsen et al., 2011 study area, with the blue dot indicating the coring sites).

Figure 4.3. ^{10}Be exposure ages and standard error from this study for historic-marginal ages (top) and Narsarsuaq moraine ages (bottom). One older statistical outlier for each group is

observable.

Figure 4.4. Late-Holocene records from southern to western Greenland (Figure 1). To facilitate comparison between figures, each relevant reference below is given with the corresponding number shown in Figure 1. (A) ^{14}C dates from intervals of organic deposition in threshold lakes (black bars) ($^{20}\text{Kaplan et al., 2002; }^{1,3,11}\text{Briner et al., 2010; 2011; 2013; }^{21}\text{Larsen et al., 2011; }^{12}\text{Kelley et al., 2012}$), and from reworked material in historical moraines that clearly document as ice being less far-reaching than its late-Holocene extent (red bars) ($^{16}\text{Kelly, 1980; }^{10,18}\text{Weidick et al., 1990; 2004; }^{2}\text{Briner et al., 2014}$), and Narsarsuaq ^{10}Be dates (blue squares; this study), (B) ice rafted debris from Ga3-2 ($^{20}\text{Nørgaard-Pedersen \& Mikkelsen, 2009}$), (C) percent agglutinated/Arctic benthic foraminifera from 248260-2 ($^{17}\text{Seidenkrantz et al., 2007}$), (D) percent Atlantic foraminifera from 344310 ($^{7}\text{Perner et al., 2011}$), (E) change in surface air temperature (SAT) at Dye 3 (purple, $^{24}\text{Dahl-Jensen et al., 1998}$), Jakobshavn (black, $^{9}\text{Axford et al., 2013}$), and Kangerlussuaq (blue, $^{15}\text{D'Andrea et al., 2011}$), (F) percent biogenic silica in Lake N14 sediment ($^{23}\text{Andresen et al., 2004}$), and (G) compilation of relative changes in Arctic temperatures (Kaufman et al., 2009). Vertical gray bar shows timing of maximum Kiagtût sermiat extent at the Narsarsuaq moraine.

Table 4.1. ^{10}Be sample data and exposure ages

Sample ^β	Latitude (°N)	Longitude (°E)	Elevation (m asl)	Thickness (cm)	Shielding Factor	^{10}Be (atoms g ⁻¹) ^γ	Uncertainty (atoms g ⁻¹) ^ε	Age (ka) ^x	Internal Uncertainty (ka) ^ε
Just within the Narsarsuaq moraine									
<i>NA08-05</i>	<i>61.2061</i>	<i>-45.3153</i>	<i>285</i>	<i>2.0</i>	<i>1.000</i>	<i>27861</i>	<i>2252</i>	<i>4.85</i>	<i>0.39</i>
NA08-06	61.2061	-45.3153	285	4.0	1.000	6683	890	1.18	0.16
NA08-24	61.2061	-45.3119	305	1.5	0.999	9966	907	1.70	0.15
NA10-03	61.2063	-45.3150	289	2.5	0.999	11338	1073	1.98	0.19
NA08-07	61.1856	-45.3618	68	1.5	0.973	7199	451	1.60	0.10
NA08-08	61.1856	-45.3618	68	1.5	0.973	9550	801	2.12	0.18
NA08-09*	61.1856	-45.3618	67	2.5	0.960	6232	805	1.41	0.18
NA08-10*	61.1851	-45.3632	76	2.0	0.980	6389	962	1.40	0.21
NA08-12	61.1847	-45.3635	59	2.5	0.965	6002	1072	1.37	0.24
NA08-13*	61.1886	-45.3590	153	1.5	1.000	6845	760	1.35	0.15
NA08-14*	61.1889	-45.3602	159	2.0	1.000	5262	1323	1.04	0.26
Ice-distal of the historical extent of Kiagtût sermiat									
NA08-01	61.2153	-45.3045	180	2.0	0.992	9354	453	1.82	0.09
NA08-02	61.2153	-45.3050	180	1.5	0.995	7706	742	1.49	0.14
<i>NA08-03*</i>	<i>61.2158</i>	<i>-45.3042</i>	<i>179</i>	<i>3.0</i>	<i>0.990</i>	<i>17712</i>	<i>1701</i>	<i>3.49</i>	<i>0.34</i>
NA08-04	61.2149	-45.3043	171	2.5	0.989	5784	1173	1.14	0.23
NA10-01	61.2159	-45.3041	185	2.0	0.994	4707	289	0.91	0.06
NA10-02	61.2159	-45.3034	181	2.0	0.991	6757	343	1.32	0.07

^βItalics indicates sample with inheritance that were excluded as outliers.

*Data measured at SUERC.

^γ ^{10}Be concentrations are blank corrected (LLNL: average blank $^{10}\text{Be}/^9\text{Be}$ of $8.8 \pm 1.5 \times 10^{-16}$, n=6;

SUERC: average blank $^{10}\text{Be}/^9\text{Be}$ of $6.1 \pm 0.7 \times 10^{-16}$, n=3) and normalized to standards

07KNSTD3110 with a reported ratio of 2.85×10^{-12} (Nishiizumi et al., 2007) at LLNL or

NIST_27900 with an assumed ratio of 2.79×10^{-11} at SUERC.

^εUncertainties are 1σ AMS uncertainties propagated in quadrature with associated blank uncertainties.

^xCalculations use standard atmosphere, density of 2.65 g cm^{-3} , zero erosion, and no inheritance in the CRONUS online calculator (Balco et al., 2008) (version 2.2, with constants version 2.2)

using the Arctic reference sea-level high-latitude spallogenic production rate $3.96 \pm 0.15 (\pm 1\sigma)$

^{10}Be atoms $\text{g}^{-1} \text{ yr}^{-1}$ (Young et al., 2013), muonogenic production after Heisinger et al. (2002a, b),

and the time-dependent Lal/Stone scaling scheme (Lal, 1999; Stone, 2000).

Table 4.S1. Complete ^{10}Be chemistry data and exposure age calculation inputs.

Sample ^β	Latitude (°N)	Longitude (°E)	Elevation (m asl)	Elevation pressure	Thickness (cm)	Density (g cm ⁻³)	Shielding Factor	Erosion rate	Quartz added(g)	OSU Blue Carrier added(g)	¹⁰ Be Carrier Added (μg)	Measured			Measured			¹⁰ Be AMS standard ^γ
												Measure d Blank ¹⁰ Be/ ⁹ Be (10 ⁻¹⁵)	Blank ¹⁰ Be/ ⁹ Be (10 ⁻¹⁵)	Measure d Sample ¹⁰ Be/ ⁹ Be (10 ⁻¹⁵)	Sample ¹⁰ Be/ ⁹ Be Uncertainty (10 ⁻¹⁵)	10Be (atoms g ⁻¹) ^γ	Uncertainty (atoms g ⁻¹) ^γ	
NA08-05	61.2061	-45.3153	285	std	2.0	2.65	1.000	0	7.33	1.033	247.9	1.250	0.378	12.330	0.997	27861	2252	07KNSTD3110
NA08-06	61.2061	-45.3153	285	std	4.0	2.65	1.000	0	13.003	1.033	247.9	1.250	0.378	5.246	0.699	6683	890	07KNSTD3110
NA08-24	61.2061	-45.3119	305	std	1.5	2.65	0.999	0	11.736	1.033	247.9	1.250	0.378	7.060	0.643	9966	907	07KNSTD3110
NA10-03	61.2063	-45.3150	289	std	2.5	2.65	0.999	0	10.715	1.037	248.9	0.394	0.277	23.243	2.232	11338	1073	07KNSTD3110
NA08-07	61.1856	-45.3618	68	std	1.5	2.65	0.973	0	29.918	1.032	247.7	0.429	0.160	13.010	0.815	7199	451	07KNSTD3110
NA08-08	61.1856	-45.3618	68	std	1.5	2.65	0.973	0	22.786	1.044	250.6	0.394	0.277	12.990	1.090	9550	801	07KNSTD3110
NA08-09*	61.1856	-45.3618	67	std	2.5	2.65	0.960	0	28.839	1.043	250.3	1.699	0.472	10.744	1.388	6232	805	NIST_27900
NA08-10*	61.1851	-45.3632	76	std	2.0	2.65	0.980	0	22.463	1.041	249.8	1.699	0.472	8.596	1.294	6389	962	NIST_27900
NA08-12	61.1847	-45.3635	59	std	2.5	2.65	0.965	0	24.56	1.04	249.6	0.936	9.156	8.838	1.578	6002	1072	07KNSTD3110
NA08-13*	61.1886	-45.3590	153	std	1.5	2.65	1.000	0	26.909	1.042	250.1	1.699	0.472	11.023	1.224	6845	760	NIST_27900
NA08-14*	61.1889	-45.3602	159	std	2.0	2.65	1.000	0	12.502	1.042	250.1	1.699	0.472	3.937	0.990	5262	1323	NIST_27900
NA08-01	61.2153	-45.3045	180	std	2.0	2.65	0.992	0	26.692	1.031	247.4	0.429	0.160	15.100	0.731	9354	453	07KNSTD3110
NA08-02	61.2153	-45.3050	180	std	1.5	2.65	0.995	0	45.738	1.041	249.8	1.154	0.351	21.110	2.033	7706	742	07KNSTD3110
NA08-03*	61.2158	-45.3042	179	std	3.0	2.65	0.990	0	21.803	1.036	248.6	1.699	0.472	23.244	2.232	17712	1701	NIST_27900
NA08-04	61.2149	-45.3043	171	std	2.5	2.65	0.989	0	14.995	1.034	248.2	1.250	0.378	5.230	1.061	5784	1173	07KNSTD3110
NA10-01	61.2159	-45.3041	185	std	2.0	2.65	0.994	0	33.271	1.034	248.2	0.429	0.160	9.444	0.579	4707	289	07KNSTD3110
NA10-02	61.2159	-45.3034	181	std	2.0	2.65	0.991	0	36.363	1.034	248.2	0.429	0.160	14.820	0.751	6757	343	07KNSTD3110

Table 4.S1 footnotes.

*β*Italics indicates sample with inheritance that were excluded as outliers.

*Data measured at SUERC.

^γ¹⁰Be concentrations are blank corrected (LLNL: average blank ¹⁰Be/⁹Be of $8.8 \pm 1.5 \times 10^{-16}$, n=6;

SUERC: average blank ¹⁰Be/⁹Be of $6.1 \pm 0.7 \times 10^{-16}$, n=3) and normalized to standards

07KNSTD3110 with a reported ratio of 2.85×10^{-12} (Nishiizumi et al., 2007) at LLNL or

NIST_27900 with an assumed ratio of 2.79×10^{-11} at SUERC.

^εUncertainties are 1σ AMS uncertainties propagated in quadrature with associated blank uncertainties.

Table 4.S2. Comparison of ^{10}Be age calculations using alternative scaling schemes

Sample ^b	Lal/Stone Constant Production (ka)	Internal Uncertainty (ka) ^c	External Uncertainty (ka) ^d	Desilets time- dependent (ka)	External Uncertainty (ka) ^d	Dunai time- dependent (ka)	External Uncertainty (ka) ^d	Lifton time- dependent (ka)	External Uncertainty (ka) ^d	Lal/Stone time- dependent (ka)	External Uncertainty (ka) ^d
NA08-05	4.85	0.39	0.43	4.87	0.44	4.92	0.45	4.86	0.45	4.85	0.43
NA08-06	1.18	0.16	0.16	1.19	0.17	1.21	0.17	1.16	0.16	1.18	0.16
NA08-24	1.70	0.15	0.17	1.70	0.17	1.73	0.18	1.67	0.17	1.70	0.17
NA10-03	1.98	0.19	0.20	1.98	0.21	2.01	0.21	1.95	0.20	1.98	0.20
NA08-07	1.60	0.10	0.12	1.58	0.12	1.60	0.12	1.55	0.12	1.60	0.12
NA08-08	2.21	0.18	0.20	2.09	0.20	2.12	0.20	2.07	0.20	2.12	0.20
NA08-09*	1.41	0.18	0.19	1.40	0.19	1.42	0.19	1.37	0.19	1.41	1.90
NA08-10*	1.40	0.21	0.22	1.39	0.22	1.41	0.22	1.36	0.21	1.40	0.22
NA08-12	1.37	0.24	0.25	1.35	0.25	1.37	0.25	1.32	0.24	1.37	0.25
NA08-13*	1.35	0.15	0.16	1.35	0.16	1.37	0.16	1.32	0.16	1.35	0.16
NA08-14*	1.04	0.26	0.26	1.03	0.26	1.05	0.27	1.01	0.26	1.04	0.26
NA08-01	1.82	0.09	0.11	1.82	0.12	1.84	0.12	1.79	0.12	1.82	0.11
NA08-02	1.49	0.14	0.15	1.49	0.16	1.51	0.16	1.46	0.15	1.49	0.15
NA08-03*	3.49	0.34	0.36	3.48	0.36	3.52	0.37	3.46	0.37	3.49	0.36
NA08-04	1.14	0.23	0.24	1.14	0.24	1.16	0.24	1.12	0.23	1.14	0.24
NA10-01	0.91	0.06	0.07	0.91	0.07	0.92	0.07	0.89	0.07	0.91	0.07
NA10-02	1.32	0.07	0.08	1.31	0.09	1.33	0.09	1.29	0.09	1.32	0.08

Italics indicates sample with inheritance that were excluded as outliers.

*Data measured at SUERC.

^xCalculations use standard atmosphere, density of 2.65 g cm^{-3} , zero erosion, and no inheritance in the CRONUS online calculator (Balco et al., 2008) (version 2.2, with constants version 2.2) using the Arctic reference sea-level high-latitude spallogenic production rate 3.96 ± 0.15 ($\pm 1\sigma$) ^{10}Be atoms $\text{g}^{-1} \text{ yr}^{-1}$ (Young et al., 2013) and muonogenic production after Heisinger et al. (2002a, b).

^cUncertainties are 1σ AMS uncertainties only, propagated in quadrature with associated blank uncertainties.

[#]Includes scaling scheme and production rate uncertainties (Balco et al., 2008).

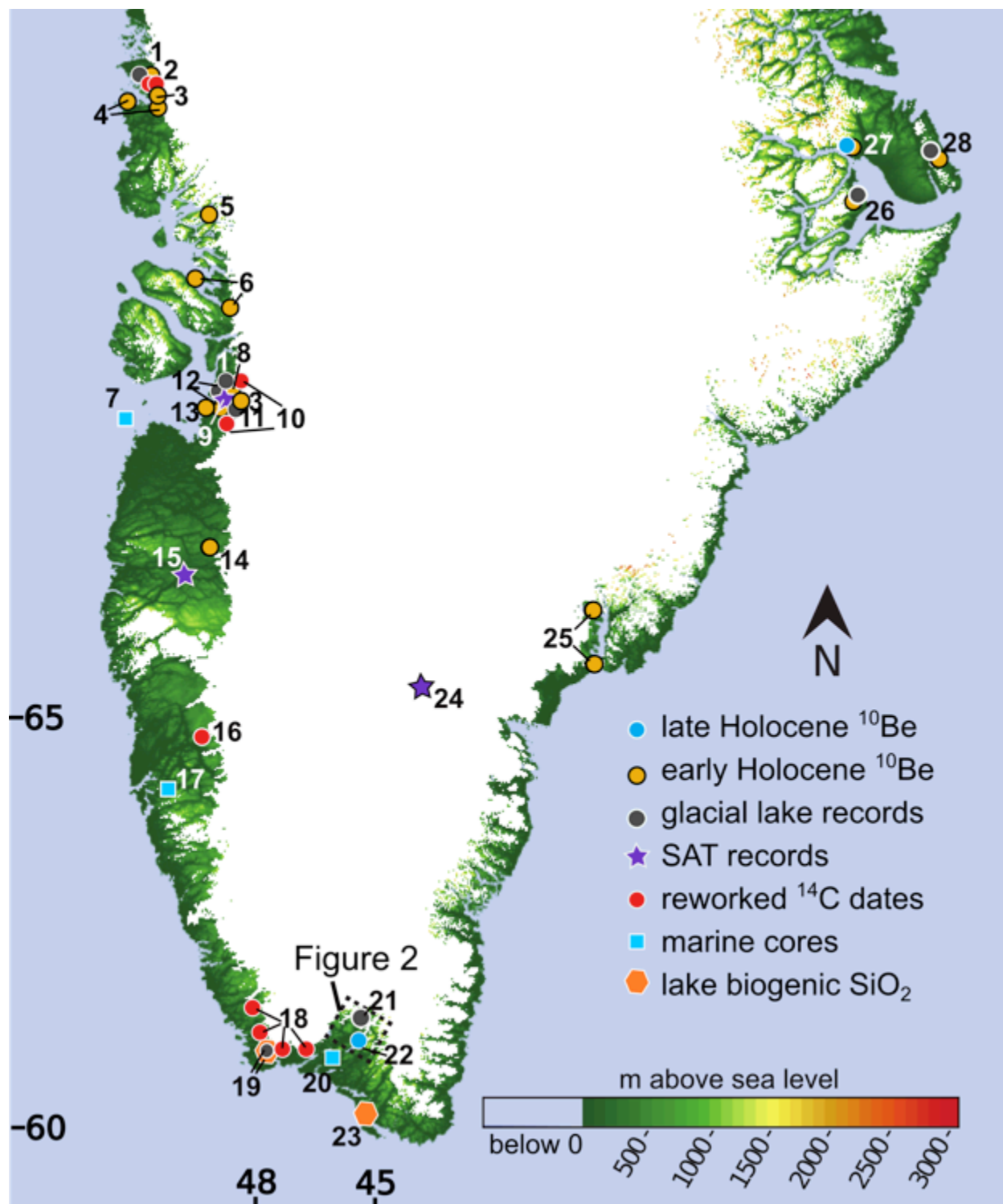


Figure 4-1.

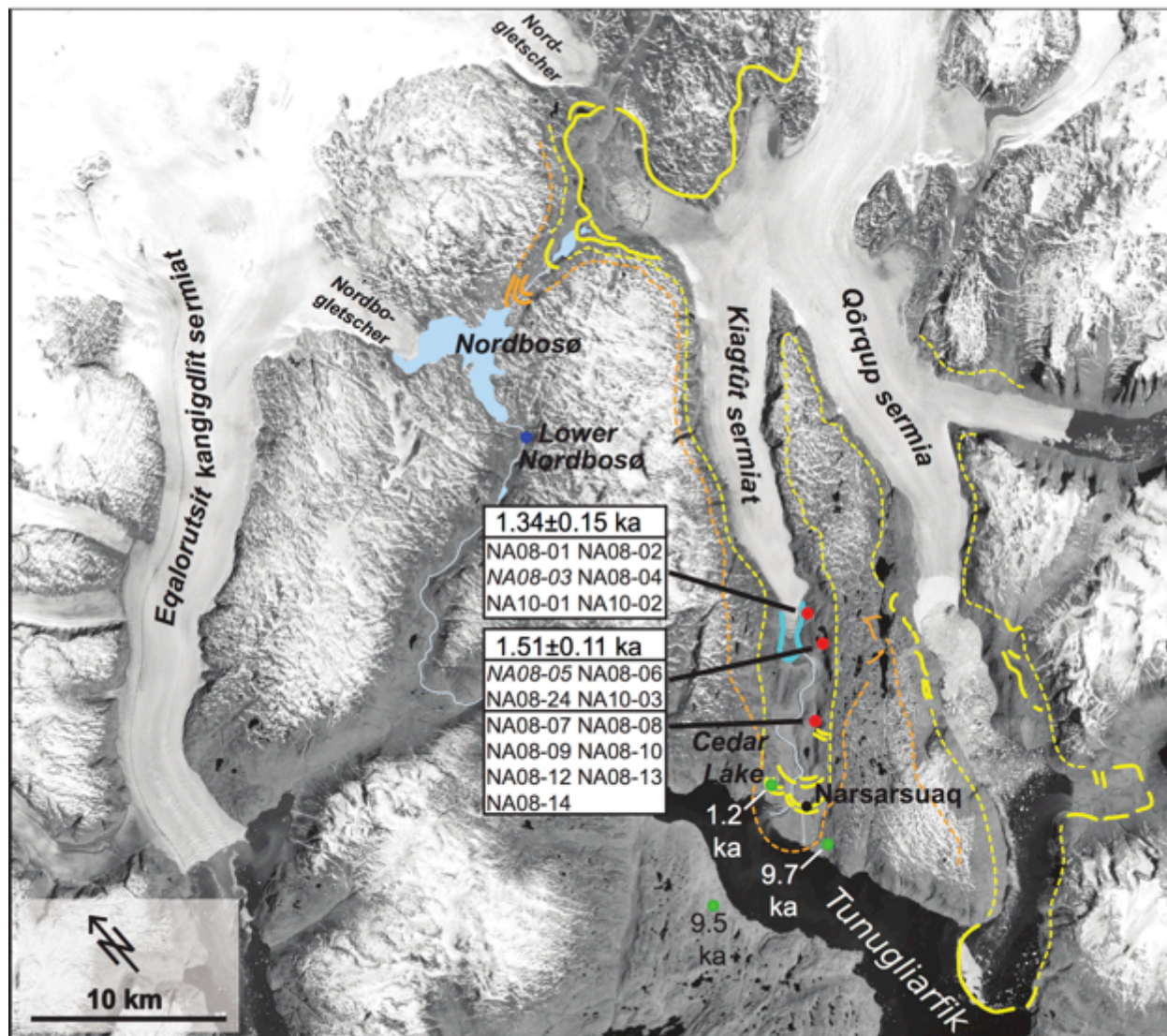


Figure 4-2.

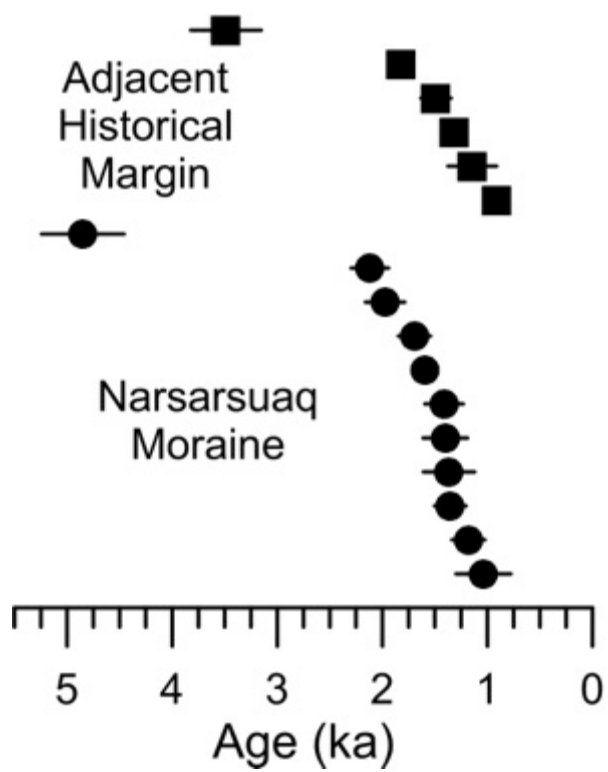


Figure 4-3.

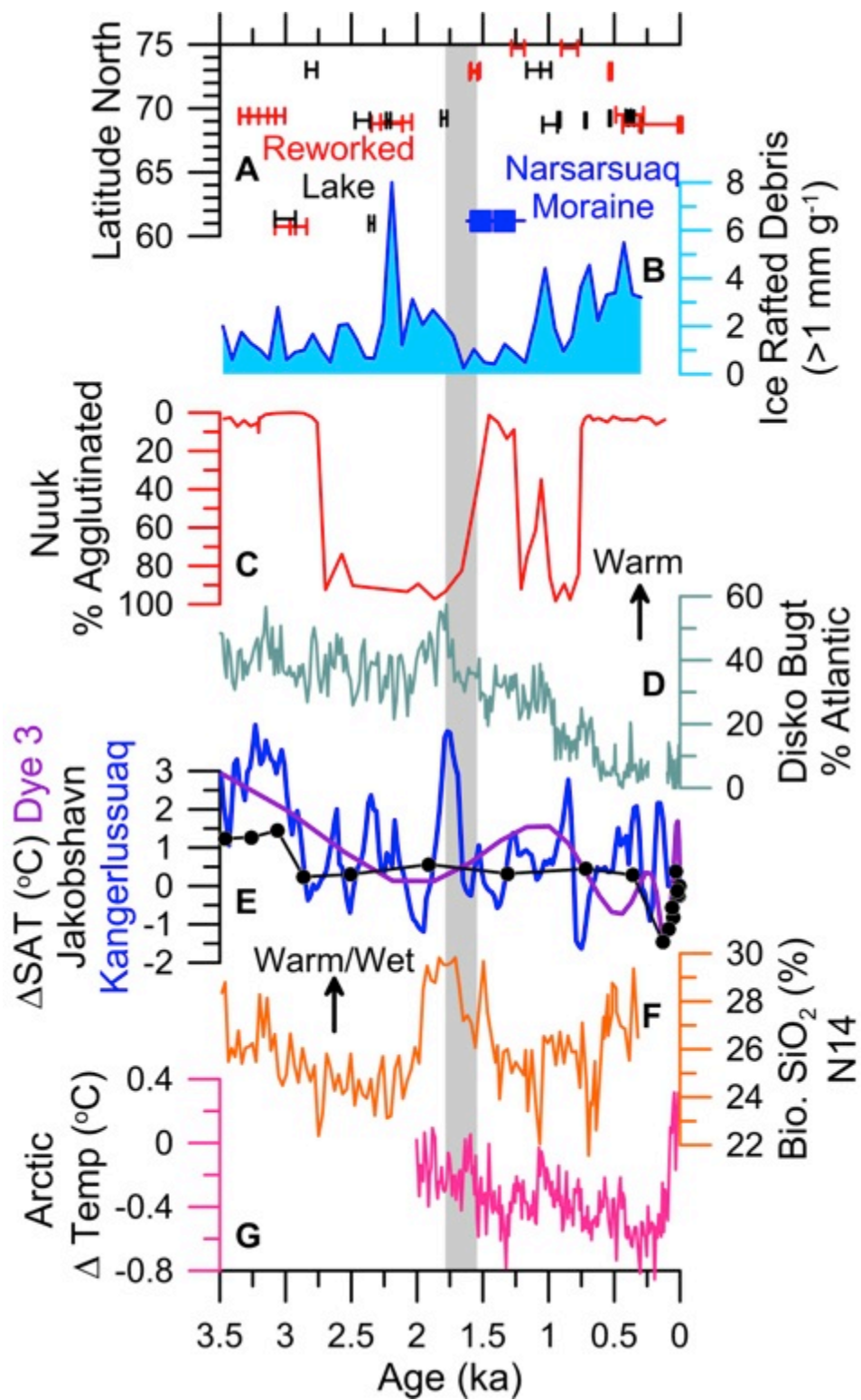


Figure 4-4.

CHAPTER V: CONCLUSIONS

5.1. Summary

This dissertation examines southwestern Greenland Ice Sheet (GrIS) retreat chronology under conditions ranging from a Last Glacial Maximum (LGM) position on the continental shelf break to a Holocene position inland of the modern coastline. During the LGM and early deglaciation, the southwestern GrIS margin rested on the middle to inner shelf after an early retreat from the shelf break, probably due to a combination of local sea level fluctuations and an increase in shortwave radiative forcing (Figure 1-1; Chapter II; Clark et al., 2009; 2012). During the late last deglaciation, exposure of the modern coastline occurred around the start of the Holocene, when boreal summer insolation was at its maximum and when the Labrador Sea upper water column warmed rapidly from glaciation-like cool temperatures (Figure 1-1; Chapter III; Berger and Loutre, 1991; Knutz et al., 2011; Winsor et al., 2012). In a purely terrestrial environment, the late-Holocene Kiagtût sermiat outlet glacier in southern Greenland responded to local environmental changes that may have deviated from average late-Holocene hemispheric climate trends (Chapter IV; Seidenkrantz et al., 2004; 2008; Mann et al., 2009; Trouet et al., 2009; Perner et al., 2012; Winsor et al., 2014). This comprehensive treatment of margin retreat is only possible due to the use of complementary marine and terrestrial records.

5.2. Retreat Forcings

The retreat chronologies discussed here suggest southwestern GrIS retreat due to small changes in sea level (Chapter II), regional oceanic warming (Chapter III), rises in radiative forcing (Chapters II and III), and local air temperature increase (Chapter IV). Each of these

drivers exists in the modern, and is projected to increase in magnitude over the coming centuries. When the GrIS margin, located on the continental shelf break, was exposed to even small sea level fluctuations of the early last deglaciation (Clark et al., 2009; 2012), it retreated to a new mid- to inner-shelf position within several centuries. Once there, however, ~100 m of deglacial sea level rise did not prompt collapse and retreat behind the modern coastline—such retreat was only achieved by warming of the waters in contact with the ice margin (Knutz et al., 2011; Winsor et al., 2012). With the onset of ocean warming, southwestern GrIS abandonment of the inner shelf and coast occurred over less than 2,000 years. Late in the Holocene, the land-terminating southernmost Greenland Kiagtût sermiat outlet glacier responded rapidly to what was most likely to centennial scale changes in atmospheric temperatures (Winsor et al., 2014).

5.3. Future research directions

5.3.1. Early deglaciation shelf retreat

Abundant opportunities for defining southwestern GrIS shelf retreat mechanisms would be provided by sediment core records and submarine geomorphology. Categorization of sand-fraction provenance would test whether ice-rafted debris (IRD) in core HU87033-008 is from southern Greenland (Knutz et al., 2011; Simon et al., 2013). Coupled with silt- and clay-fraction provenances, this would determine whether the source of sand-transporting icebergs was measurably different from the source of silts and clays, a difference that would not be expected under the sedimentation mechanisms proposed in this dissertation. Grain size analysis to examine sortedness of the silt fraction of HU87033-008 would point to an IRD source if poorly sorted (Andrews, 2000), and a meltwater plume or Deep Western Boundary Undercurrent source if well sorted (Fagel et al., 1997). The sand, silt, and clay weight percentages discussed in

Chapter II, and previous work on the undercurrent (Fagel et al., 1997), suggest a meltwater plume deposition, but additional provenance studies and grain size analyses would lend support (or opposition) to this hypothesis.

The southwestern Greenland continental shelf remains largely unmapped (Kelly, 1985). Early bathymetric soundings performed in the 1960s and 70s documented moraine-like landforms on the inner shelf and in cross-shelf troughs (Figure 2-1b; Rvachev, 1964; Brett and Zarudzki, 1979; Roksandic, 1979). However, these possible moraines are not dated, nor can they offer detailed constraints on ice sheet behavior at the time of deposition. High-resolution bathymetric mapping on the southwestern Greenland shelf would enable identification of glacially derived landforms, which, if radiocarbon dated, could define periods of ice margin stabilization (Ó Cofaigh et al., 2012). Furthermore, several large cross-shelf troughs on the shelf near Nuuk and Paamiut may have housed ice streams. If present, these ice streams would have been strong controls on southwestern GrIS behavior (Roberts et al., 2010; Ó Cofaigh et al., 2012; 2013; Dowdeswell et al., 2013; Simon et al., 2013). Without bathymetric mapping capable of defining potential ice stream behavior, a comprehensive understanding of southwest GrIS retreat is not possible (Roberts et al., 2010).

An intriguing potential course of study stemming from this work is the influence of a 19 ka meltwater pulse, which may have rapidly increased sea levels by 10 m immediately after the LGM sea-level minimum (Figure 2-4; Clark et al., 2004; 2009). Sea-level fingerprinting indicates that a northern hemisphere origin for this meltwater is likely (Clark et al., 2009; Carlson and Clark, 2012). Local sea level changes in southwestern Greenland would have been dependent on the precise location of this northern hemisphere ice loss, and been influenced by the competing and compounding potential contributions of eustatic sea level rise (Simpson et al.,

2009), possible Laurentide Ice Sheet forebulge drop (Long et al., 2011), and reduction of gravitational pull of the ice body (Clark et al., 2002). While I suggest that sea level change destabilized the southwestern GrIS at ~19 ka, it is not possible to differentiate, using the present sedimentological evidence, an advance to the shelf break from a retreat from that location, as both of these events would have enabled the high sedimentation rates observed in HU87033-008.

If the source of the 19 ka meltwater pulse were determined, model simulations of the resulting sea level fingerprint could identify whether the southwestern GrIS was compelled to advance or retreat (Clark et al., 2002; Clark et al., 2004; Carlson and Clark, 2012). Alternatively, if an advance or retreat at this time were identified, this data would be a valuable contribution to restricting the possible source locations for the 19 ka meltwater pulse (G. Milne, personal communication). Unfortunately, such identification would likely require radiocarbon dating of glacially derived shelf landforms, which, as explained above, are largely unmapped and not sampled.

5.3.2. Marine vs. terrestrial late deglaciation retreat

The primary finding of Chapter III is that retreat from the modern coastline to the modern ice margin occurred far more slowly in a region without strong marine influence than in fjord systems with a strong marine influence (Figure 3-6). If retreat inland from Sisimiut occurred steadily between 14 and 7 ka (Chapter III), as suggested by the lack of substantive moraines in the intervening land, no further causes of the relatively slow retreat could be defined. However, if hiatuses did occur, it may be possible to attribute specific changes in atmospheric temperatures, particularly during the Younger Dryas cold period (Figure 1-1, Svensson et al., 2008), to this terrestrial-dominated ice margin retreat. If a hiatus did occur during the Younger

Dryas, it would suggest that oceanic forcing of thinning and retreat at the southern locations was stronger than the countering atmospheric drivers. A high-resolution ^{10}Be exposure-dated transect between Sisimiut and the Kangerlussuaq sites of Levy et al. (2012) and Carlson et al. (in press) would identify potential dates and locations of hiatuses in retreat.

Data from Chapter III also demonstrate that coastal exposure occurred earlier near the town of Sisimiut than at the more southern three locales. An early southwestern GrIS onset of retreat is supported by a marked drop in HU87033-008 sedimentation rates (Chapter II; Figure 2-3) and by nearby, high-elevation ^{10}Be exposure dates (Rinterknecht et al., 2009; Roberts et al., 2009; Figure 3-4). Why did shelf retreat from the LGM to the modern coastline occur more quickly at Sisimiut? As suggested in section 5.3.2, high-resolution bathymetric mapping of the southwestern Greenland continental shelf would greatly improve our understanding of deglacial GrIS behavior. Dating of submarine moraines offshore of Sisimiut would point to an LGM ice extent more specific than ‘middle to outer shelf’ (e.g., Roberts et al., 2010), thereby providing the distance variable required for calculating retreat rates.

5.3.3. *Late Holocene glacial maxima*

In Chapter IV, I discuss evidence for a late-Holocene, southernmost Greenland Kiangtût sermiat glacier maximum preceding the Little Ice Age (LIA). However, the cause of this timing is unknown (Winsor et al., 2014). Was pre-LIA late Holocene moraine abandonment due to local ice dynamics or to local climate change? Some records of late-Holocene southern Greenland climate suggest warming at the time of Kiangtût sermiat moraine abandonment (Andresen et al., 2004; D’Andrea et al., 2011), though others are in disagreement (Kaplan et al., 2002). Two study directions will enable identification of the causes of Kiangtût sermiat moraine abandonment. First,

high-precision dating of additional southern Greenland outlet glaciers will determine if the Kiagtût sermiat chronology is unique, and therefore likely driven by ice dynamics. If the chronology is representative of other margins, it is likely driven by climate changes. Second, additional high-resolution, well-dated, late-Holocene climate records would test whether for a coherent regional change (warming at ~ 1.5 ka) that drove retreat.

References:

- Andresen, C.S., Björck, S., Bennike, O., Bond, G., 2004. Holocene climate changes in southern Greenland. *Journal of Quaternary Science*, 18, 783-795.
- Andrews, J.T., 2000. Icebergs and iceberg rafted detritus (IRD) in the North Atlantic: facts and assumptions. *Oceanography*, 13, 100-108.
- Berger, A., and Loutre, M.F., 1991. Insolation values for the climate of the last 10 million years. *Quaternary Science Reviews*, 10, 297-317.
- Brett, C.P., and Zarudzski, E.F.K., 1979. Project Westmar. A shallow marine geophysical survey on the West Greenland continental shelf. *Rapport Grönlands Geologiske Undersøgelse*, 87, 27 pp.
- Carlson, A.E., and Clark, P.U., 2012. Ice sheet sources of sea level rise and freshwater discharge during the last deglaciation. *Reviews of Geophysics*, 50, RG4007, doi:10.1029/2011RG000371.
- Carlson, A.E., Winsor, K., Ullman, D.J., Brook, E., Rood, D.H., Axford, Y., LeGrande, A.N., Anslow, F., and Sinclair, G., Earliest Holocene south Greenland ice-sheet retreat within its late-Holocene extent. in press at *Geophysical Research Letters*.
- Clark, P.U., Mitrovica, J.X., Milne, G.A., and Tamisiea, M.E., 2002. Sea-level fingerprinting as a direct test for the source of global meltwater pulse 1A. *Science*, 295, 2438-2441.
- Clark, P.U., McCabe, A.M., Mix, A.C., and Weaver, A.J., 2004. Rapid rise of sea level 19,000 years ago and its global implications. *Science*, 304, 1141-1144.
- Clark, P.U., Dyke, A.S., Shakun, J.D., Carlson, A.E., Clark, J., Wohlfarth, B., Mitrovica, J.X., Hostetler, S.W., and McCabe, A.M., 2009. The Last Glacial Maximum: *Science*, 325, 710-714.
- Clark, P.U., Shakun, J.D., Baker, P.A., Bartlein, P.J., Brewer, S., Brook, E., Carlson, A.E., Cheng, H., Kaufman, D.S., Liu, Z., Marchitto, T.M., Mix, A.C., Morrill, C., Otto-Bliesner, B.L., Pahnke, K., Russell, J.M., Whitlock, C., Adkins, J.F., Blois, J.L., Clark, J., Colman, S.M., Curry, W.B., Flower, B.P., He, F., Johnson, T.C., Lynch-Stieglitz, J., Markgraf, V., McManus, J., Mitrovica, J.X., Moreno, P.I., and Williams, J.W., 2012. Global climate evolution during the last deglaciation. *Proceedings of the National Academy of Sciences*, 109, 1134-1142.
- D'Andrea, W.J., Huang, Y., Fritz, C.S., Anderson, N.J., 2011. Abrupt Holocene climate change as an important factor for human migration in West Greenland. *Proceedings of the National Academies of Science*, 108, 9765-9769.

- Dowdeswell, J.A., Hogan, K.A., and Ó Cofaigh, C., 2013. Submarine glacial-landform distribution across the West Greenland margin: a fjord-shelf-slope transect through the Ummannaq system (70° to 71°N): In, Dowdeswell, J.A., Canals, M., Jakobsson, M., Todd, B.J., Dowdeswell, E.K., and Hogan, K.A. (eds), *Atlas of Submarine Glacial Landforms: Modern, Quaternary and Ancient*. Geological Society, London, Memoirs, 2015.
- Joughin, I., Alley, R.B., and Holland, D.M., 2012. Ice-sheet response to oceanic forcing. *Science*, 338, 1172-1176.
- Holland, D.M., Thomas, R.H., De Young, B., Ribergaard, M.H., and Lyberth, B., 2008. Acceleration of Jakobshavn Isbræ triggered by warm subsurface ocean waters. *Nature Geoscience*, 1, 659-664.
- Kaplan, M.R., Wolfe, A.P., Miller, G.H., 2002. Holocene environmental variability in southern Greenland inferred from lake sediments. *Quaternary Research*, 58, 149-159.
- Knutz, P.C., M.-A. Sicre, H. Ebbesen, S. Christiansen, and A. Kuijpers 2011. Multiple-stage deglacial retreat of the southern Greenland Ice Sheet linked with Irminger Current warm water transport: *Paleoceanography*, 26, PA3204, doi:10.1029/2010PA002053.
- Long, A.J., Woodroffe, S.A., Roberts, D.H., and Dawson, S., 2011. Isolation basins, sea-level changes and the Holocene history of the Greenland Ice Sheet. *Quaternary Science Reviews*, 30, 3748-3768.
- Mann, M.E., Zhang, Z., Rutherford, S., Bradley, R.S., Hughes, M.K., Shindell, D., Ammann, C., Faluvegi, G., and Ni, F., 2009. Global signatures and dynamical origins of the Little Ice Age and Medieval Climate Anomaly. *Science*, 326, 1256-1260.
- Murray, T., Scharer, K., James, T.D., Dye, S.R., Hanna, E., Booth, A.D., Selmes, N., Luckman, A., Hughes, A.L.C., Cook, S., Huybrechts, P., 2010. Ocean regulation hypothesis for glacier dynamics in southeast Greenland and implications for ice sheet mass changes: *Journal of Geophysical Research*, 115, F03026, doi:10.1029/2009JF001522.
- Ó Cofaigh, Andrews, J.T., Jennings, A.E., Dowdeswell, J.A., Hogan, K.A., Kilfeather, A.A., and Sheldon, C., 2013. Glacimarine lithofacies, provenance and depositional processes on a West Greenland trough-mouth fan. *Journal of Quaternary Science*, 28, 13-26.
- Ó Cofaigh, C., Dowdeswell, J.A., Jennings, A.E., Hogan, K.A., Kilfeather, A., Hiemstra, J.F., Noormets, R., Evans, J., McCarthy, D.J., Andrews, J.T., Lloyd, J.M., and Moros, M., 2013. An extensive and dynamic ice sheet on the West Greenland shelf during the last glacial cycle: *Geology*, 41, 219-222.
- Perner, K., Moros, M., Lloyd, J.M., Kuijpers, A., Telford, R.J., and Harff, J., 2011. Centennial scale benthic foraminiferal record of late Holocene oceanographic variability in Disko

- Bugt, West Greenland. *Quaternary Science Reviews*, 30, 2815-2826.
- Pritchard, H.D., Arthern, R.J., Vaughan, D.G., and Edwards, L.A., 2009. Extensive dynamic thinning on the margins of the Greenland and Antarctic ice sheets. *Nature*, 461, 971-975.
- Raymo, M.E., and Mitrovica, J.X., 2012. Collapse of polar ice sheets during the stage 11 interglacial. *Nature*,
- Rignot, E., Koppes, M., Velicogna, I., 2010. Rapid submarine melting of the calving faces of West Greenland glaciers: *Nature Geoscience*, v. 3, p. 187-191.
- Rinterknecht, V., Gorokhovitch, Y., Schaeffer, J., and Caffee, M., 2009, Preliminary ^{10}Be chronology for the last deglaciation of the western margin of the Greenland Ice Sheet: *Journal of Quaternary Science*, v. 24, no. 3, p. 270-278, doi:10.1002/jqs.1226.
- Roberts, D.H., Long, A.J., Schnabel, C., Davies, B., Xu, S., Simpson, M.J.R., and Huybrechts, P., 2009. Ice sheet extent and early deglacial history of the southwestern sector of the Greenland Ice Sheet: *Quaternary Science Reviews*, 28, 2760-2773.
- Roberts, D.H., Long, A.J., Davies, B.J., Simpson, M.J.R., and Schnabel, C., 2010. Ice stream influence on West Greenland Ice Sheet dynamics during the Last Glacial Maximum: *Journal of Quaternary Science*, doi:10.1002/jqs.1354.
- Roksandic, M.M., 1979. Geology of the continental shelf off West Greenland between 61°15'N and 64°00'N: an interpretation of sparker seismic and echosounder data. Rapport Grönlands Geologiske Undersøgelse, 92, 15 pp.
- Rvachev, V.D., 1964. Relief and bottom deposits of the shelf of southwestern Greenland. *Deep Sea Research*, 11, 646-653.
- Seidenkrantz, M.-S., Aagaard-Sørensen, S., Sulsbrück, H., Kuijpers, A., Jensen, K.G., and Kuzendorf, H., 2007. Hydrography and climate of the last 4400 years in a SW Greenland fjord: implications for Labrador Sea paleoceanography. *Holocene*, 17, 387-401.
- Seidenkrantz, M.-S., Roncaglia, L., Fischel, A., Heilmann-Clausen, C., Kuijpers, A., and Moros, M., 2008. Variable North Atlantic climate seesaw patterns documented by a late Holocene marine record from Disko Bugt, West Greenland. *Marine Micropaleontology*, 68, 66-83.
- Simon, Q., Hillaire-Marcel, C., St-Onge, G., and Andrews, J.T., 2013. North-eastern Laurentide, western Greenland and southern Inuitian ice stream dynamics during the last glacial cycle: *Journal of Quaternary Science*, doi:10.1002/jqs.2648.
- Simpson, J.R.M., Milne, G.A., Huybrechts, P., and Long, A.J., 2009. Calibrating a glaciological model of the Greenland ice sheet from the Last Glacial Maximum to present-day using

- field observations of relative sea level and ice extent. *Quaternary Science Reviews*, 28, 1630-1656.
- Straneo, F., Hamilton, G.S., Sutherland, D.A., Stearns, L.A., Davidson, F., Hammil, M.O., Stenson, G.B., and Rosing-Asvid, A., 2010. Rapid circulation of warm subtropical waters in a major glacial fjord in East Greenland. *Nature Geoscience*, 3, 182-186.
- Svensson, A., Andersen, K.K., Bigler, M., Clausen, H.B., Dahl-Jensen, D., Davies, S.M., Johnsen, S.J., Muscheler, R., Parrenin, F., Rasmussen, S.O., Röthlisberger, R., Seierstad, I., Steffensen, J.P., and Vinther, B.M., 2008. A 60 000 year Greenland stratigraphic ice core chronology: *Climate of the Past*, 4, 47-57.
- Trouet, V., Esper, J., Graham, N.E., Baker, A., Scourse, J.D., and Frank, D.C., 2009. Persistent positive North Atlantic oscillation mode dominated the medieval climate anomaly. *Science*, 324, 78-80.
- Winsor, K., Carlson, A.E., Klinkhammer, G.P., Stoner, J.S., and Hatfield, R.G., 2012. Evolution of the northeast Labrador Sea during the last interglaciation: *Geochemistry, Geophysics, Geosystems*, 13, doi:10.1029/2012GC004263.
- Winsor, K., Carlson, A.E., and Rood, D.H., 2014. ^{10}Be dating of the Narsarsuaq moraine in southernmost Greenland: evidence for a late-Holocene ice advance exceeding the Little Ice Age. *Quaternary Science Reviews*, 98, 135-143.